Technical Report

TR-14-19

Canister Retrieval Test

Final report

Ola Kristensson, Lennart Börgesson
Clay Technology AB

January 2015

Svensk Kärnbränslehantering AB
Swedish Nuclear Fuel
and Waste Management Co

Box 250, SE-101 24 Stockholm
Phone +46 8 459 84 00

ISSN 1404-0344
SKB TR-14-19
ID 1451477

Canister Retrieval Test

Final report

Ola Kristensson, Lennart Börgesson
Clay Technology AB

January 2015

Summary

The Canister Retrieval Test was a full scale field experiment simulating a deposition hole in a high level radioactive waste repository of KBS-3V design. The main purpose was to demonstrate that canister retrieval is technical feasible after full water saturation of the bentonite buffer encapsulating the canister.

The in-situ experiment was carried out at Äspö Hard Rock Laboratory from 1999 to 2006. The experiment consisted of a cylindrical deposition hole hosting a canister encapsulated in clay buffer. Cables attached between the host rock and a plug on top of the buffer retained the buffer vertically and simulated the reaction force of a tunnel backfill. The canister was equipped with heaters to simulate the thermal activity of nuclear waste and strips of plastic filter were installed at the deposition hole's wall and connected to a water supply to provide a controllable simulated groundwater inflow. After 5 years in operation the experiment was shut down and dismantled.

Besides retrieval of the canister, the possibility to perform additional studies was exploited. These concerned: canister handling and equipment operation during installation; evaluation of thermo-hydro-mechanical processes taking place in the buffer during operation; the effect of repository-like conditions on density and water content, microorganisms, hydro-mechanical properties, chemistry/mineralogy; and capabilities of modelling the experiment.

The hydrodynamic/chemical technique used when freeing the canister, from canister mid-height down to about canister bottom, performed well. When the canister was freed, the retrieval from the deposition hole was unproblematic using the machinery for canister deposition in a reversed process order.

When analysing buffer samples it was found that considerable density homogenization had taken place during the water uptake, but that the buffer still had remaining density heterogeneity. It was also concluded that the buffer on top of the canister was still unsaturated but saturation had been achieved elsewhere.

Autotropic acetogens and sulphate-reducing bacteria were found in buffer samples. The number of them was however low as compared to the surrounding groundwater. Viable bacteria were mostly found at locations where the maximum temperature had not been too high.

Buffer material analyses regarding chemistry/mineralogy and hydro-mechanics showed that properties of the buffer had not been significantly changed by the repository-like conditions.

The thermal processes seem to be well captured by the numerical simulations undertaken. When considering hydraulics, the models appear to be capable of simulating the processes fairly accurately for the conditions prevailing in the experiment. The models are however, formulated using certain assumptions which may not be valid for other conditions. The performance of the mechanical part of the models is considered to be most uncertain. Present mechanical models show process dependence and have often to be recalibrated for different situations in order to capture the mechanical processes accurately.

Sammanfattning

Återtagsförsöket var ett fullskaligt fältförsök som simulerade ett av deponeringshålen i ett KBS-3V slutförvar av radioaktivt kärnbränsleavfall. Det huvudsakliga syftet var att visa att det är tekniskt genomförbart att återta kapslar efter full vattenmättnad av bentonitbufferten.

Experimentet genomfördes vid Äspölaboratoriet från 1999 till 2006. Det bestod av en kapsel inbäddad i lerbuffert som placerats i ett cylindriskt deponeringshål. Buffertens vertikala svällning begränsades av en plugg som var förbunden med berget via nio stålkablar vilka simularade reaktionskraften av en återfylld tunnel. Kapseln var utrustad med värmare för att simulera den termiska aktiviteten av kärnbränsleavfall och remsor av plastfilter installerades på deponeringshålsväggen och kopplads till vattenförsörjning för att ge ett kontrollerbart grundvatteninflöde. Efter fem års drift avbröts försöket och nedmonterades.

Förutom återtagande av kapseln, utnyttjades möjligheten för ytterligare studier. Dessa berörde: hantering och utrustning under installationen; termo-hydro-mekaniska processer som ägde rum i bufferten under drift; hantering och utrustning under återtagande; effekten av förvarsliknande förhållanden på densitet och vattenhalt, mikroorganismer, hydromekaniska egenskaper, kemi/mineralogi; och kapaciteten för att modellera experimentet.

Den hydrodynamiska/kemiska teknik som användes vid frigörande av kapseln, från kapselns mitthöjd ned till kapselbotten, fungerade tillfredställande. Själva återtagandet av kapseln ur deponeringshålet, då installationsutrustningen användes i omvänd ordning jämfört med installationen, var oproblematiskt.

Analyser av buffertprover visade att densiteten hade homogeniserats under vattenupptaget, men också att bufferten fortfarande hade en återstående heterogenitet. Det visade sig också att bufferten ovanpå kapseln var omättad men för övrigt vattenmättad.

Autotrofa acetogener och sulfatreducerande bakterier hittades i buffertproverna . Antalet av dem var emellertid låg jämfört med det omgivande grundvattnet. Livskraftiga bakterier hittades till största delen där den maximala temperaturen inte hade varit för hög.

Materialanalyser av bufferten med avseende på kemi/mineralogi och hydromekanik visade att egenskaper hos bufferten inte hade ändrats nämnvärt av de förvarsliknande förhållandena.

De termiska processerna verkar kunna modeleras tillförlitligt. Lösningarna som fås med de hydrauliska modellerna återger också de uppmätta processerna relativt väl. De är emellertid formulerade under vissa antaganden som inte nödvändigtvis alltid gäller. De mekaniska modellerna får anses som mest osäkra. De nuvarande uppvisar ofta processberoende och behöver kalibreras för olika situationer för att ge lösningar som överensstämmer med uppmätta mekaniska beteenden.

Contents

1 Introduction

1.1 Aim and scope

The Canister Retrieval Test (CRT) was a full scale field experiment simulating conditions prevailing in a deposition hole of a repository of high level radioactive waste according to the Swedish KBS-3V design. The main purpose was to demonstrate that retrieving a canister is technically feasible after full water saturation of the bentonite buffer encapsulating the canister has been achieved (Svemar 1999).

Besides the overall main purpose of demonstrating retrievability, the possibility to perform additional studies was exploited. These involved:

- Handling and equipment during installation.
- Evaluating Thermo-Hydro-Mechanical (THM) processes taking place in the buffer during operation.
- Handling and equipment during retrieval.
- The HM state (in terms of density and water content) of a buffer have being subjected to repository-like conditions.
- The effect of repository-like conditions on:
  - Microorganisms present in the buffer.
  - Hydro-mechanical and chemical-mineralogical properties of the buffer.
- The capabilities of modelling the experiment and developing models.

Tunnel backfill was not included in the setup. The mechanical influence from a backfilled tunnel was however simulated by using a vertically mobile retaining system. To enable a controlled wetting an artificial water supply at the deposition hole wall was utilized. The canister freeing technique was tested from canister mid-height and downwards. The experiment did not consider factors such as radiation hazard and radioactive pollution, which might complicate actual application of the technique being evaluated.

1.2 Brief overview of CRT

The in-situ experiment was carried out at Äspö Hard Rock Laboratory (HRL) from 1999 to 2006. One target area of Äspö HRL is to ”Demonstrate technology for and function of important parts of the deep disposal system” (Svemar 1999). This target area in turn, can be described as concerning: ”Function”, ”Handling techniques”, and ”Development and testing of equipment” (Svemar 1999). The CRT fit all of these criteria.

The CRT project contained a full scale experiment in close accordance with the KBS-3V design. A schematic view showing the geometry and equipment used in the experiment is given in Figure 1-1. As can be seen, the experimental design is composed of a canister encapsulated in a clay buffer, emplaced in a cylindrical deposition hole and restrained vertically by cables attached between the rock and a rigid lid on top of the buffer. The term “buffer” in this study is defined as consisting of the volume initially occupied by the bentonite clay together with initially empty volumes in the deposition hole.

The canister was equipped with internal heaters in order to simulate the thermal activity of the nuclear waste.

The buffer was made from Wyoming bentonite (Volclay MX-80) in different geometric and physical forms (see Figure 1-1):

- Cylinders, one below and three above the canister, C1 and C2-C4, respectively.
- Rings, R1–R10 , mainly between the canister and deposition hole wall.
- Bricks, filling the volume between the top of the canister, R10, and C2.

- Pellets, filling an open vertical slot between the deposition hole wall and the cylinders and rings.
- Powder, for additional backfilling of voids.

In the KBS-3V design, the cylinders and rings are so dimensioned that an inner and outer slot facilitates installation. The outer slot, at the borehole wall, was filled with pellets and water in CRT.

On top of the buffer an impermeable mat was placed before casting of a concrete plug that was part of the retaining system. The plug could be displaced vertically, but the motion was restrained by nine "rock anchors", i.e. steel cables anchored in the rock and connected to a steel lid emplaced on top of the concrete plug. The elasticity of the pre-tensioned cables mimicked the reaction force of the backfill in the tunnel, present in a real repository, and thereby prevented uncontrolled upward swelling of the buffer when absorbing water.

In order to control, homogenize (orientation wise), and speed up the saturation process of the experiment, strips of a porous plastic filter material were installed at the deposition hole wall and connected to a water supply that was supplied with groundwater taken from an adjacent bore-hole.

During the operational phase, the heater power and filter water pressure were controlled, with the heaters mimicking the thermal activity of a "live" canister. The rock (temperature and stress), canister (temperature and strain), retaining system (force and displacement), and buffer (temperature, relative humidity, pore pressure, and total pressure) were all monitored, and during the operational phase the monitored data was continuously logged and transferred to a computer connected to the Äspö data network.

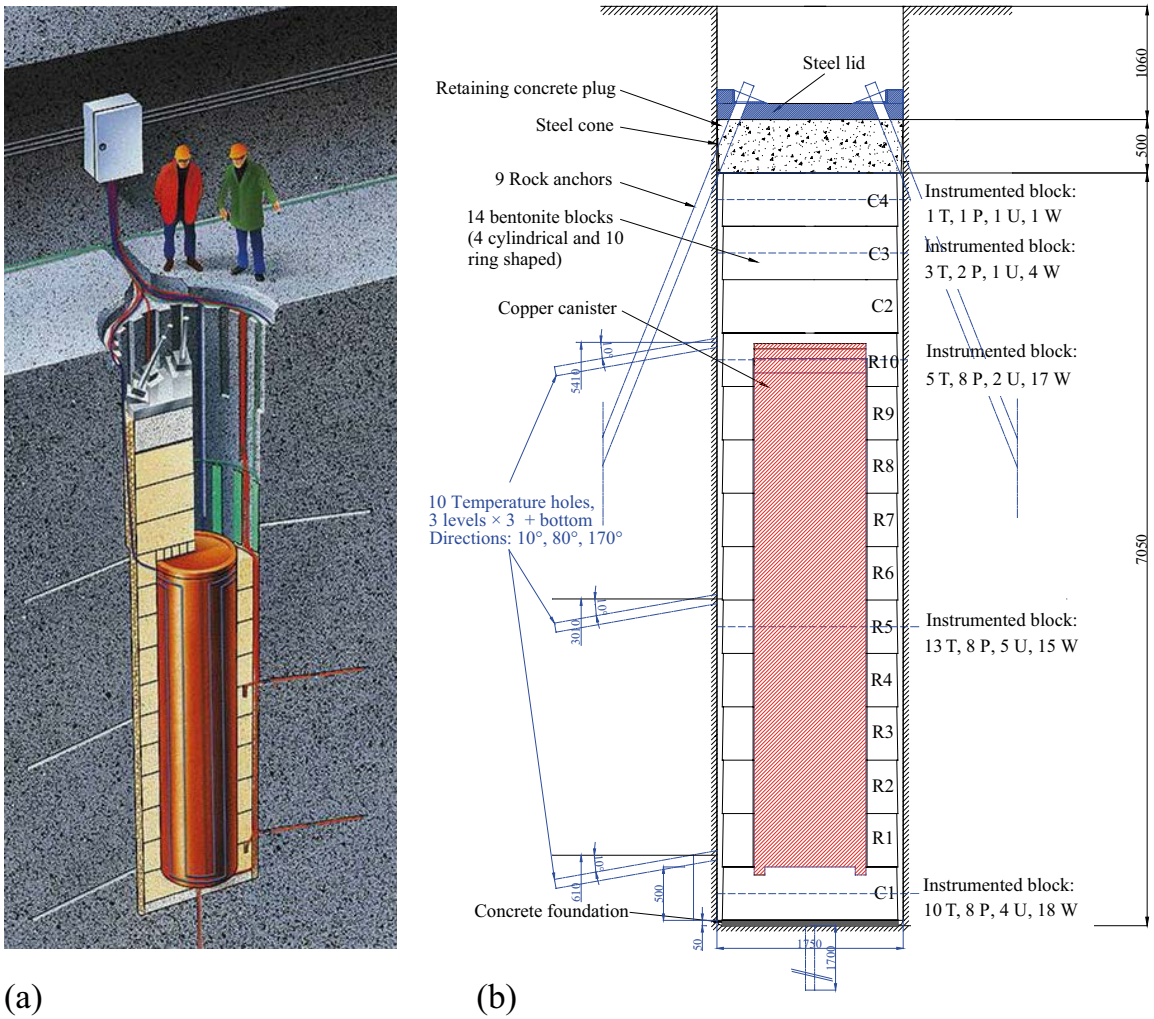

Figure 1-1. *(a) Schematic overview of CRT and (b) geometry and equipment, where the type of sensor (T=temperature, P=total pressure, U=pore pressure, and W=relative humidity) and number of sensors installed are indicated for the instrumented blocks. Dimensions indicated are given in mm.*

After having the experiment running for five years it was dismantled. The buffer, from the top to the canister's mid-height was extensively sampled. Density and water content were determined for the sampled material. The buffer from canister mid-height down to close to the canister's base was removed by using the most promising technique for freeing the canister, as evaluated by Kalbantner and Sjöblom (2000). The technique used was the so called *low pressure hydrodynamic technique* (also referred to as the *hydrodynamic/chemical technique*) in which a dilute calcium chloride solution is flushed over the buffer's exposed surface with a turbulent flow. This process disaggregates the compact buffer into a slurry which can be pumped away from the deposition hole.

When the canister was freed, the machinery used for canister deposition was used in the reverse order to that used in installation, to retrieve the canister from the deposition hole. The buffer below the canister was removed manually.

The buffer analyses that followed were performed on the samples taken from the upper half of the buffer. They investigated the effect of repository-like conditions regarding:

- Density and water content of the buffer.
- Microorganisms in the buffer.
- Hydro-mechanical and chemical-mineralogical properties of the buffer.

As a part of the project, modelling was carried out, mainly in order to evaluate and develop models representing the barrier materials. CRT became the subject for analysis in one of the assignments (2.2) of the Task-Force on Engineered Barrier Systems (EBS-TF). At the time of publishing of this report, some more modelling of CRT is planned to be carried out within EBS-TF.

The activities within CRT can be categorized into distinctive phases, somewhat overlapping but with subsequent initialization. The time when these started and the initial activities associated with them are given in Table 1-1.

In addition to the phases given in Table 1-1, "Modelling" could be added. It is not accounted for in Table 1-1 since, as mentioned above, modelling of CRT mainly has been carried out in the framework of EBS-TF, whereas the CRT-assignment was introduced in 2007.

Table 1-1. Phases of CRT, their starting time, and initial activity.

Phase	Starting time	Initial activity
Preparation	1998	Tunnel excavation
Installation	2000, Autumn	Buffer installation
Operation	2000, October 26	Outer slot pellet/water filling
Dismantling	2005, October 11	Switching the heaters off
Analysis	2006, January 18	Determining the density and water content

1.3 Report structure

This report is intended as a general overview of the CRT experiment, briefly presenting the experiment execution and the main findings. The retrieval technique and the final use of the technique for freeing the lower half of the canister at the end of the test are also briefly described. The information given here was obtained from addressed references, where more detailed descriptions are provided. The report is structured so that it follows the timeline of the experiment, and descriptions of vital components are given when they appear in the experimental process. The report is divided into chapters with following self-explanatory titles: Preparation, Installation, Operation, Dismantling, Material analyses, Modelling, and Conclusions.

2 Preparation

2.1 Tunnel

CRT was located on the 420 m level in the inner most section of the 100 m TASD-tunnel, Figure 2-1. In 1998 the 6 m wide and 6 m high CRT tunnel-section was excavated using conventional drilling and blasting and following this, geological mapping of the tunnel was carried out (Hardenby 2002). The tunnel floor was cast with concrete to obtain a flat surface for the boring machine and the machine handling the canister.

2.2 Deposition hole

Initially, the experiment was planned to include retrieval from two equally equipped deposition holes, 1.762 m in diameter, 8.75 m deep, and 6 m spacing, in order to be able to test different recovery techniques (Svemar 1999). This plan was subsequently changed to incorporate only the innermost of the two excavated deposition holes (DD0092G01), see Figure 2-2. As a consequence, only one freeing technique was tested. The unused deposition hole was later used for hosting the Temperature Buffer Test (TBT). Geological mappings were done for pilot and deposition holes (Hardenby 2002), pressure and inflow measurements for the pilot holes (Gentzschein 1999) and acoustic emission monitoring was utilized to investigate the host rock's reaction to the deposition hole boring process (Pettitt et al. 1999).

The geological mapping of the CRT deposition hole is shown in Figure 2-3. The pressure and inflow measurements from 0.3 m – 8 m depth for the pilot hole KD0092G01, 8 m deep and with a diameter of 76 mm, gave a pressure of 5 bar and a flow rate of 7.1 ml/min. Hardenby (2002) noted that, "Although, some water leakage has been recorded there is not a great deal of water in the hole."

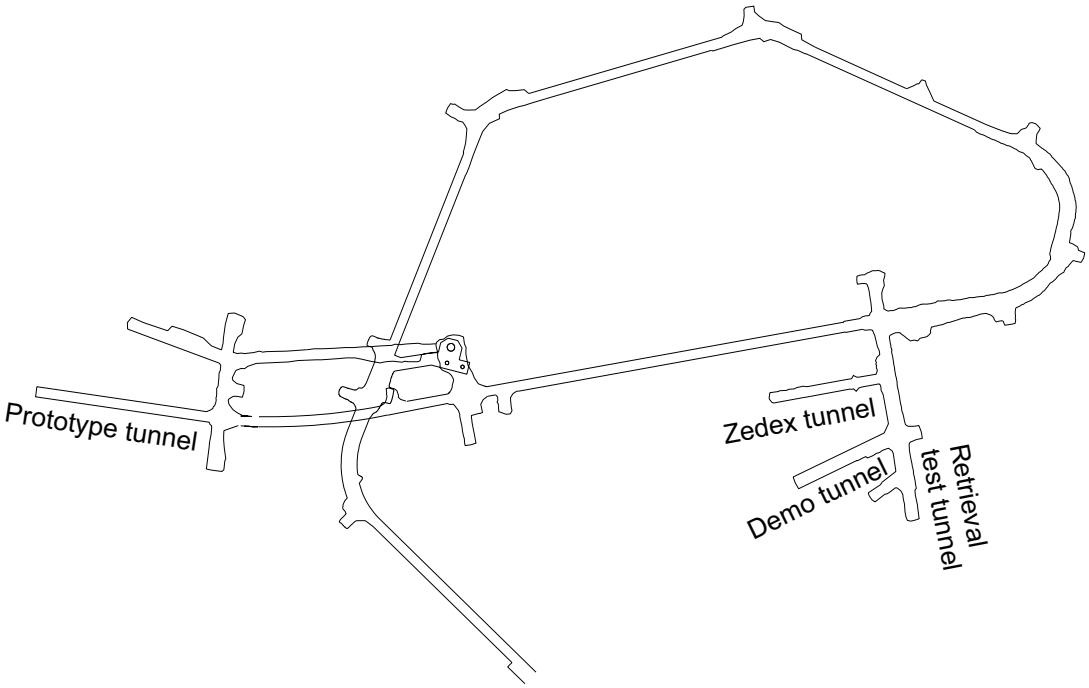

Figure 2-1. *Äspö HRL tunnel layout for 420–450 m depth.*

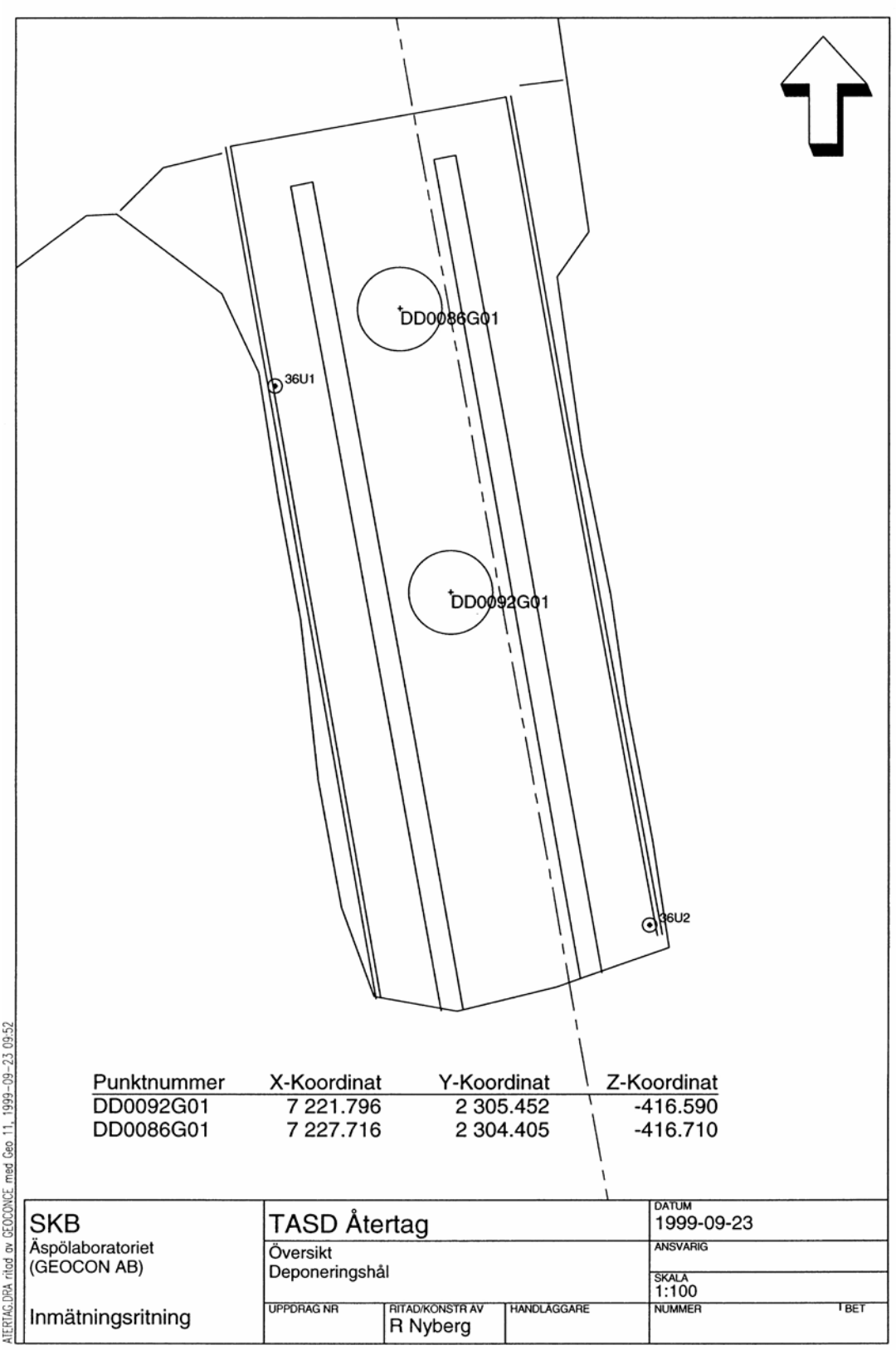

Figure 2-2. *Overview of the CRT tunnel with the two boreholes. The inner most, DD0092G01, hosted the CRT experiment and the outer, DD0086G01, hosted the Temperature Buffer Test.*

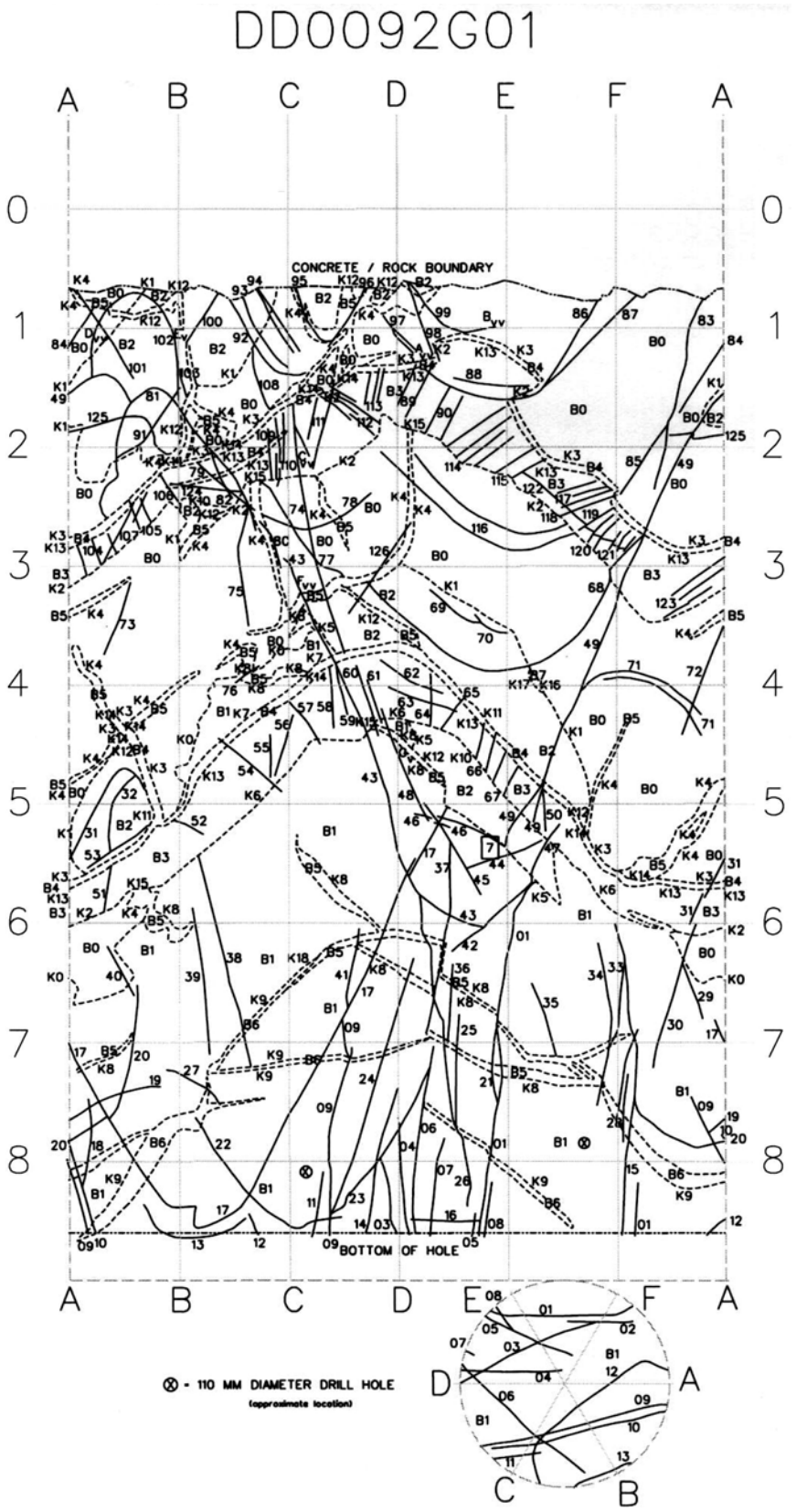

Rock types:

B0 = Greenstone, medium-grained, gneissified/granitized variety

B1 = Äspö diorite

B2 = Greenstone, medium-grained, mainly homogenous variety

B3 = Fine-grained granite, fine-grained and reddish variety

B4 = Pegmatite

B5 = Fine-grained granite/pegmatite hybrid

B6 = Fine-grained granite, fine-grained and grey variety

B7 = Pyrite lens

Contacts:

K0-K18 and dashed line

Fractures:

01-126 and continuous line

Water:

A-G and v-vv. (v-vv = damp – wet)

Figure 2-3. *Geological mapping of the CRT deposition hole.*

Prior to the installation of the buffer and canister, preparations of the deposition hole or adjacent rock mass were carried out as described by Thorsager et al. (2002), and consisted of the following:

- Casting of concrete foundation in the bottom of the hole.
- Installation of drainage system.
- Cutting of slots in the rock wall and tunnel floor.
- Installation of rock anchors and instruments in the rock.
- Installation of plug formwork, a steel cone, at top of the hole wall.
- Installation of artificial wetting system.
- Installation of a climate control system for regulating relative humidity in the hole during installation.

The artificial wetting system consisted of strips of a porous plastic filter material, installed at the deposition hole wall, connected to a water supply, that was fed with groundwater taken from an adjacent borehole (hole ID = HD0025A). A schematic drawing of the filter strip installation is shown in Figure 2-4.

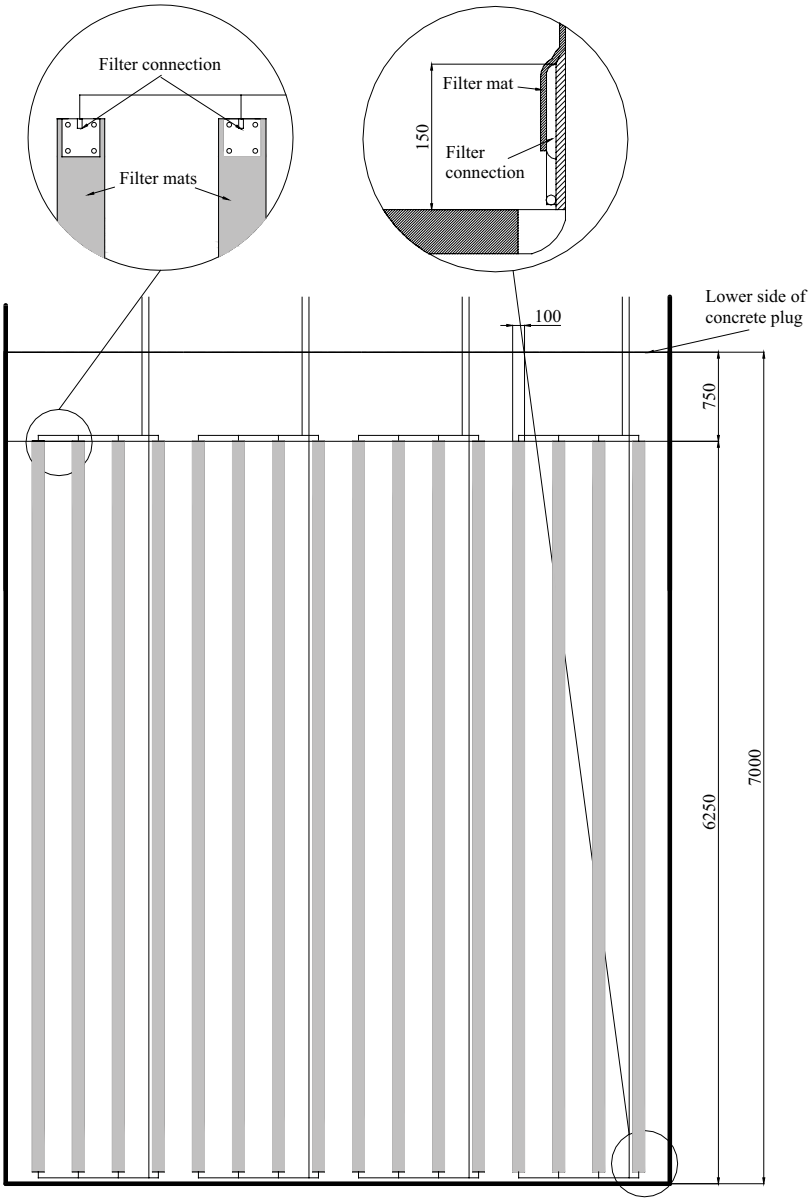

Figure 2-4. *Schematic drawing of the location of the filter strips and connecting tubes in the artificial wetting system. The surface of the deposition hole has been unfolded. Dimensions indicated are given in mm.*

2.3 Buffer

All buffer clay components were made from sodium dominated Wyoming bentonite (Volclay MX-80) delivered from the processing plant at Volclay Limited in Liverpool, England. All calculations in this report were performed using 2,780 kg/m^3 as the solid density of the clay (Karnland et al. 2006) and 1,000 kg/m^3 as the water density.

Large cylinder-shaped and ring-shaped blocks

The manufacturing of the large blocks is described in Thorsager et al. (2002) and Johannesson (1999). Bentonite powder was mixed with water at Hackman-Rörstrand AB in Lidköping to obtain the desired water content of 17% for use in manufacturing the cylinder-shaped and ring-shaped blocks in CRT. The mix was then transported to Hydroweld AB in Ystad where the powder was uniaxially compacted in a mould. Table 2-1 presents the results of block compaction (as measured directly after production) and also the water content of the materials used, demonstrating the uniformity of the materials and products. After removal from the form, the block was placed on a pallet by specially designed lifting equipment, and a cap was placed over the block in order to prevent the block from drying. On average, the outer diameter of both types of the large blocks was 1.64 m and the inner diameter of the rings was 1.07 m.

Preparation of blocks for installation of sensors and cables, described in Sandén and Börgesson (2000), was carried out in a controlled climate prior to shipment to Äspö HRL. Spaces for the instrumentation, holes and groves, were excavated by careful drilling and cutting. The bottom-most block, C1, was prepared differently than the others since instrumentation was installed prior to block placement. For all other blocks, installation of instrumentation was carried out after their placement in the deposition hole.

Brick-shaped blocks

Höganäs Bjufv AB in Bjufv produced bentonite bricks for the CRT. The bricks had dimensions of 115x234x64 mm. They were compacted under high pressure in a machine built for compaction of fire-clay bricks. The average dry density of a brick was 1,800 kg/m^3 and the water content 10%.

Pellets

Bentonite pellets were produced by Sahut-Conceur in France. The pellets were shaped like pillows and had the dimensions 16x16x8 mm. They were compacted in double rollers under high pressure. The average dry density of a pellet was 1,800 kg/m^3 and the water content 10%.

Table 2-1. Data for the large blocks in CRT.

ID	Water content	Density (kg/m^3)	Weight (kg)	Height (mm)	Degree of saturation	Void ratio
R1	0.173	2,091.9	1,280	506.5	0.859	0.558
R6	0.171	2,102.7	1,282	505.0	0.867	0.548
R8	0.171	2,099.8	1,286	507.1	0.865	0.551
R9	0.171	2,098.3	1,288	508.0	0.861	0.551
R7	0.172	2,099.5	1,290	508.7	0.866	0.552
R3	0.167	2,102.7	1,280	503.9	0.855	0.543
R2	0.172	2,095.4	1,288	508.5	0.861	0.555
R4	0.170	2,116.3	1,290	504.6	0.879	0.537
R5	0.175	2,086.5	1,278	506.9	0.859	0.565
R10	0.171	2,069.1	1,272	509.2	0.83	0.574
C4	0.173	2,016.4	2,156	505.4	0.78	0.617
C3	0.171	2,004.8	2,094	493.7	0.761	0.623
C2	0.170	2,003.1	2,104	496.7	0.759	0.624
C1	0.173	1,987.7	2,128	506.3	0.751	0.641

3 Installation

For the purposes of describing the installation process it should be noted that unless otherwise noted the information given in this chapter was obtained from Thorsager et al. (2002).

The installation started in the autumn of the year 2000 and was carried out in the following sequence:

1. Emplacement of bentonite blocks and rings including installation of instruments.
2. Deposition of canister.
3. Continuation of 1.
4. Removal of climate control system used for regulating relative humidity in the hole during installation.
5. Filling of gap between rock and blocks with pellets and water.
6. Casting of concrete plug and placement of steel lid.
7. Pre-stressing of retaining system.

3.1 Buffer blocks

The first activity of the installation was to emplace the buffer blocks (cylinder C1 and rings R1–R10). The canister was then installed in the centre of the buffer rings. The volume on top of the canister, up to the upper surface of R10 was subsequently filled with brick-shaped buffer blocks, pellets and bentonite powder. Cylindrical blocks C2–C4 were then emplaced on top.

To facilitate installation, the bentonite buffer of KBS-3V is designed so that gaps, ideally 10 mm and 50 mm, are present at the inner (canister) and outer (rock) interfaces, respectively. In CRT the average width of the outer gap was estimated to be 61 mm due to an imperfect borehole. Initial average dimensional and density data for the buffer blocks are as given in Table 3-1. Values of dry density and water content for these materials are given in Johannesson (2007).

Installation of sensors and cables in the previously prepared blocks was performed after emplacement of each block, except for the bottom block C1, which was instrumented beforehand to facilitate its installation. Bentonite powder was used for backfilling the open spaces around the instrumentation.

Table 3-1. Average data for buffer blocks at installation, dimensions from Thorsager et al. (2002) and other parameters from Johannesson (2007).

Type	Dimensions (mm)	Density (kg/m^3)	Water content	Dry density (kg/m^3)	Void ratio
Cylinders	H=504[1]	1,991	0.172	1,699	0.636
Rings	H=510[1]	2,087	0.171	1,782	0.560
Bricks[2]	H=217/125[3]	1,883	0.165	1,616	0.720

[1]The average value of the data in Table 2-1 and an additional 3 mm representing interface volumes between blocks.

[2]Based on the total volume filled with bricks, pellets, and powder.

[3]The first value is reported in Thorsager et al. (2002) and the latter is obtained from subtracting the canister height from the height of 10 rings as described in the table. The difference could come from shape imperfections of the blocks and imperfect installation which leads to a total height larger than the theoretical.

3.2 Canister

The canister was in addition to the ordinary KBS-3V specification, equipped with heaters internally to simulate the thermal activity of the nuclear waste. An additional top-lid installed on the canister protected the heater power cables, adding 140 mm of additional height to the unmodified canister height dimension of 4,835 mm. The canister diameter, 1,050 mm, was unchanged. The empty space between the two canister top-lids, the reference dimension and the additional connector component, was backfilled using a mix of bentonite/sand in the proportions 30/70.

3.3 Pellets and water

Removal of the climate control system was undertaken before four tubes to be used for subsequent water filling of the outer (pellet filled) slot at installation were placed in the outer gap. After this the pellets were blown into the slot using specially design equipment. When the gap was filled to the brim of the hole, the four tubes were connected to a water supply and the gap was filled with water (estimated to be 950 l) (Thorsager et al. 2002). During the water filling the four tubes were subsequently withdrawn as not to get stuck in the swelling bentonite pellets. The pellets and subsequent water filling of the outer slot occurred on October 26, 2000 and is considered to be the start of the test.

The pellet-filled slot, in average 61 mm wide, had the initial average properties given in Table 3-2 obtained from Johannesson (2007).

Table 3-2. Data for pellet filled gap at installation, from Johannesson (2007).

Type	Width (mm)	Density (kg/m^3)	Water content	Dry density (kg/m^3)	Void ratio
Pellet slot (dry)	61	1,101	0.1	1,001	1.778
Pellet slot (wet[1])	61	1,574	0.572	1,001	1.778

[1]The state when the pore volume between the pellets has been water filled.

3.4 Retaining system

As described above in Section 2.2, the rock anchors were fixated at the rock and plug formwork were installed before the buffer installation. Each anchor consisted of a wire with inclination = 22°, free wire length = 5 m, and nominal anchor area = 19 strands · 98.7 mm^2. A rubber mat was emplaced on top of the buffer after the buffer installation.

The next step, taking place at the same day as the test start, October 26, 2000, was to cast the vertically mobile, conical, concrete plug in a stainless steel mould that was coated with mould release oil. This was followed by emplacement of the steel lid on top of the concrete and then attaching the rock anchors. Three of the rock anchors were activated, i.e. pre-tensioned to 20 kN, 5 days after test start. The remaining six anchors were activated and thereby all anchors equilibrated on days 46–48 after the test start, when the total anchor force exceeded 1,500 kN.

3.5 Instrumentation

Information about the instrumentation can be found in Sandén and Börgesson (2000), Thorsager et al. (2002), and Goudarzi et al. (2006). A listing of the instruments used in the CRT and a schematic overview of the buffer instrumentation is provided in Figure 3-2.

Rock mass

- Temperature was measured using Type K thermocouples from BICC.
- Strain was measured using Geokon 4200 vibrating wire strain gauges.
- Stresses in the horizontal plane were measured using vibrating wire Geokon 4350 embedded biaxial stressmeters.

Canister

- Temperature inside the canister was measured using PT-100 gauges.
- The canister surface temperature was measured using an optical system, fibre temperature laser radar, from BICC.
- Strain gauges were used for measuring strains on the inner surface of the upper half of the canister.

Retaining system

- Glötzl force transducers measured the force in 3 of the 9 rock anchors (no. 3, 6, and 9, indicated in Figure 3-1) in order to evaluate the vertical force acting on the plug.
- The vertical displacement of the plug was measured in three points (indicated in Figure 3-1) with differential transformer displacement transducers. The location of the points were:
  - no.1 between anchors 4 and 5
  - no.2 between anchors 7 and 8
  - no.3 between anchors 1 and 2

Buffer

- Temperature was measured using thermocouples from BICC. Temperature sensors were also available in: capacitive relative humidity sensors, vibrating wire pressure sensors, and psychrometers.
- Relative humidity/Suction was measured using two different sensors, Vaisala capacitive relative humidity sensor and Wescor PST-55 psychrometers.
- Pore pressure was measured using two different pore pressure cells, Geokon, with vibrating wire transducers, and Kulite, with piezo resistive transducers.
- Total pressure (stress in the direction of the sensor) was measured using two different total pressure sensors, Geokon, with vibrating wire transducers and Kulite, with piezo resistive transducers.

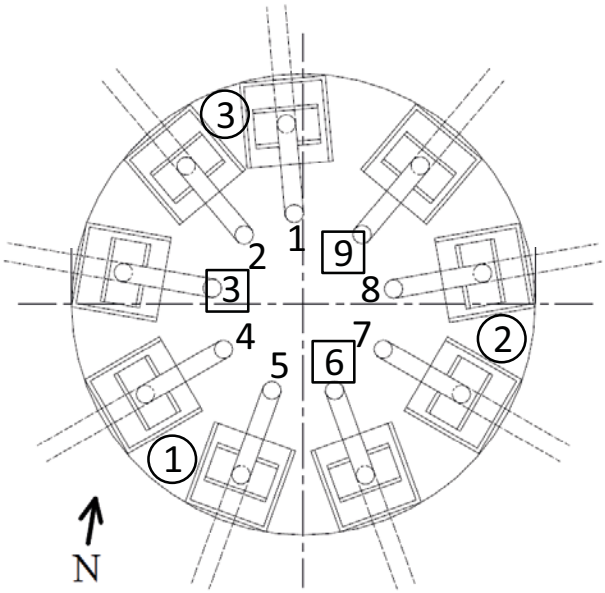

Figure 3-1. *Schematic overview of the instrumentation of the retaining system in CRT.*

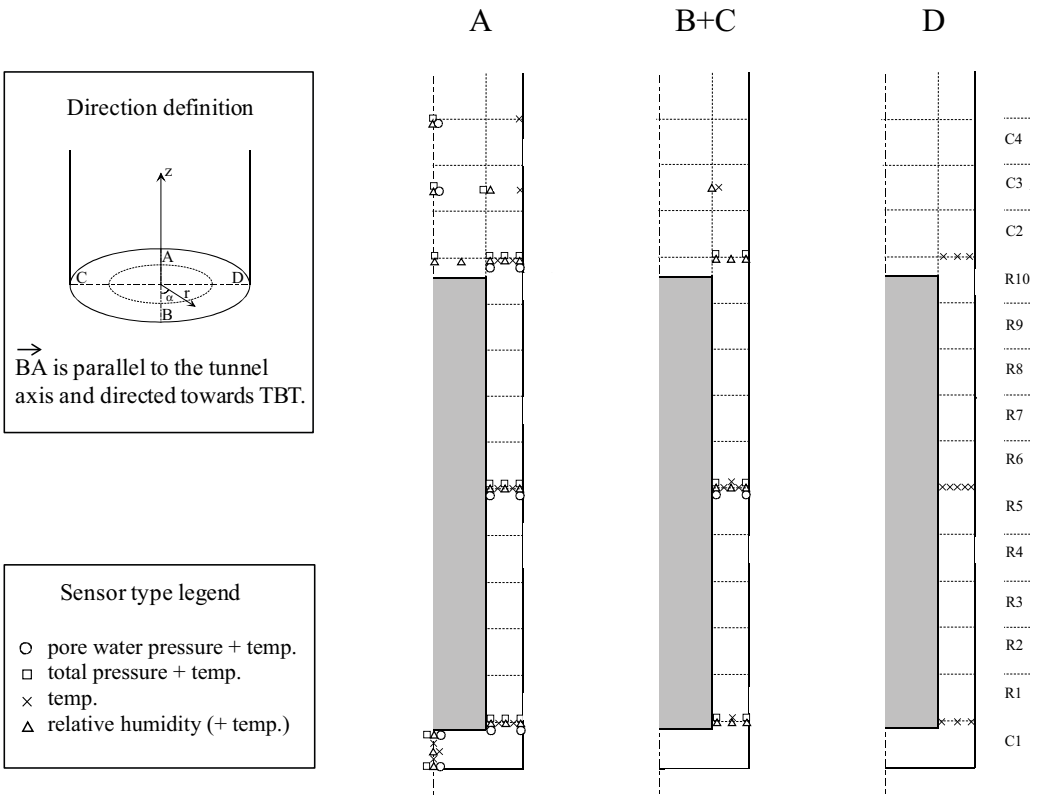

Figure 3-2. *Schematic overview of the buffer instrumentation in CRT.*

4 Operation

It should be noted that unless otherwise stated, the information given in this chapter was obtained from the sensor data reports provided twice yearly during experiment operation. The last report produced is Goudarzi et al. (2006).

The starting date of the operational phase was defined as 26-October-2000, when pellets and subsequently water were installed in the outer slot. One day later the canister heaters were turned on and the following heating stages are shown in Figure 4-1. Suitable heater power, with respect to maximum canister surface temperature had been estimated beforehand (Ageskog and Blix 2000). On 2-November-2000, the water supply tank having a 1 m water head, was connected to the filter system. The filter pressure history also shown in Figure 4-1 followed.

In the course of the CRT operation, some of the heaters malfunctioned and the total heater power available to the canister was successively reduced due to the failures. The response resulting from some of the failures is clearly visible in Figure 4-1. From a total of 36 initially operating heater units there were only 4 working heaters left in the canister when the power was turned off at the end of the test 11-October-2005 (indicated with the grey vertical line in Figure 4-1).

When dismantling the experiment, it was found out that the mechanically protective plastic shield of the power cables was severely damaged at the top of the canister. This damage together with the moist conditions most probably caused short circuits which led to the heater failures. The heaters themselves were tested and had full functionality when reconnected using new wiring. The investigation of the heater malfunction is described by Eng (2008).

4.1 Global THM-processes

4.1.1 Temperature

In Figure 4-2 temperatures on the deposition hole wall, at canister mid-height in the direction of, and the opposite to, the TBT experiment, are shown. Before the start of TBT on 27-March-2003, 2.5 years into the operation-phase of the CRT, the temperatures observed in the CRT showed axisymmetry. After this date the temperatures diverge from this pattern and attain different magnitudes due to asymmetric heat supply.

Measured maximum canister surface temperature is shown in Figure 4-3. The temperature is less or equal to 100 °C, as aimed for. The TBT can be seen to have had an influence since the local temperature rises somewhat after 2.5 years, despite constant canister power in CRT.

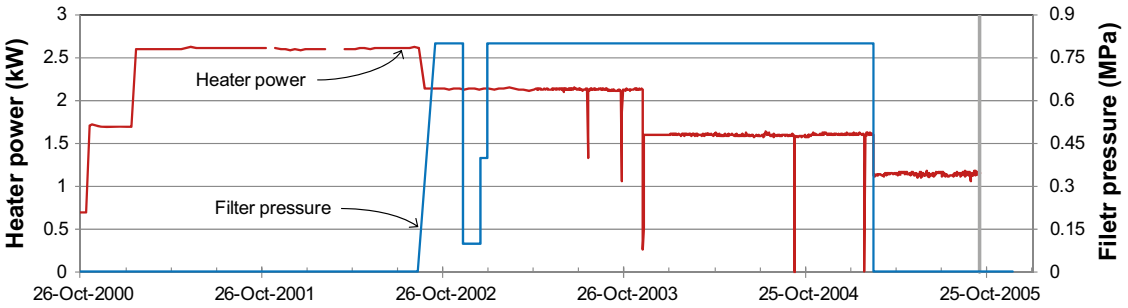

Figure 4-1. *Heater power (kW) and filter pressure (MPa) during the operational phase.*

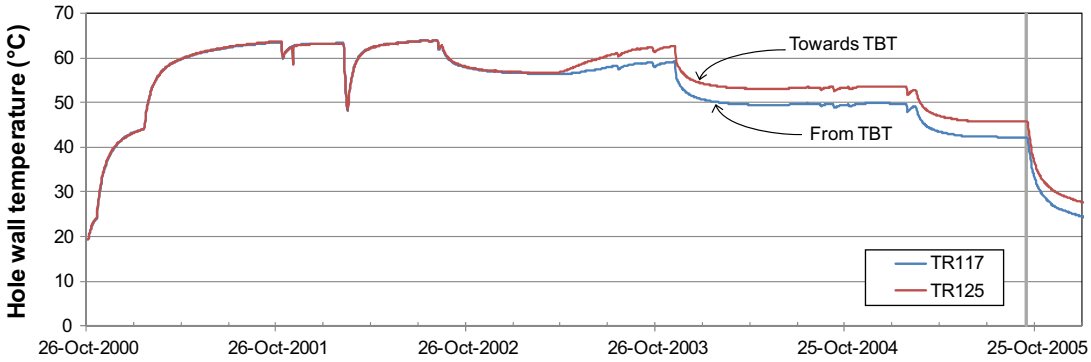

Figure 4-2. *Temperature at the deposition hole wall in direction from (TR117) and towards (TR125) TBT.*

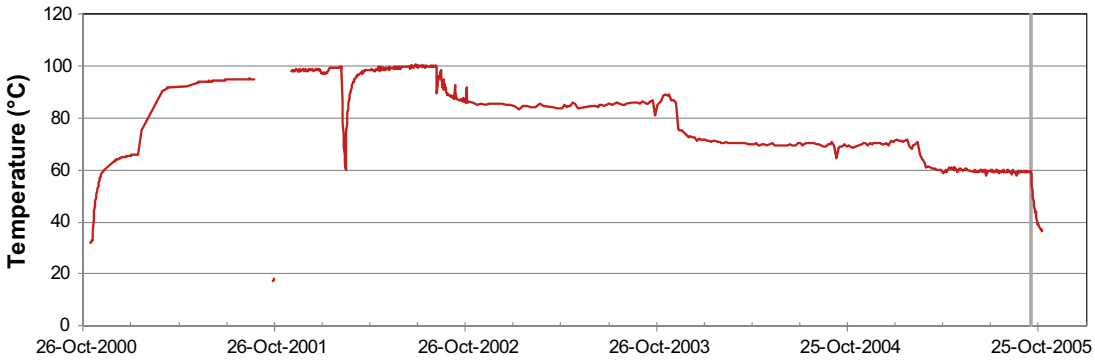

Figure 4-3. *Measured maximum canister surface temperature.*

4.1.2 Added water

Figure 4-4 shows the volume of artificially supplied water to the experiment. During CRT operation the accumulated filter inflow evolution was as shown in Figure 4-4 (reading the left-side y-axis). At installation, however, about 950 litres of water was added to the outer slot (Thorsager et al. 2002) and so, reading the right-side y-axis in Figure 4-4, the accumulated total volume of added water is given (approximately 1,620 litres at the end of test).

An effect from changing the filter water pressure, shown in Figure 4-1, is clearly visible in water inflow evolution given in Figure 4-4. When the filters were fed by atmospheric pressure only during the first two years of the operational-phase, the inflow rate decreased considerably with time. After pressurizing the filters the inflow rate increased significantly and when depressurizing at the end of the test, the inflow rate decreased significantly (but measurements still indicated a small inflow).

In order to analyse the decreasing inflow during the first two years, almost to standstill, the Abaqus simulation reported in Åkesson et al. (2010) and Börgesson et al. (2015) was utilized. The simulation was controlled by prescribing the filter pressure protocol given in Figure 4-1 at the deposition hole wall. In Figure 4-5 the measured water volume added through the filters is shown together with the simulated result.

As can be seen, the simulation does not agree well with the measured inflow evolution with predicted rate being much higher than that measured. The most probable explanation is that the supply of water into the filter mats was not sufficient to keep the filter mats water saturated due to clogging or air entrapment. Laboratory flow tests of the filter mats showed that the connectivity was rather poor for some mats unless sufficient water pressure was applied. Hence, as seen in Figure 4-5, when after 680 days the water pressure was increased to 800 kPa the filter mat flow resistance was overcome and the wetting of the bentonite could proceed.

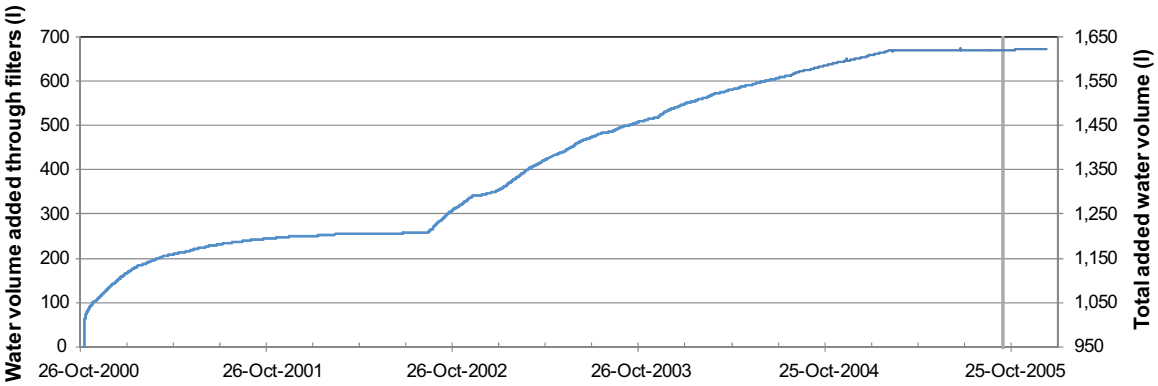

Figure 4-4. *Accumulative water volume added through filters (left scale) and accumulative total volume added water (right scale).*

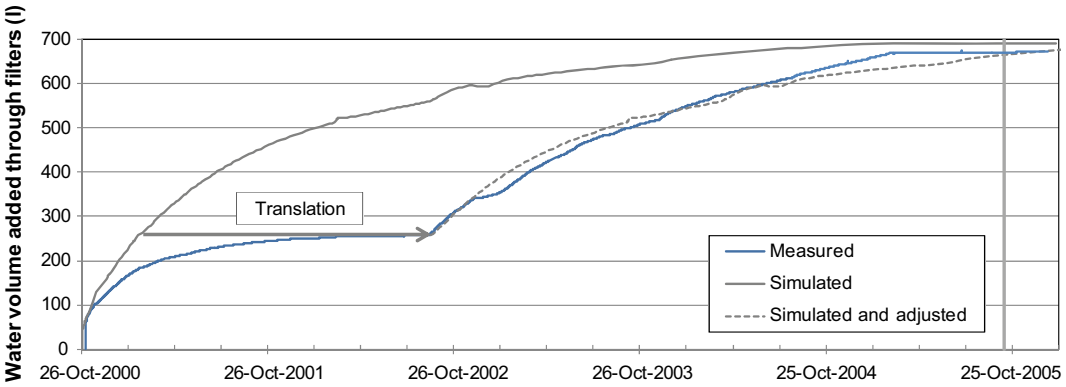

Figure 4-5. *Accumulative water volume added through filters: measured, simulated, and simulated and adjusted (transferred according to the arrow).*

The curve denoted *Simulated & adjusted* in Figure 4-5 was obtained by adjusting the output obtained from the simulation by simply shifting the curve as indicated by the translation-arrow. The translation was defined as starting when the simulated inflow was 260 litres and ending at the time when the water pressure was increased to 800 kPa. This response can be thought of as obtained by a model where the entire state of the model is ”frozen” after 260 litres of inflow and then ”released” at the time when the water pressure was increased to 800 kPa.

The agreement between the measured and adjusted (delayed) simulation data in Figure 4-5 strengthens the hypothesis that the filters could not provide the buffer with water when the filter water pressure was low and when it was substantially increased, water was one again available for absorption into the buffer.

The total volume of added water to the experiment is summarized in Table 4-1 and can be described as follows:

First, as a starting point, an estimate of the initial available pore volume can be obtained from using the information given in Table 3-1 and Table 3-2 together with the specified geometry, see Appendix A. This volume, also accounting for the empty 1 cm slot between canister and rings and a 36 mm heave of the plug (motivated from the data shown below in Figure 4-7), becomes 2,269 litres.

The measured total added water volume was, as mentioned before, 1,620 litres. The total added water volume can also be estimated as described in Appendix A using density and water content data from excavated buffer samples (See chapter 6.1 for details). This estimation concludes that 2104 litres was added in total. The difference of 484 litres between this estimate and the measured value of 1,620 litres is significant.

Table 4-1. Compilation of the volumes discussed in the text.

Description	Volume [litres]	Ratio [%]
Estimation of available pore volume at installation	2,269	100
Added water volume 1: Reported at pellet filling + Measured filter inflow	1,620	71
Added water volume 2: Calculated from excavation data	2,104	93
Added water volume 3: Calculated available ”macro pore volume” in pellet filling and volume of inner slot + Measured filter inflow	1,931	85

One possible reason for the 484 litre difference is that the water volume added to the pellet slot at installation might be more than the reported 950 litres, see Appendix A. If calculating the initially available ”macro-pore” volume, i.e. between pellets and between canister and buffer, a volume of 1,261 litres is obtained. Together with the measured water volume added through the filters, a total added water volume of 1,931 litres is given.

The added water volumes discussed above, given in Table 4-1, show that the water taken up by the bentonite as calculated from the excavation data is slightly higher than or in fair agreement with the estimates obtained from the inflow measurements. The degree of agreement depends on if the water filling at installation is taken as the reported volume or as the calculated available ”macro-pore” volume is used.

This shows that it is not probable that any water has been lost to the rock in spite of the water pressure applied to the mats. Alternatively, the lack of available water during the first 680 days (before the water pressure increase), shows that it is not likely that there is any water inflow from the rock. The rock thus seems to be very tight which is confirmed by the inflow measurements of the test hole before installation when no inflow could be measured. Also, the filter mats were fastened to a cement smoothing component that was applied on the rock wall, which further hindered water exchange between the rock and the filters.

4.1.3 Force on plug and plug displacement

In Figure 4-6 the measured forces in three of the anchors (no. 3, 6, and 9) and the corresponding vertical force on the plug calculated by considering the 22° inclination of the anchors and the number of anchors in operation, three from Day 5 to Day 46 and nine thereafter. Note the different multiplication factors for anchor force (1 kN) and vertical force on plug (10 kN) in Figure 4-6.

The appearances of the anchor force responses are as anticipated with a rapid increase at installation when only three anchors were in operation and a reduction to one third after the installation of all nine anchors. The measurements for different anchors are also consistent when comparing them; no large deviations can be seen either qualitatively or quantitatively. The vertical force acting on the plug ends up at approximately 8 MN, which translates to an average pressure of 3.3 MPa when acting on a circular surface with diameter equal to the deposition hole (1.76 m).

In Figure 4-7 the estimated total vertical displacements of the plug are given, 13 mm free swelling before installation of the rock anchors (Thorsager et al. 2002) together with the measurements of the three transducers installed at the top of the plug during constrained conditions. Also, a curve designed to be representative to the real vertical displacement of the plug is given in Figure 4-7. The reasoning behind this designed displacement curve is given below.

When studying the measured displacements it can be seen that they differ quite a lot in the initial phase when the filters were not pressurized. After pressurizing the filters transducers 1 and 3 seemed to be malfunctioning based on their erratic readings. Transducer 2, however, seems to give a consistent, smoothly increasing set of values after the pressurization of the filters. The question of what a representative response during the initial stages should appear remains and is unclear. Could any of the three transducers be considered representative in this phase?

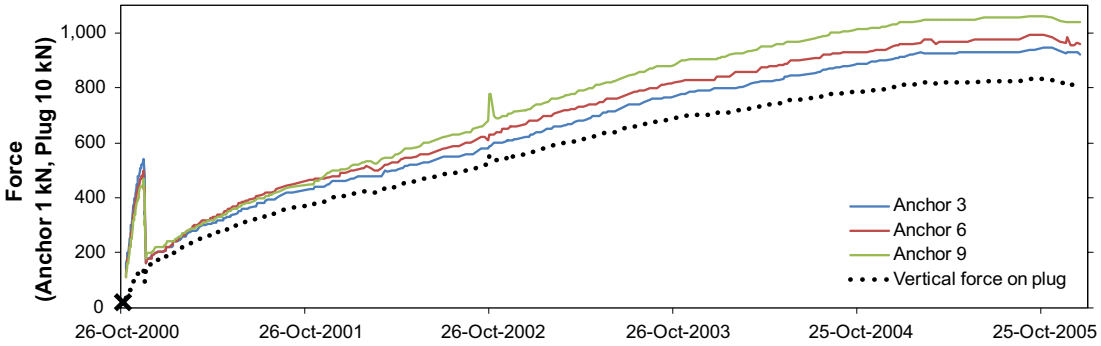

Figure 4-6. *Measured force in three of the anchors (1 kN) and estimated vertical force on the plug (10 kN).*

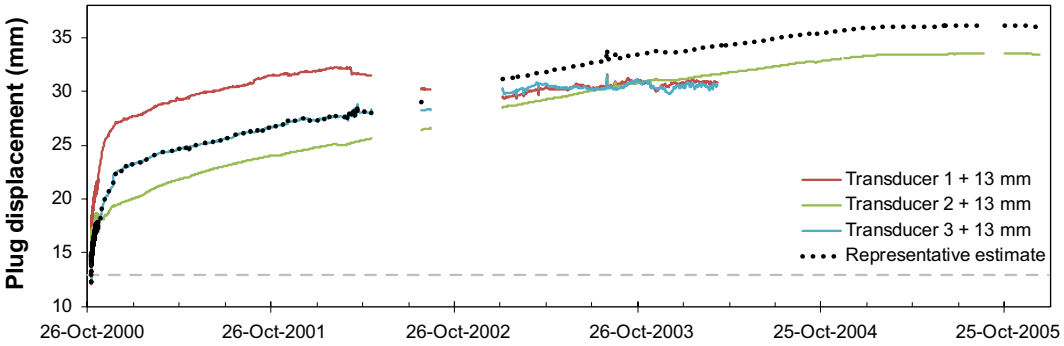

Figure 4-7. *Measured vertical displacements with 13 mm additional free swelling and a representative estimate of total vertical plug displacement.*

To begin assessment of the sensor outputs, a quick check of the correlation between the force and displacement measurements in Figure 4-6 and Figure 4-7, respectively, were undertaken. The Young's modulus for the wires is calculated from the force – displacement data over the interval December 27th 2000 to June 15th 2005, together with using the known geometry (wire inclination = 22°, free wire length = 5 m, and nominal anchor area = 19 strands · 98.7 mm^2). A value of 164 GPa is obtained from this assessment. In the manufacturer data sheets for the wire, Young's modulus is specified as approximately 197 GPa. This indicates that the correlation between the force and displacement measurements is appropriate.

To evaluate a representative initial plug displacement evolution under confined conditions when three rock anchors were in operation, a plug displacement was calculated. This is shown to the right in Figure 4-8 and is calculated from the measured anchor force evolution (shown to the left in Figure 4-8) together with the Young's modulus (determined to 164 GPa) and the known geometry.

In studying the anchor forces in Figure 4-8, it can be seen that they are relatively smooth and consistent. The black cross in Figure 4-8 indicates the initial force of 20 kN at October 31th 2000, which stems from the pre-straining. The curves may be back-extrapolated to this point. December 12th – 14th 2000 all nine anchors were taken into operation by equilibrating the total force of 1,500 kN between them. This can be seen as the kink in the curves at this time.

Comparing the calculated displacement curve with the measurements in Figure 4-8 shows that transducer 3 agrees well with the calculated curve. Transducer 1 and transducer 2 produce too large and small displacements as compared to what is expected from the measured forces, respectively. The measurements of transducer 3 may also be back extrapolated as to match the very small change in displacement stemming from the initial pre-straining.

The evaluation of the plug displacement measurements indicates that the data obtained from transducer 3 should be considered representative from the start until about May 14th 2002 and thereafter 2.6 mm should be added to the data obtained from transducer 2 in order to match the transducer 3 data and obtain a representative plug displacement consistent with the anchor force measurements. The resulting curve is shown in Figure 4-7 with the maximum displacement 36 mm of which 23 mm was generated during restrained conditions.

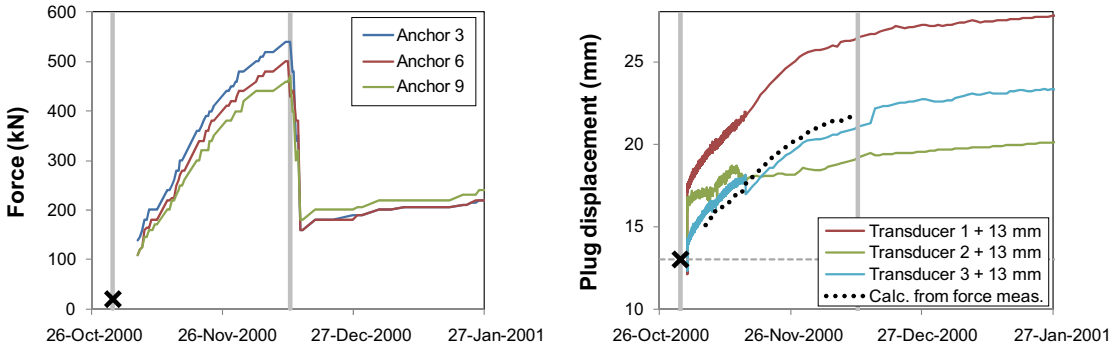

Figure 4-8. *Mechanical processes of the plug for the initial operational phase. (Left) Measured anchor forces and initial force, 20 kN. (Right) Measured vertical displacements with 13 mm additional free swelling, calculated initial and total vertical plug displacement obtained from using the force measurements and Young's modulus of the anchors. The left and right vertical grey lines indicate the time when three and nine rock anchors where taken into operation, respectively.*

To further evaluate the plug force and heave described above, an Abaqus simulation reported in Åkesson et al. (2010) and Börgesson et al. (2015) is utilized.

The simulated and measurement based estimate of the vertical force on the plug, shown in Figure 4-9, are first compared. The responses can be seen to agree reasonable well even though the simulation has a faster pick up in force which later on slows down relative to the measurement based estimate. Since the force is generated by the swelling of the buffer which in turn comes from water absorption, the simulation is, due to the initial fast water inflow discussed earlier, expected to generate this discrepancy as compared to measurements. With this in mind the relation between the responses is considered to be explainable which strengthens the confidence for both measurements and simulation.

Next, as shown in Figure 4-10, the representative measurement-based estimate and simulated plug displacement of +13 mm is shown together with a "post calculated" response from the simulation +13 mm. This 13 mm was the reported heave prior to the attachment of the anchors to the plug and this was not included in the model.

If comparing the plain simulation response with the measurement-based estimate, it can be seen that the simulation underestimates the plug heave and also gives rise to a significant initial compression (≈ 4 mm) of the buffer.

The *Post calculated simulation* response was obtained from using the plug force evolution obtained from the simulation and a representative elastic modulus of the retaining system. In the model a 200 mm thick disc above the steel lid was used to represent the retaining system. The disc was equipped with a varying elastic modulus, 13.1 MPa when three anchors were active and 39.4 MPa when all nine anchors were active. The obtained response agrees better with the measurement based estimate as compared to the plain simulation response. After the activation of all nine anchors the adjusted simulation response overestimates the displacement and has a decreasing trend that agrees with what was discussed earlier concerning the connection between the force and buffer water uptake.

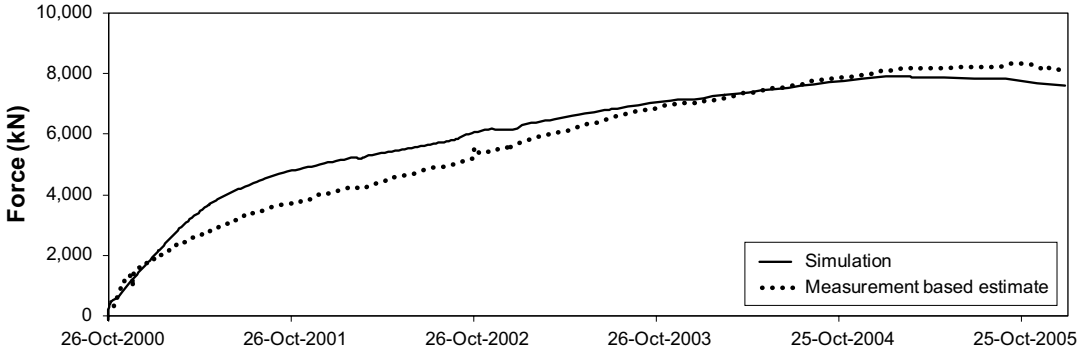

Figure 4-9. *Simulated and measurement based estimate of vertical force on the plug.*

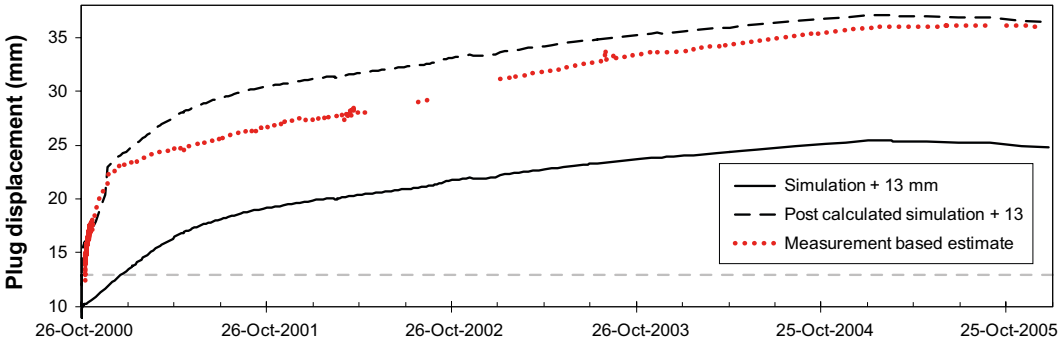

Figure 4-10. *Plain simulation response, post calculated simulation response and measurement based estimate of plug displacement. The horizontal grey hatched line indicate 13 mm plug displacement, the reported heave prior to the attachment of the rock anchors.*

4.1.4 An analysis of upward swelling based on excavation data

The axial displacement of the buffer can be estimated by using the relationship between initial and final dry density. When performing the estimation three assumptions are made; the solid mass is constant within a considered control volume (buffer section), this volume has a constant thickness also at the final state, and excavation samples taken at a given radius are representative for that radius in the block. The obtained vertical swelling of the buffer sections are given in Table 4-2, where also initial and final dry densities are shown.

The data as well as the graph in Table 4-2 indicate that swelling has occurred from block R9 and upwards. A total swelling of 51 mm is obtained which is 15 mm in excess of the 36 mm which is considered to be representative when evaluating sensor data. One reason for the discrepancy, besides uncertainties concerning measurements and numerical integration, could be that open gaps between blocks have not been considered when calculating the initial dry density and this might therefore be somewhat overestimated. The qualitative trend of the buffer swelling is however considered to be properly represented.

Table 4-2. Average dry density at installation and at dismantling in different sections of the buffer together with the calculated vertical swelling of the sections. To the right accumulated calculated vertical swelling of the buffer sections is show.

Block No	Average dry density at installation. [kg/m^3]	Average dry density at dismantling [kg/m^3]	Calculated vertical swelling of buffer section [mm]
C4	1,606	1,552	17.3
C3	1,606	1,583	7.0
C2	1,606	1,560	14.7
R10[1]	1,617	1,576	3.2
R10[2]	1,583	1,551	7.9
R9	1,583	1,570	4.1
R8	1,583	1,586	–1.0
R7	1,583	1,586	–1.2
R6	1,583	1,585	–0.8
Σ			**51.2**

[1] Above the canister top.
[2] Underneath the canister top.

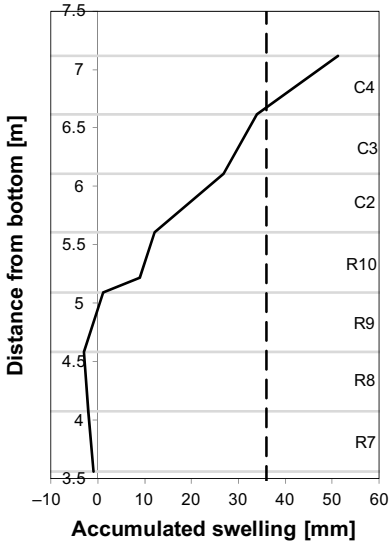

4.2 THM-processes in the buffer

The responses of sensors in the buffer are shown for positions at the top, mid, and bottom of the canister. The chosen sensors all belong to the A-direction as defined in Figure 3-2, in order to provide a simple overview of the processes taking place in the buffer during operation. The A-direction, see Figure 3-2, is towards the TBT and has been chosen since this was most heavily instrumented direction. In the charts provided as Figure 4-11, Figure 4-12, Figure 4-13, and Figure 4-14, the bracketed number after the sensor ID is the radial distance of the sensor from the borehole centre-line in mm as defined in Figure 3-2. The plotted data were recorded by the sensors identified in Table 4-3.

In connection to the description of the processes within the buffer (as perceived when studying the sensor data shown in Figure 4-11 through Figure 4-14), it is useful to also evaluate/discuss the sensor responses and issues associated with them that might relate to monitoring of the processes.

In the recorded buffer temperatures of the CRT shown in Figure 4-11 the effect of starting the nearby TBT can be seen at approximately 2.5 years (i.e. in between 26-Oct-2002 and 26-Oct-2003) in the form of an increasing temperature trend despite a constant heat load in CRT and previously stable temperature condition (from 26-Oct-2002). When comparing the data for sensors at the same radial distances (635 mm or 735 mm) it is found that the mid-height (R5) temperatures were, as expected, the highest. Then follow the bottom (C1) temperatures and last the top (R10) temperatures. Figure 4-11 also shows the temperature decay associated with loss of heater elements in the CRT beginning in mid-2002, leading to the end of the CRT in October 2005.

Suction

The different sensor types have different ranges of validity and different accuracy within these ranges. As general rules, Vaisala capacitive relative humidity sensors, with RH as output, can be said to work well for RH<95%. The Wescor psychrometers on the other hand, with their suction readings as output, work well for RH>95% (or below 5 MPa in suction). Hence, the data obtained from the capacitive relative humidity sensors (Vaisala) should probably not be given too much credibility at suction below about 20 MPa due to their limited accuracy in that range. In Figure 4-12 RH data has been transformed to suction and the output variable of the sensors, RH or S for suction, are indicated after the sensor ID and radial position.

In order to be able to accurately evaluate the water saturation process the RH and corresponding suction were determined for Äspö water, 99.5–99.7% and 0.40–0.68 MPa at 20°C respectively, see Appendix B. These relationships were then used in evaluating the sensor outputs.

The two innermost sensors, W134 and W135, for the top position in R10 show a significant magnitude of drying during the first year of CRT operation after which wetting takes place at a slow pace. An initial wetting-drying-wetting sequence occurred at r = 585 mm; this pattern was rather modest for the W136 sensor at the top, and more pronounced for the W119 sensor at mid-height. There is no indication of initial drying at the bottom of the borehole, but the wetting process seems to have been slower as compared to mid-height. The data at the end of the test indicate that the buffer was saturated except for the innermost part of the top-section, which means that the W138-data cannot be taken as quantitative.

Pore water pressure

Common for all three vertical positions was that the pore water pressures increased rapidly in connection with increase in filter pressure after approximately two years (Sept 2002) (qualitatively indicated at the top of each chart). Also, when the filter pressure was decreased in the 2nd quarter of the 5th year (end of 2004), the pore water pressure decreased rapidly. This reduction probably also came from decreasing the canister power (qualitatively indicated at the top of each chart) at this time. During operation, changes in canister power can be seen to correlate well with subsequent changes in pore water pressure.

Table 4-3. Sensors used for the overview of the processes in the buffer.

Variable	Position	Block	Sensor ID							
Temperature	Top	R10	T124	T125						
	Mid	R5	T111	T112						
	Bottom	C1	T104	T105						
RH/Suction[1]	Top	R10	W134	W135	W136	W137	W138	W139	W140	W141
	Mid	R5	W119	W120	W121			W122	W123	W124
	Bottom	C1	W104	W105	W106			W107	W108	W109
Pore pressure	Top	C3	U113							
		R10	U112	U211						
	Mid	R5	U105							
	Bottom	C1	U103	U104						
Vertical stress[2]	Top	R10	P118	P119	P120					
	Mid	R5	P110	P111	P112					
	Bottom	C1	P103	P105						

[1] Vaisala with RH as output / Wescor with suction as output. Wescor sensor IDs are underlined.
[2] Geokon only.

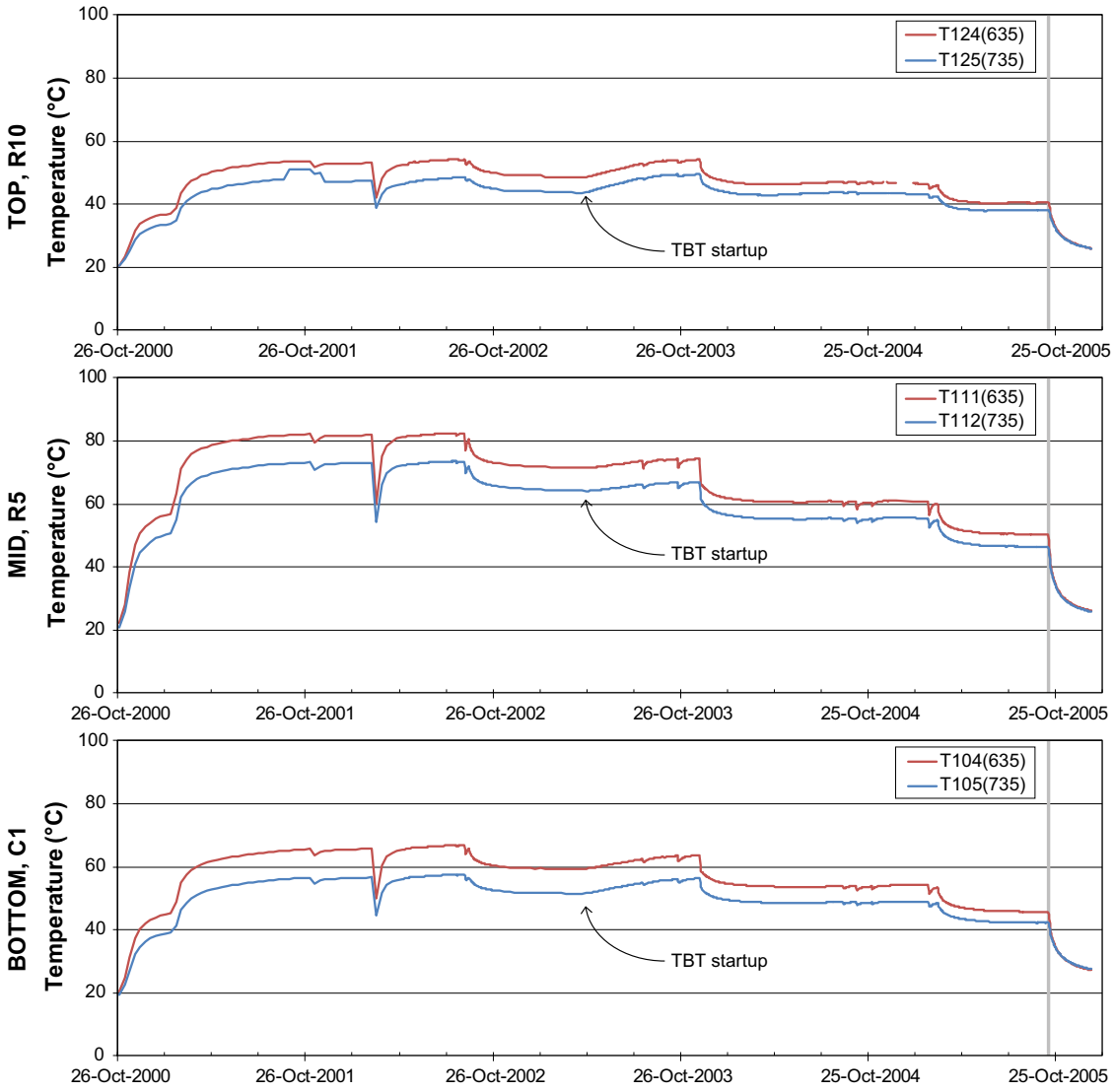

Figure 4-11. *Examples of recorded buffer temperatures.*

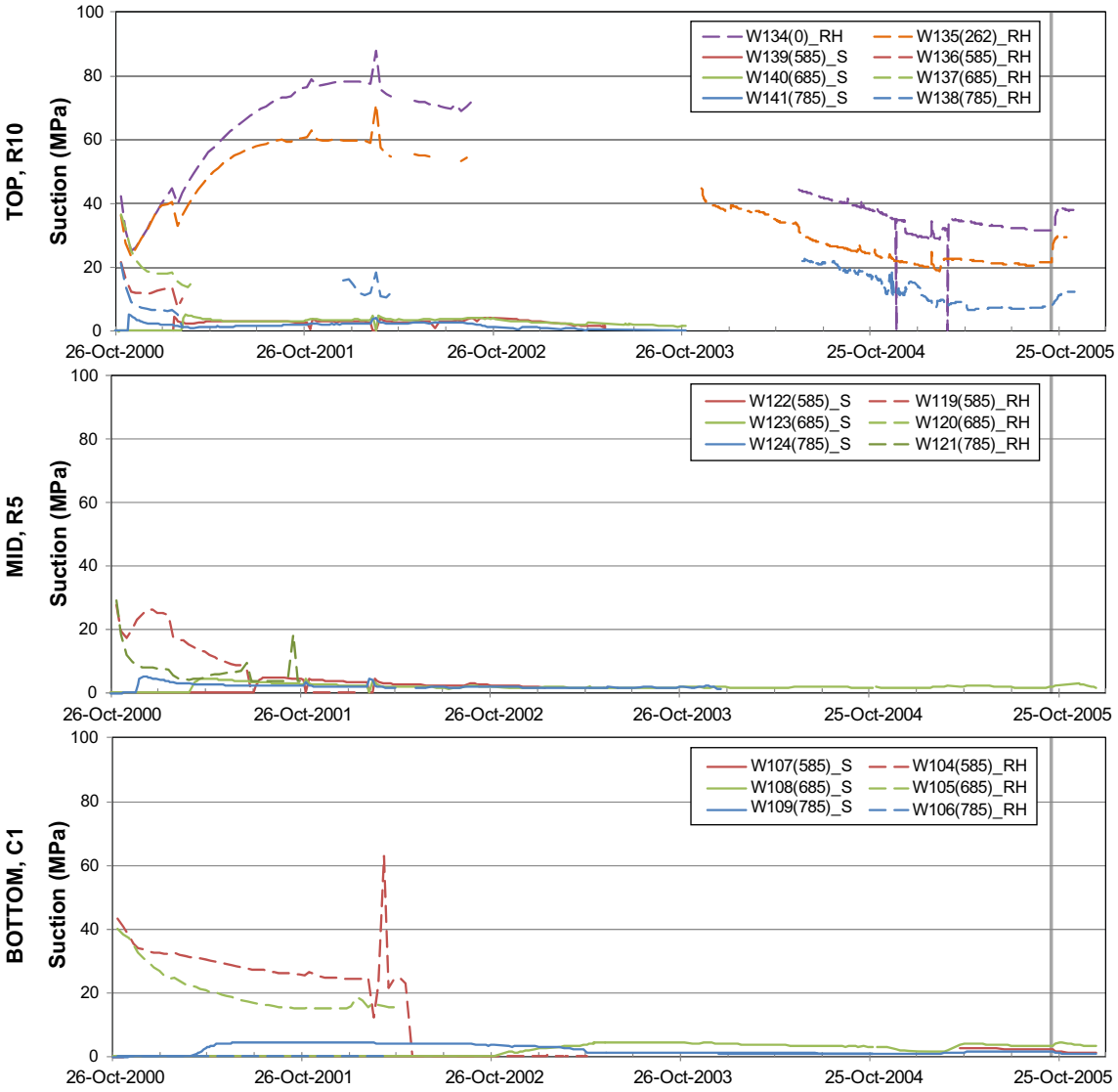

Figure 4-12. *Examples of recorded suction in the buffer.*

The sensor graphs in the upper chart in Figure 4-13 indicate that the outer part of R10 was more saturated as compared to the inner part of R10 and C3 since U112 located at the radius 785 mm gave positive pore water pressure after pressurizing the filters but the other ones did not react. At the middle chart of this figure the data show that significant pore water pressure has developed in the inner part (r = 585 mm) of R5 indicating saturated conditions. The bottom-most chart shows that for the bottom block (C1) significant pore water pressure is present at the outermost position, at 785 mm (U104), but only marginally so for the inner position, at 585 mm (U103). The temporary shutdown of the heaters in the 1st quarter of the 4th year (late 2003) can be seen to have a substantial and long-lasting effect on the response of U105 and U104.

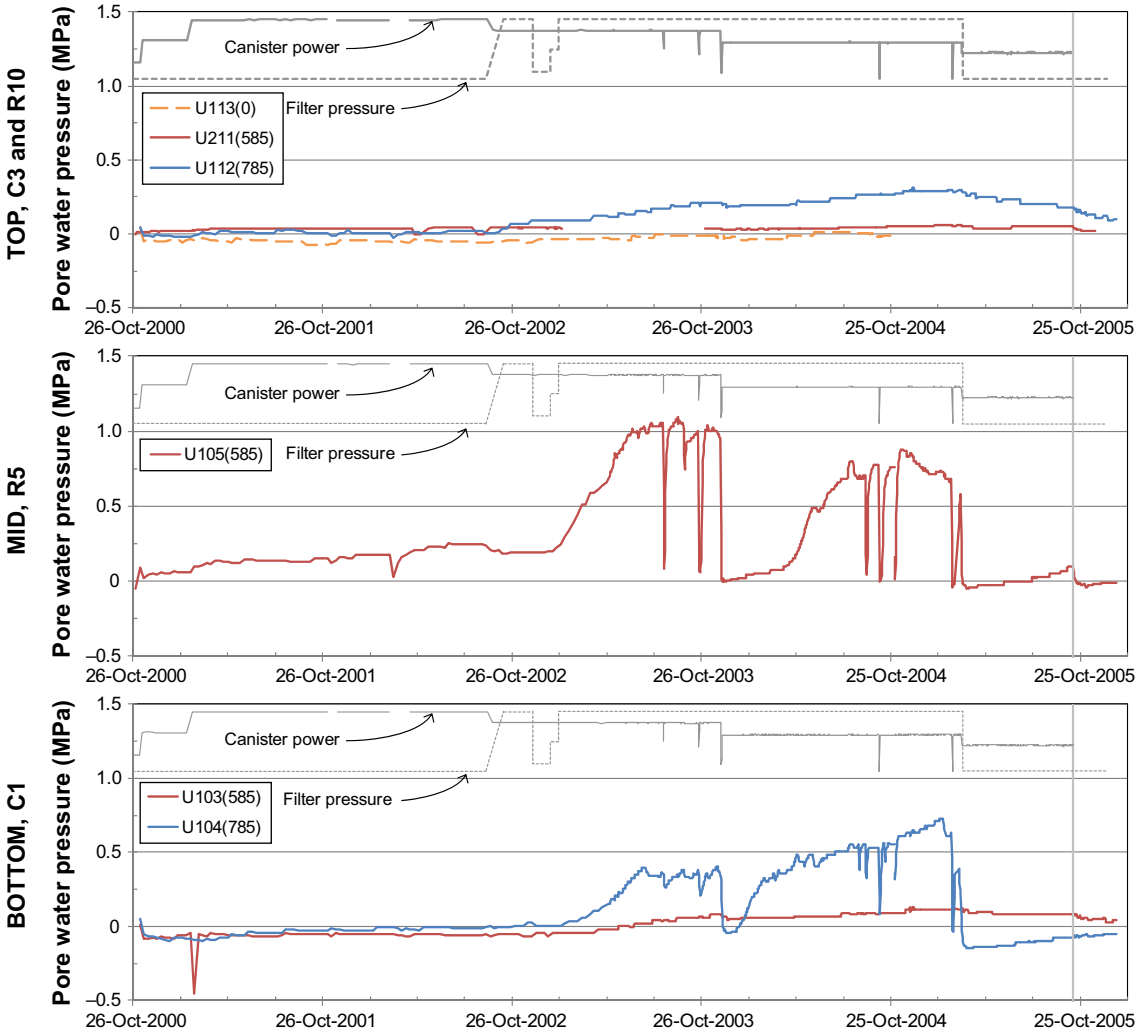

Figure 4-13. *Examples of recorded pore water pressures in the buffer. The canister power and filter pressure are included without scale.*

Vertical stress

As well as for the pore water pressure, the rate of the vertical stress development increased when the filter pressure (qualitatively indicated at the top of each chart) was increased in the 4st quarter of the 2st year of operation (late 2002). This is most pronounced for the top responses. Also, in accordance with the pore water pressure, events regarding the canister power (qualitatively indicated at the top of each chart) had a significant effect on the measurements of vertical stresses.

The canister power and filter pressure are included in Figure 4-14 without scale for the purposes of comparing response to power changes. For comparison, the retaining system's response in terms of average plug pressure is also given in Figure 4-14. The monitored locations close to the plug should show responses that resemble the average plug pressure, both in character and magnitude. With increasing distance from the plug, larger magnitudes of vertical stress could be expected due to the effect of friction against the rock wall, change in geometry by the canister, etc. Local variations of the magnitude of each of these effects would be expected.

When comparing the vertical stress responses with the average plug pressure, the stresses are often found to be less then, or roughly equal to, the plug pressure (excepting for P105 at the bottom). Also, when comparing the rapid initial increase in plug pressure with the evolution of the stresses, only P105 and P118 (which after approximately 3 months had decreased again) show the same character.

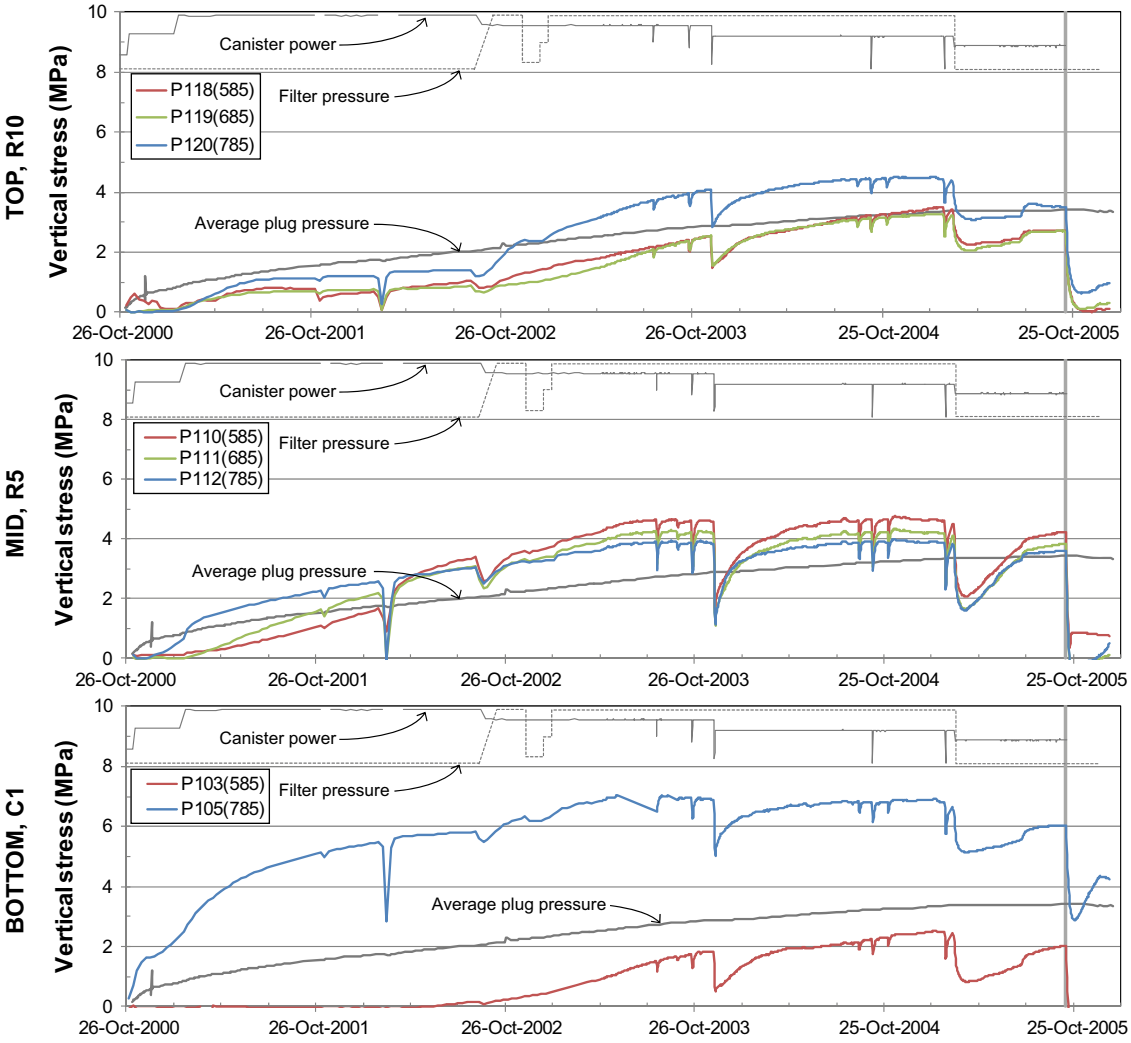

Figure 4-14. *Examples of recorded vertical stress in the buffer and average vertical pressure on the plug.*

To obtain an estimation of the magnitudes of expected vertical stress at canister mid-height (block R5), data obtained from two reports in the project can be used. Johannesson (2007) estimated the average density of block R6 and R7 to be 1,575 kg/m^3 and Dueck et al. (2011b) found that samples, with dry densities in the range 1,560 to 1,590 kg/m^3, taken from R7, showed a swelling pressure at full saturation ranging from 6.3 to 9.3 MPa, see Figure 4-15.

If this range (6.3–9.3 MPa) is compared to what the sensors recorded (about 3–5 MPa), it is found that the total pressure measurements in the CRT are lower than expected. Thus, the CRT sensor measurements are approximately 0.3–0.8 of the determined swelling pressure of the sampled buffer.

All vertical stresses given in Figure 4-14 were obtained by Geokon sensors which were retested after dismantling. The testing showed that with the exception of P210, the sensors were reading about 2–4% lower than initially set values, see Appendix D. Thus, the discrepancy between the measurements and the estimated range in typical swelling pressures (6.3–9.3 MPa) is not likely to come from changes in the calibration values of the sensors.

Geokon sensors have a cigar-shape, see Figure 4-16, with relatively a small end-surface area to monitor pressure. In the CRT puck-shaped Kulite pressure sensors with a larger pressure-area were also installed, but these produced unreliable data, probably due to weak sensor cable connections which were not able to withstand the pressures in the buffer. The geometry of the Geokon sensors, with their small sensing surface area could also make them rather sensitive to local variations in buffer properties around the sensors.

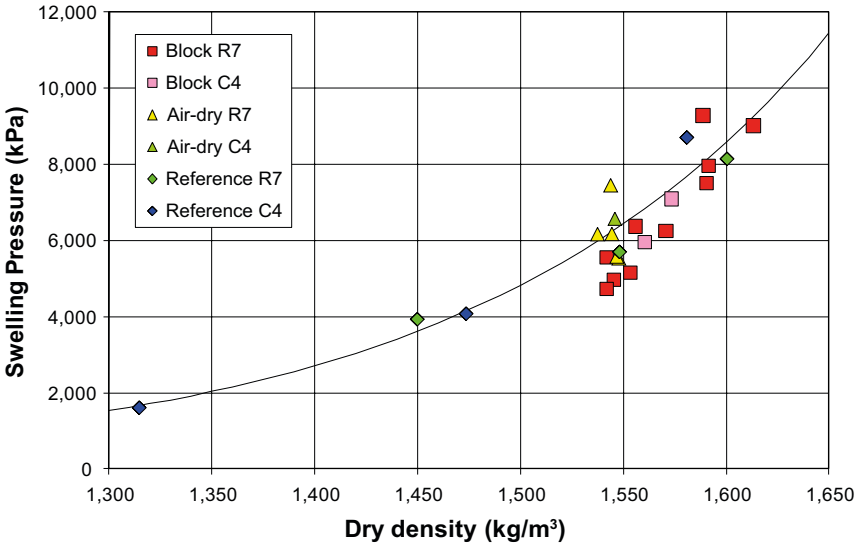

Figure 4-15. *Swelling pressure vs dry density for recovered CRT buffer samples and reference material.*

Figure 4-16. *Geokon pressure sensor.*

To investigate the local conditions at the sensor tips, profiles of dry density in the direction of the sensor axis have been determined for three sensor positions (P113, P115, and P116) in block R5. In Figure 4-17 these profiles are shown, normalized with regard to the value obtained at the outer-most position, which is considered most representative for undisturbed buffer conditions.

For all three sensors a clear decrease in dry density can be seen with decreasing distance from the sensor tip. The dry density at the sensor tip is approximately 0.95–0.97 of the dry density measured farthest (50–100 mm) from the sensor tip. With the undisturbed dry density taken as 1,575 kg/m^3, an estimated dry density in the range 1,496–1,528 kg/m^3 is obtained at the sensor tip if the previous ratios are used. At these dry densities swelling pressures about 5 MPa are expected based on data in Figure 4-15. This indicates that local variation in the density around the sensor tip is a possible cause for the low levels of measured stress.

To investigate the "sensor installation effect" further, a laboratory study was undertaken as described in Appendix C. This showed that a sensor installed using the same installation technique as used in CRT measured stresses approximately 0.6 of the level of stress as recorded by a load cell measuring stresses for undisturbed material.

It should be noted that the laboratory study of the installation effect is very limited in terms of data volume, it was also performed on a slightly higher dry density material, and that more issues connected to the installation of the sensors might exist, which cannot be investigated with the used setup.

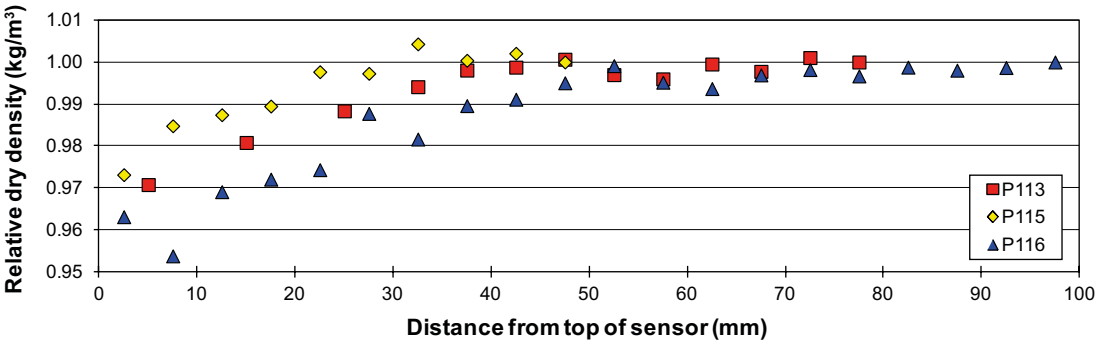

Figure 4-17. *Profile of relative dry density from the sensor tip and outwards.*

4.3 Sensor functionality

A listing of the sensors in CRT with short comments about their functionality is provided below. For the sensors in the buffer, the number of sensors working at the end of test and the number of sensors installed are indicated. Testing of recovered sensors is described in Appendix D.

Rock mass

- BICC type K thermocouples: OK
- Geokon 4200 vibrating wire strain gauges: Have not been evaluated, but this type of sensor did not work well in the subsequently installed Prototype Repository experiment.
- Geokon 4350 embedded biaxial stressmeter: Have not been evaluated, but this type of sensor did not work well in the subsequently installed Prototype Repository experiment.

Canister

- PT-100 gauges: All temperature sensors inside the canister were non-functioning in less than 3 years.
- BICC fibre temperature laser radar: Initially, 26-October-2000 to 1-May-2001, there were problems with the data collection system.
- Strain gauges: The strain measurements on the canister were not reported due to question marks regarding the quality of the data.

Retaining system

- Glötzl force transducers: OK
- Differential transformer displacement transducers: Transducer no. 3 is considered to have produced the most representative data until mid2002. Thereafter transducer no. 2 (added with a +2.6 mm offset) is considered to give the most representative response.

Buffer (Number of sensors working at end of test/Number of sensors installed)

- BICC thermocouples: (32/32)
- Relative humidity/Suction
  - Vaisala capacitive relative humidity sensor: Most finished to provide usable data due to high water saturation. Rather poor accuracy (7/25)
  - Wescor PST-55 psychrometers: (24/26)
- Pore pressure
  - Geokon vibrating wire transducers: (10/11)
  - Kulite piezo resistive transducers: (0/2)
- Total pressure (stress in the direction of the sensor)
  - Geokon, with vibrating wire transducers: (20/21)
  - Kulite piezo-resistive transducers: Produced unreliable data due to faulty cable connections (1/5)

5 Dismantling

It should be noted that unless otherwise noted the information regarding dismantling of the CRT given in this chapter was previously reported by Eng (2008).

The following quotation, taken from Goudarzi et al. (2006), provides a brief overview of the dismantling schedule:

"*The plug was dismounted 060116 (day 1908) and the excavation of the buffer started shortly after. The manual excavation and sampling was finished 060316. Testing of the heaters was done in April (days 1979–2002) by applying a power of 2,000 W. The retrieval of the canister with salt water flushing was done in May.*"

The dismantling phase was, for the purposes of the present report, taken to be started with the shut-down of the heaters 11-October-2005. After three months the measured buffer temperature at canister mid-height had decreased from above 50 °C to 26 °C. At that time the dismantling continued with removal of the restraining system (rock anchors, steel lid, and concrete plug) and rubber mat emplaced above the buffer.

By 18-January-2006, when the buffer was exposed, the sampling as described by Johannesson (2007), was begun. The majority of the buffer samples were obtained by core drilling with some taken manually. Cores were drilled as close as possible to predefined patterns, shown in Figure 5-1. The sampling was performed block by block, where the part of the block not being core-sampled was excavated manually before the next round of sampling of the next block was undertaken. When the canister top was revealed, the sampling was briefly interrupted as dismantling of the power cables occurred. The sampling, from the top (C4) down to canister mid-height (R6), was finished March 21, 2006.

The general finding during the sampling was that the buffer had experienced a homogenisation process and where fully water saturated, no open volumes could be found in the buffer. At the locations of the pellet filled slot, inner initially empty slot, powder back filled routed slots for cables, no open voids were found and the buffer had undergone a homogenisation process. The only location where it might have been open voids was in between the two canister lids at the very top of the canister where the buffer still was unsaturated.

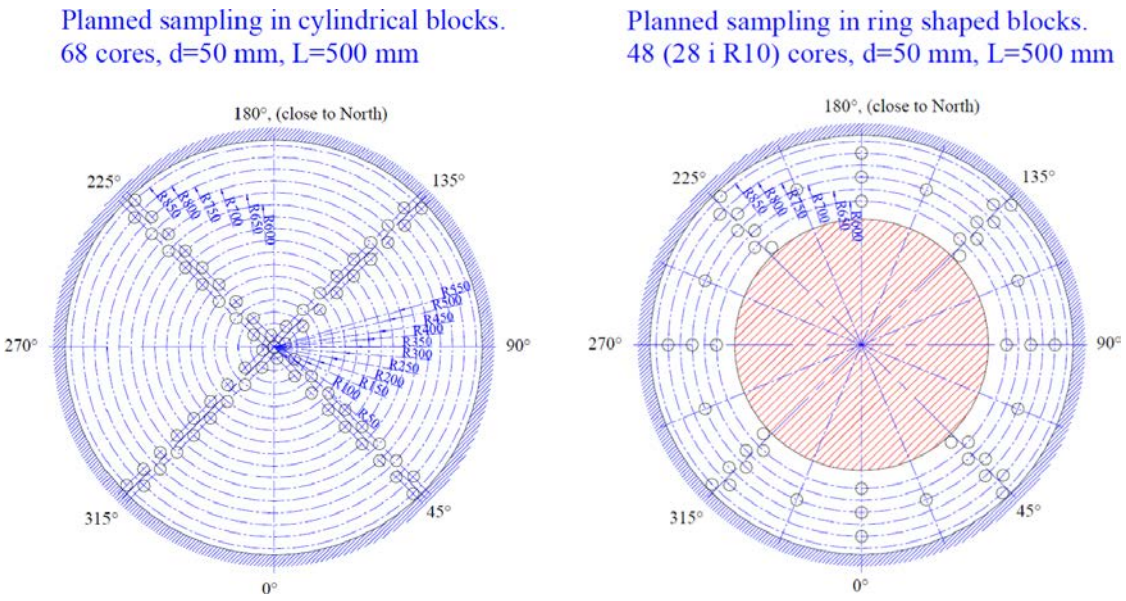

Figure 5-1. *Planned sampling pattern in cylinder-shaped buffer blocks (left) and ring-shaped buffer blocks (right).*

No trace of the initially open inner slot at the canister could be found. An interface was visible between the bentonite blocks and the pellet filled slot. At some locations a granular structure originating from the individual pellets could still be seen.

When taking samples of the buffer including the interface between blocks or between block and the pellet filled slot, the samples often broke at the interface. Thus, the interfaces were mechanically weaker as compared to the bulk materials. This property was in fact utilized during the sampling where the vertically core drilled samples broke at the block interfaces. When all core drilling had been performed for one block the remaining volume of the block could be removed manually down to the interface and the sampling of the next block could be started.

On completion of the mechanical sampling program the freeing of the canister from the buffer was started. The freeing process, performed by using the hydrodynamic/chemical technique (see Kalbantner and Sjöblom 2000), is described by Nirvin (2007) and Eng (2008). The technique uses a dilute calcium cloride solution which is flushed on the upper surface of the buffer under turbulent flow conditions. This disaggregates the compacted buffer into a slurry that can be pumped away from the deposition hole.

A schematic illustration of the freeing equipment/process is given in Figure 5-2. Part A corresponds to the deposition hole with a given volume of salt solution above the bentonite buffer and with the slurrying equipment in the working position. Part B corresponds to a decanter which separates bentonite and generates a clarified liquid that was recycled into the slurrying process. Part C corresponds to a blending vessel for preparation of salt solution and checking of the clarified liquid.

In Figure 5-3 the slurrying process and equipment used are schematically described in more detail. Salt solution from the blending vessel enters the deposition hole opening and frees buffer material chemically. Mixers and pumps connected to a suction nozzle provide a hydrodynamic freeing process and one of the three pumps is used to remove the slurry from the deposition hole to the decanter.

Figure 5-4 shows a drawing and a picture of the suction nozzle arrangement, with three mixture chambers, pumps, and mixers.

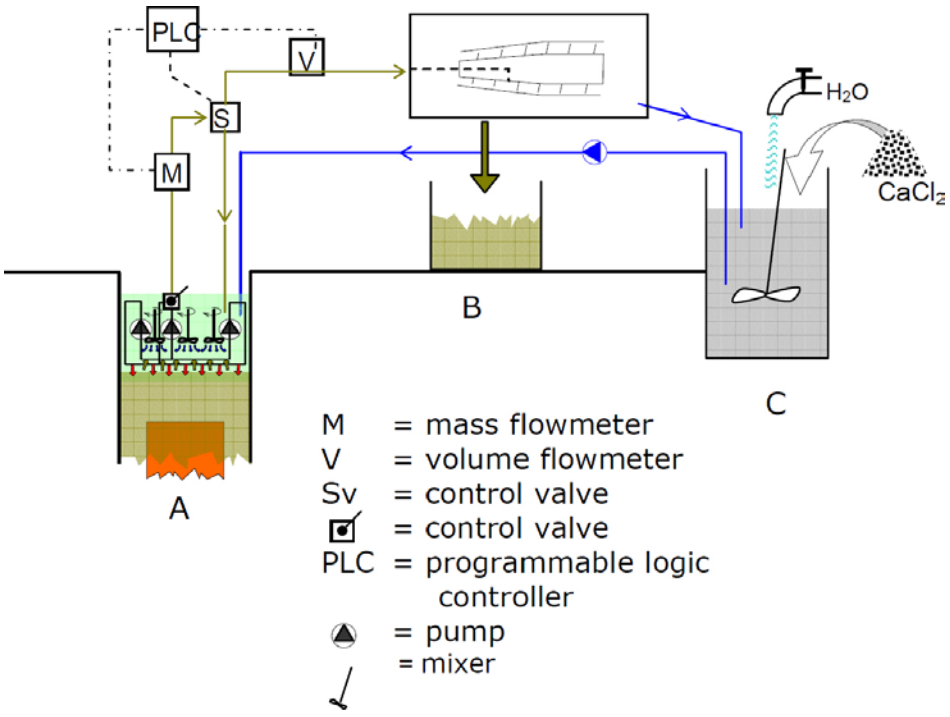

Figure 5-2. *Schematic illustration of the freeing equipment.*

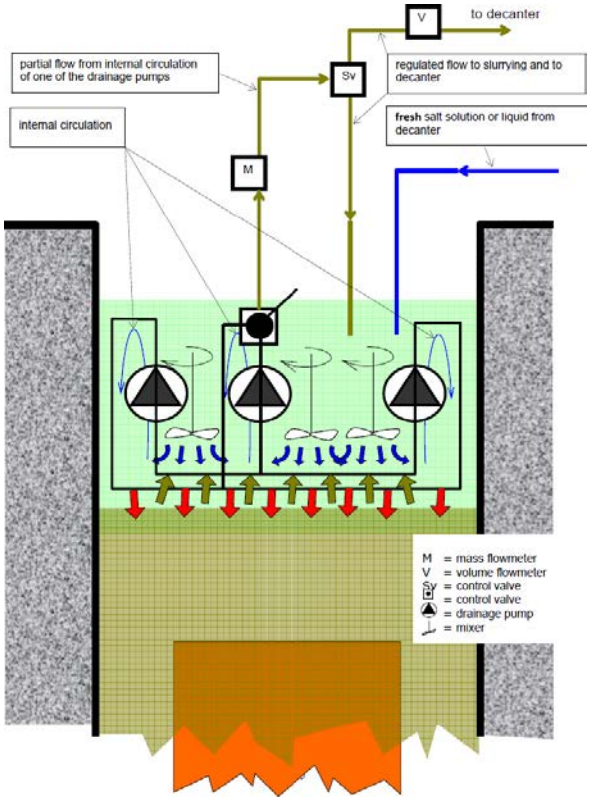

Figure 5-3. *Detailed schematic illustration of the slurrying equipment and process.*

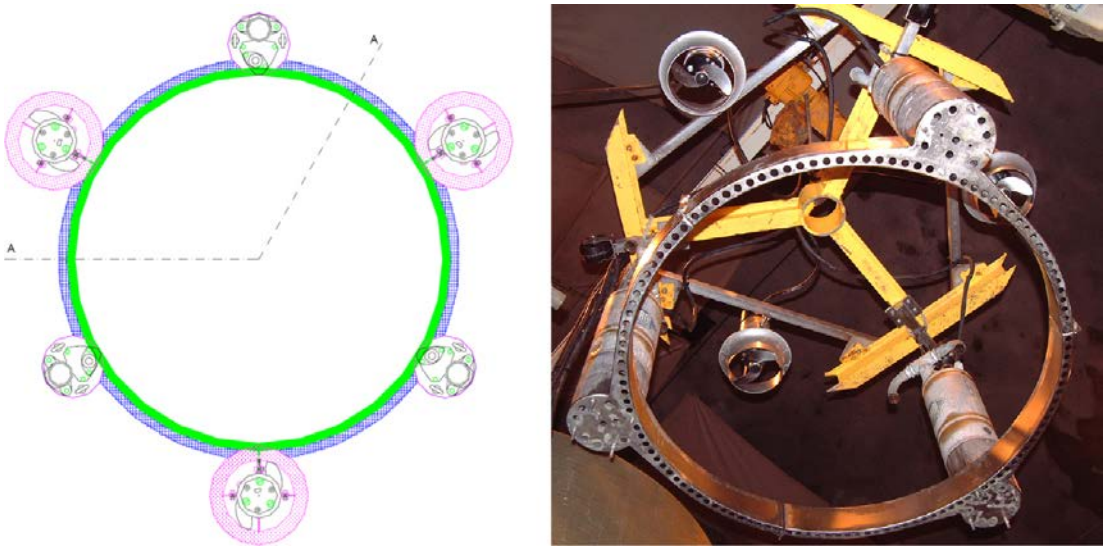

Figure 5-4. *Drawing and picture of the suction nozzle, mixture chambers and connected pumps, and mixers***.**

This freeing technique/equipment was used from canister mid-height (R5) until the bottom of the canister, resting on R1, could be seen. Figure 5-5 shows a picture taken during the recovery process. The tested freeing technique was disturbed by parts of the experimental setup which would not be present in a real repository. Pieces of filter mats, strings, gauge pipes, and tubing became stuck in the equipment. So it was concluded that the hydrodynamic/chemical technique *"... works very well for dissolution and removal of bentonite. However, a prerequisite for its efficiency is that it is used in an environment free of disruptive materials such as bits of tubing, rags, strings etc."* (Nirvin 2007). Due to the multiple interruptions the efficiency of the freeing process was hard to estimate with high statistical significance, but based on the longest continuous running period, an estimate of 180 hours was obtained for freeing a canister embedded according to KBS-3V design.

Figure 5-5. *The buffer disintegration system in operation. The canister is visible to the left.*

The retrieval of the canister was then performed without any problems using the same machine utilized when depositing the canister. The freeing of the buffer had not been entirely even around the perimeter of the canister. The height of the buffer around the canister-base therefore varied from 0 to 100 cm. This did, however, not give rise to any problems during the retrieval.

Due to the extensive instrumentation in the buffer remaining below the canister (block C1), manual removal was preferred in this part.

The final aspect discussed in the present report on the dismantling phase relates to sampling of the host rock. A total of 12 rock samples were obtained from six sub-horizontal boreholes. The six boreholes were divided into three pairs, each pair at a different depth in the deposition hole. Within each of the pairs, one borehole was directed parallel to the major and the other parallel to the minor rock stress axis. These rock samples were analysed regarding heat-induced stress damage by comparison to properties of cores taken prior to the installation of the canister (Luo 2006).

6 Material analyses

Analyses of the material taken from the experiment started right after the sampling of the buffer (January 18, 2006) with determination of density and water content (Johannesson 2007). Buffer samples were further analysed with respect to microorganisms (Lydmark and Pedersen 2011) and chemical-mineralogical and hydro-mechanical properties (Dueck et al. 2011a, b). The rock samples were analysed regarding thermally induced stress damage (Luo 2006).

6.1 State at dismantling, buffer density and water content

Density and water content of a geomaterial are basic properties important for characterizing its state. Therefore, these were determined after sampling the upper part of the buffer. The data were to be used for verification of models predicting the saturation and homogenization process of the buffer and also to support the following analyses with basic input.

Johannesson (2007) concluded that the obtained data "*... show that the buffer was far from saturated above the canister lid, while the buffer at the canister level was fully saturated. The data is also showing that the initial large variation in dry density for different part of the buffer has been reduced during the saturation although there are still noticeable differences in the density at the dismantling...*". Furthermore, it was concluded that for the analysed properties of the samples, "*Very small differences can be seen between the four directions*" (Johannesson 2007), which means that the spatial distribution of the analysed properties was close to axisymmetric.

The dry buffer volume above the canister and the fully saturated buffer at canister mid-height are clearly seen in the iso-maps shown in Figure 6-1. Also clearly visible are the small differences between the four directions, implying approximately but not perfect axisymmetrical conditions.

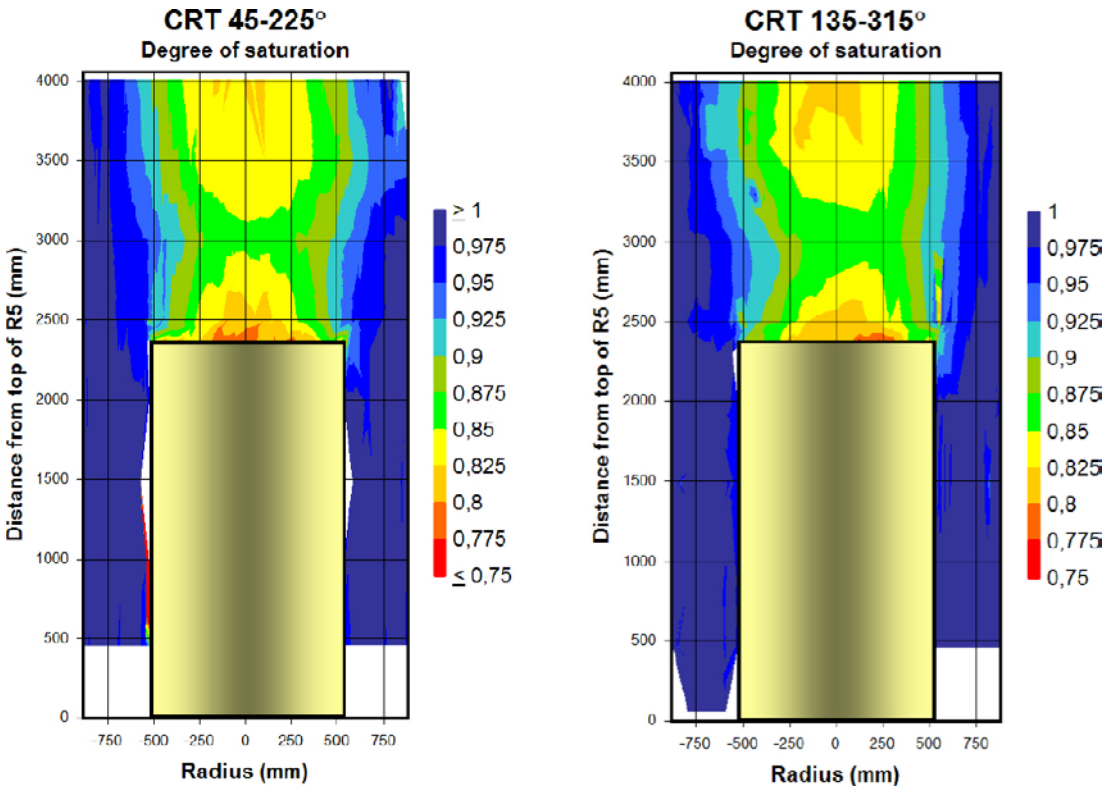

Figure 6-1. *Iso-maps of degree of saturation of the buffer samples in four directions.*

Also in the iso-maps over the dry density shown in Figure 6-2 the approximately axisymmetrical conditions are visible. The heterogeneity of the dry density of the buffer is obvious in the iso-maps. In the plot of the dry density profiles for ring R6 shown in Figure 6-3, the decreased heterogeneity from the initial state is clearly seen. The level of remaining heterogeneity of the buffer (in terms of dry density) when being fully water saturated may also be studied in detail from the dry density profiles in Figure 6-3, since block R6 was fully water saturated.

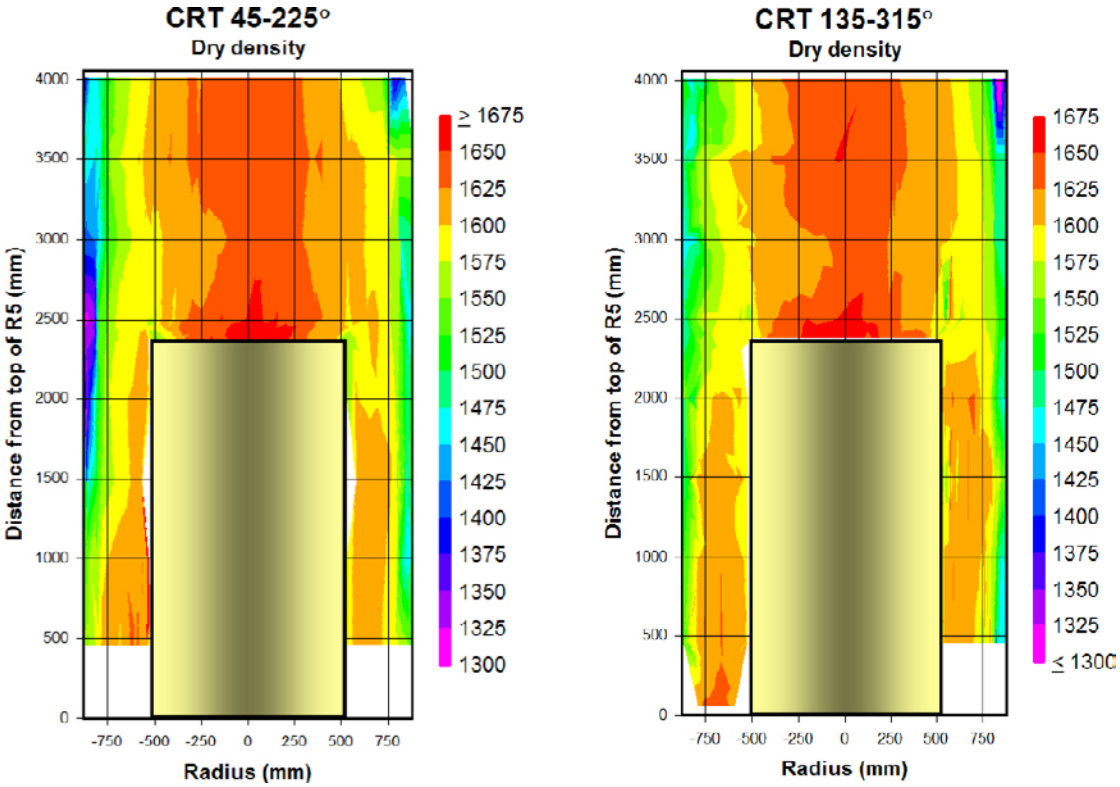

Figure 6-2. *Iso-maps of dry density [kg/m³] of the buffer samples in four directions.*

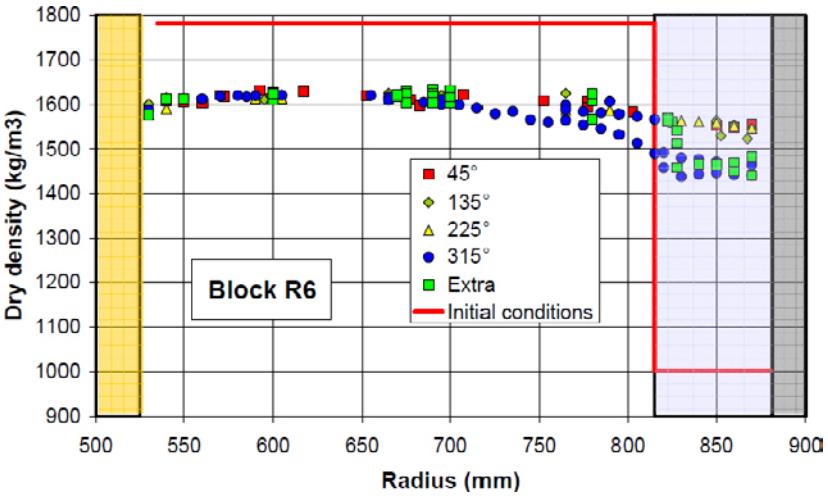

Figure 6-3. *Dry density profiles in block R6.*

6.2 Microorganism analyses of the buffer

Sulphate-reducing bacteria (SRB), producing sulphide, has commonly been observed in groundwater environments typical of possible future repositories. Therefore, consideration of the potential for sulphide corrosion of the copper canisters is of high importance. According to a proposal of a deep hydrogen-driven biosphere hypothesis (Pedersen 1993), presence of autotrophic acetogens (AAs), could be an indicator of the potential for SRBs, since AAs are considered the organisms at the base of these ecosystems.

Lydmark and Pedersen (2011) concluded that: "*AA and SRB were present in the CRT bentonite after five years of storage. The numbers of AA and SRB were low compared to the surrounding groundwater, which can be expected because of the harsh conditions in the bentonite. Nevertheless, they could be found repeatedly in many of the CRT bentonite samples. The results show that the bacteria from various distances from the rock and the inside the CRT bentonite were viable and had a potential to produce both sulphide and organic carbon in form of acetate, also in bentonite with a density over 2,000 kg/m^3. Especially, this was evident in bentonite where the maximum temperature was not too high. The elevated temperature in the R6 bentonite where the maximum temperature reached 85°C during some stage of the experiment obviously made it more difficult for the bacteria to survive compared to the sampled C2 and R9 bentonite where the maximum temperature reached 55°C.*".

6.3 Chemical-mineralogical and hydro-mechanical analyses of the buffer

These analyses aimed at studying the effect of five years of exposure to repository-like conditions on the buffer. The effect was determined by comparing hydro-mechanical and chemical-mineralogical properties of samples from the buffer with those of reference material. The tests/analyses performed were: bentonite composition, aqueous leachates, exchangeable cations and cation exchange capacity, X-ray diffraction analysis, swelling pressure, hydraulic conductivity, and unconfined compression tests.

Dueck et al. (2011a) concluded that the study "… *suggested that:*

- *under the thermal and hydration gradients that prevailed during the test period, calcium sulfate (anhydrite) accumulated near the canister in the heated part of the buffer,*
- *the equilibration of the exchangeable cation pool against the Na-Ca-dominated groundwater resulted in a small decrease in the proportion of exchangeable Mg in the peripheral parts of both blocks,*
- *at the surface of the copper canister, Cu was incorporated in the bentonite in a non-exchangeable, insoluble form,*
- *the crystal chemistry, the X-ray diffraction characteristics and the cation exchange properties of purified, Na-converted < 1 µm fractions provided no evidence of any structural changes in the montmorillonite,*
- *the swelling pressure of the field test material was in the same range as that of the reference material,*
- *the hydraulic conductivity of the trimmed specimens taken from the field experiment was somewhat lower than that of the reference tests, especially at higher densities,*
- *compared to the reference tests, a reduction of strain at failure was observed on re-saturated material taken close to the canister in the heated part of the buffer,*
- *no influence on deviator stress at failure was seen on re-saturated specimens of intact material from the field experiment compared to reference tests.*"

The final overall conclusion was that: "*Based on this study the conditions imposed by the CRT's thermal and hydraulic evolution have not resulted in significant changes of the buffer properties.*" (Dueck et al. 2011a).

6.4 Rock analysis

To investigate development of heat-induced stress damage in the rock close to the deposition hole, Luo (2006) compiled and analysed: the uniaxial compression strength (UCS), Young´s modulus, the crack initiation stress (CIS), crack damage stress (CDS), and the crack volumetric strain. The material analysed were the 12 core samples taken from different parts of sub-horizontal core boreholes drilled parallel and perpendicular to the direction of the major principal stress around the CRT deposition hole. In addition to the laboratory work, modelling of the experiment was carried out.

Concerning the laboratory analyses, Luo (2006) concluded that: "*Judged from relatively higher values of crack volumetric strain at CIS, damage of small extent in the form of micro-fracturing probably occurred in the rock near the deposition hole wall in the direction perpendicular to the major principal stress after excavation of the deposition hole and during the later heating stage. There was no evidence of any damage by UCS, Young's modulus, CIS and CDS.*" Thus, the evidence for heat-induced stress damage was minor.

The modelling, however, showed that " … *at depth 3.1m and 5.4m, in the rock near the deposition hole wall in the direction perpendicular to the major principal stress, the tangential stresses were higher than CIS after excavation, and at all three depths in the mentioned rock, the calculated tangential stresses at the temperature peak were higher than corresponding CIS and even near to CDS for depth 3.1m and 5.4m.* " (Luo 2006).

Suggestions of the origin for the discrepancy between sample analyses and modelling were also given by Luo (2006). It was said that, "*This discrepancy is probably due to the existence of important influence of minor principal stress on crack formation and development.*", which was not considered in the modelling. Furthermore, uncertainties in the laboratory testing were suggested as a possible cause: "*The comparison in this study for UCS testing was conducted among samples taken from different locations after heating and not among samples of the same location taken prior to and after heating. The inherent spatial geological difference might have masked the damage to some extent.*" (Luo 2006).

7 Modelling

7.1 Modelling within EBS-TF

In 2007 CRT was introduced to the Task Force on Engineered Barrie Systems (EBS-TF) as a full size experiment assignment (task 2.2). The assignment was divided into three sub-tasks:

1. Thermal modelling of CRT and TBT with host rock.
2. Detailed THM modelling of a disc of engineered buffer at canister mid-height.
3. THM modelling of the entire experiment.

The first sub-task was not considered as important as the two following with respect to the task force framework, so results from such a model were provided for use as input to the two other tasks.

The second sub-task was suitable for investigations of material models and couplings between (THM) processes. Model responses could be compared with sensor data at canister mid-height as well as the determined mid-height conditions at the time of excavation.

The third sub-task aimed at using the best setup found in the former detailed study, in order to investigate the agreement of the model with buffer sensor data and "global" responses such as heave of and force acting on the lid.

Several of the teams participating in the EBS-TF contributed to the CRT modelling assignment (CIMNE, POSIVA, SKB1, SKB2, BGR, and AECL). In this report however, only the work financed by and produced for SKB is briefly presented. Additional information about work related to modelling of CRT within EBS-TF can be found in Nowak and Kunz (2010) and Börgesson et al. (2015).

In the following three sub-chapters, some results from the sub-tasks are given and briefly discussed. Code_Bright models have been developed for sub-task 1 and 2 and Abaqus has been used for modelling sub-task 2 and 3.

7.1.1 Sub-task 1: Thermal modelling of CRT and TBT

Figure 7-1 shows the position and name of the sensors measuring the temperature in the rock and canister, which the Code_Bright model results are verified against and the geometry used in the 3D thermal calculation.

The comparison between the rock temperature measured by the chosen sensors and the temperature obtained by the simulation is given in Figure 7-2. In Figure 7-3 the experimental and simulated temperatures of the canister temperature are shown.

The buffer thermal conductivity (TC) does not appear to affect the temperature evolution in the rock significantly. Therefore the results in Figure 7-2 are obtained using the base case value of buffer TC only. The simulated temperatures agree well with those measured.

When the canister surface temperatures were simulated, both base case and alternative buffer TC were used in order to evaluate the effect of the water saturation process in the buffer on the canister temperatures. The "true" simulated temperature evolution is considered to go from the temperature curve obtained from using the lower TC-value (1.0 W/(m·K) = dry conditions) towards the curve obtained using the higher TC-value (1.2 W/(m·K) = wet conditions). Figure 7-3 shows that the simulated temperatures fit quite well to the measured temperature evolution when in thought considering the water saturation process by interpolating between the two curves. Initially, the temperature is underestimated. This could be an effect of not considering the initially open inner slot in the model.

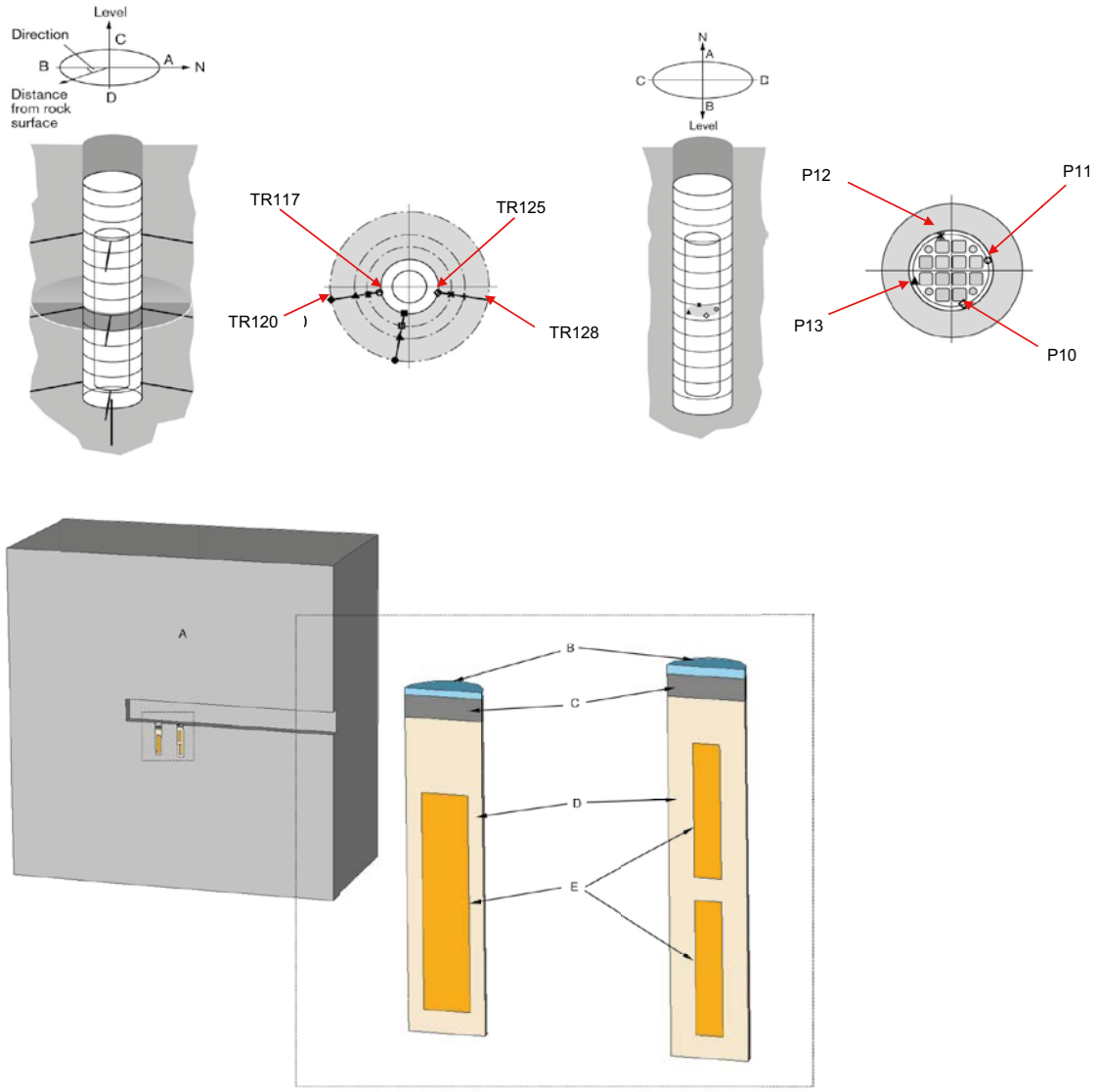

Figure 7-1. *Rock and canister temperature sensor positions/ID and the geometry of a 3D model used for thermal simulation of the CRT and TBT environment.*

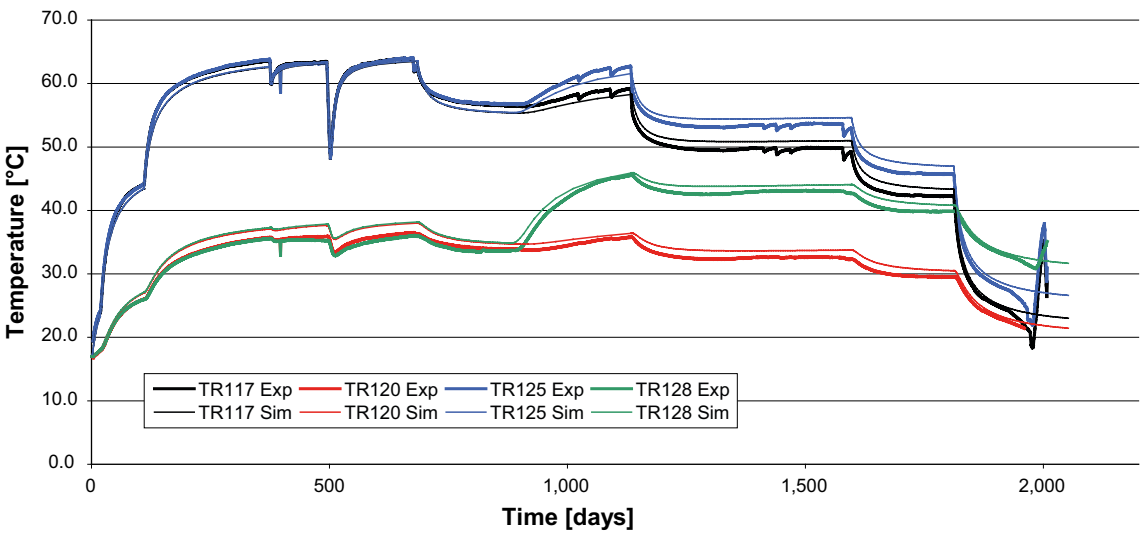

Figure 7-2. *Experimental and simulated rock temperatures at canister mid-height.*

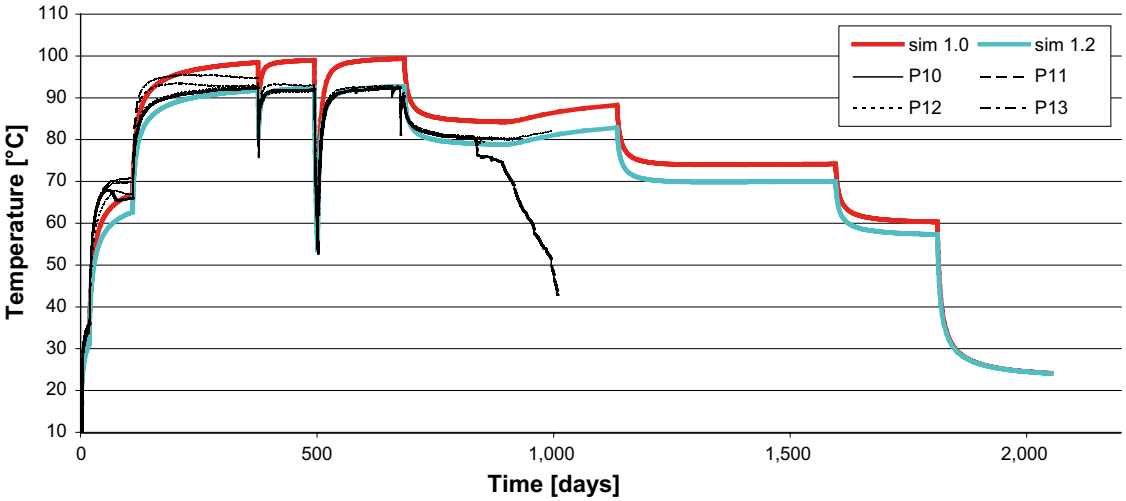

Figure 7-3. *Experimental and simulated canister surface temperatures at canister mid-height.*

7.1.2 Sub-task 2: THM modelling of a disc of CRT buffer

This sub-task was analysed using the finite element solvers Abaqus and Code_Bright. Below, some results from the simulations are shown together in order to facilitate comparisons. The Abaqus and Code_Bright models are not identical, neither on the level of balance equations nor in terms of constitutive relations. For more information about the models the references given should be studied. When available, experimental data is given to enable evaluation of the computed results.

Suction

Figure 7-4 shows suction evolutions at various radial distance at canister mid-height. In the Abaqus model a slightly wetter initial condition, where initial suction is about 37.5 MPa, has been used as compared with the Code_Bright model, where initial suction is defined as 45 MPa. The measurements of the middle graphs of each trio shown in Figure 7-4 indicate that the initial suction should be above 43 MPa.

The two models capture the main trends of the evolutions. Both models underestimate the amount of drying after the initial wetting at the innermost position, shown in the top graphs. The Abaqus model has slightly lower saturation rate as compared to the Code_Bright model. Which of the models produce the most representative result cannot however, really be distinguished based on the available data.

Total stress

As can be seen in Figure 7-5 both models produce stress levels that agree reasonable well with each other but are in excess of what is measured. Most probable, as mentioned in Chapter 4.2, is that this stems from “installation effects” where local low density volumes around the sensors give rise to lower swelling pressure as compared to the buffer material replaced with sensors and bentonite backfill powder.

The innermost response at r = 540 mm in the Code_Bright solution can be seen to be very sensitive to changes in temperature as compared to other points. Some of the effect probably comes from unfortunate choices when designing a fictitious material, intended to mimic the initially open slot at the canister. This fictitious material seems to have adversely affected the simulation close to the canister. It should be noted that it is likely that the material properties could be chosen as not to obtain this disturbance, this is however left to investigate.

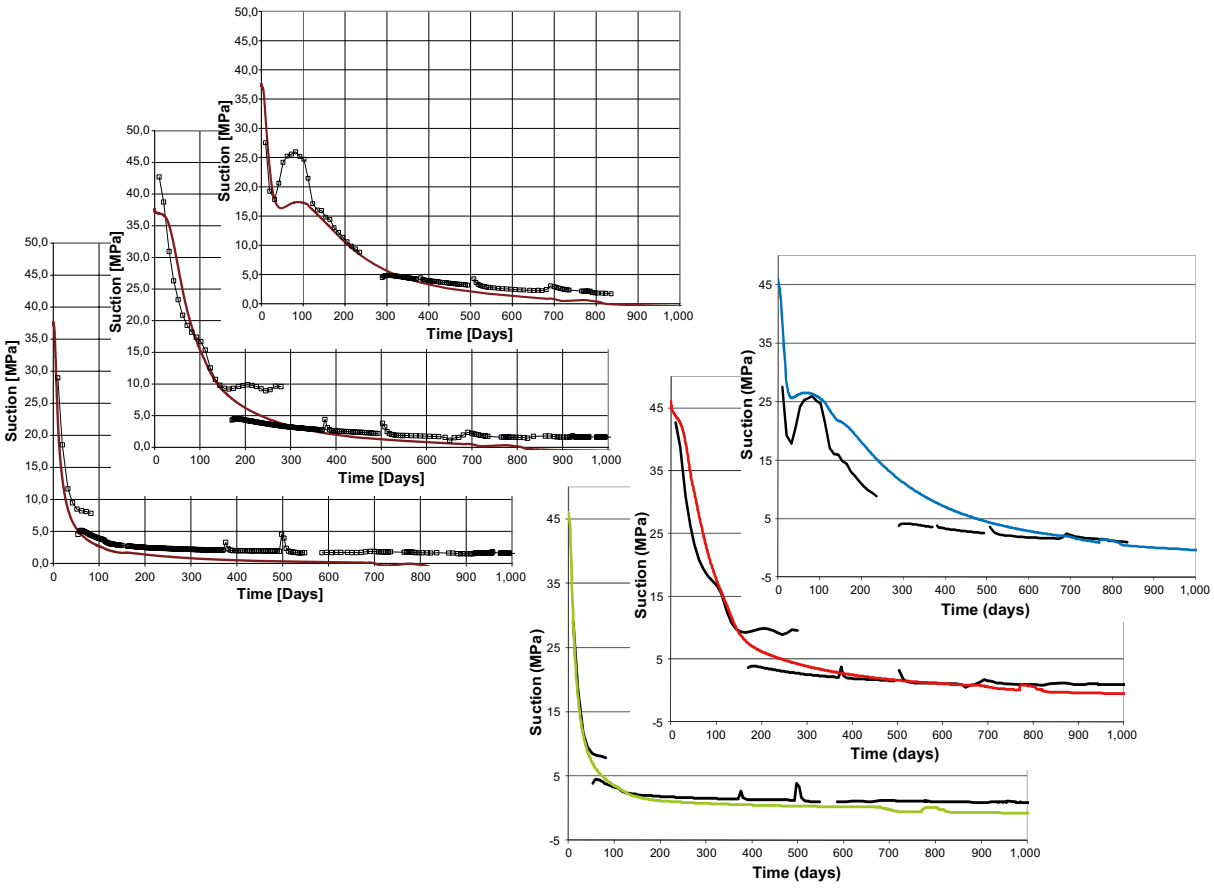

Figure 7-4. *Compilation of suction evolutions; measurements, Abaqus (left sequence), and Code_Bright (right sequence). The sequences are showing evolutions in points at radius 585 mm (top), 685 mm (middle), and 785 mm (bottom).*

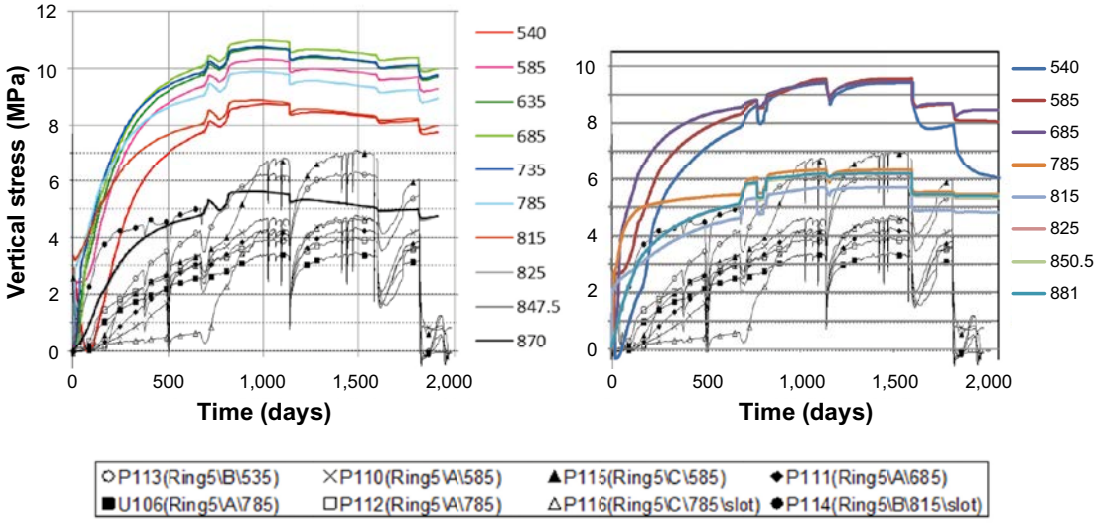

Figure 7-5. *Compilation of vertical stress evolutions at the radii indicated to the right of the graphs, Abaqus (left), and Code_Bright (right). Measured stress is also given (the black thin curves with symbols) at canister mid-height at the positions indicated below the graphs.*

Dry density distribution

Figure 7-6 shows evolutions of dry density at the radii indicated to the right of the graphs. The appearance of the curves are similar for both the models except for r=540 mm which has a very strong initial compaction phase in the Code_Bright model. This is the same as for the vertical stress histories; very likely a consequence of somewhat inappropriate properties chosen for representing the initially open slot.

In Figure 7-7 profiles of dry density are given. The analysed field samples were taken in four different directions in block R7, which was positioned close to the canister mid-height. The calculated profiles, given as the solid black line in each of the graphs, agree very well with the results from the analysed samples. Initial dry densities in the materials, given by the red curve, are also indicated in Figure 7-7.

There are, however, two slight anomalies in the profiles.

i) The Abaqus solution shows a distinct discontinuity at the interface between block and pellet slot material, and

ii) Locally, close to the canister, the Code_Bright solution produces high dry densities.

For the Code_Bright model, the properties of the pellet slot material model (a modified version of Barcelona Basic Model) were calibrated to produce a continuous dry density profile over the block/pellet slot interface, and again, the inner slot material model (or rather, unsuitable choice of parameter values) is most likely to blame for the appearance close to the canister. The Abaqus model, however, did not rely on calibration of the pellet slot parameters in the same way as the Code_Bright model, and might therefore be considered a more realistic representation of the predictive capacity. In addition, the inner 1 cm slot was represented by contact surfaces and thus modelled as an open gap in the Abaqus simulation.

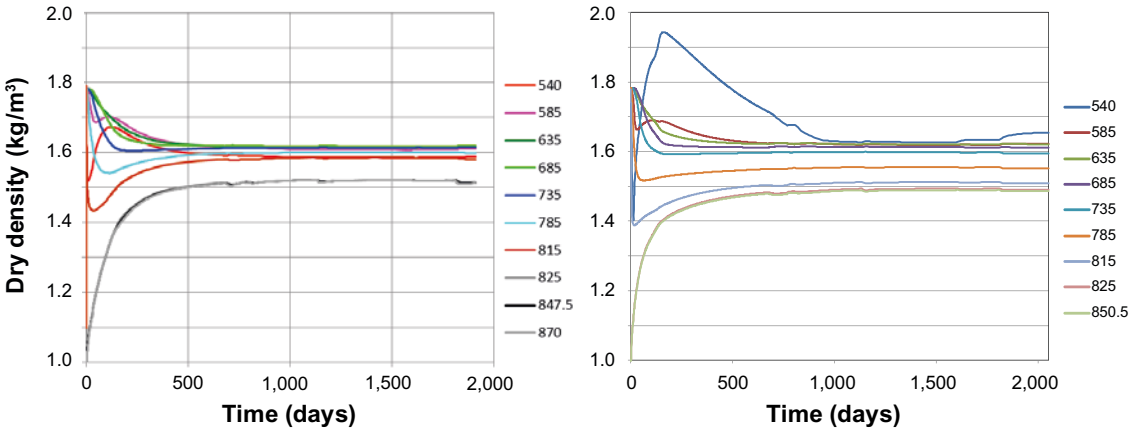

Figure 7-6. *Compilation of simulated dry density evolutions from Abaqus (left) and Code_Bright (right).*

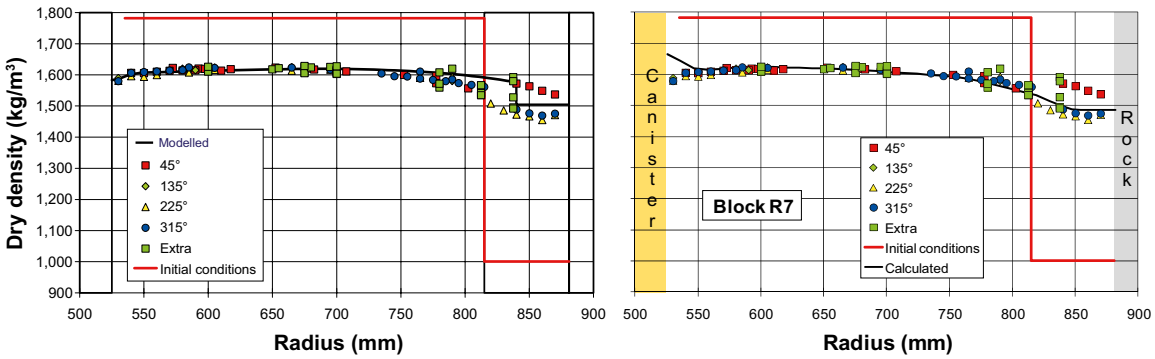

Figure 7-7. *Compilation of dry density profiles at time of buffer excavation; comparison of measurements to Abaqus (left), and Code_Bright (right).*

7.1.3 Sub-task 3: THM modelling of the entire CRT

A 2D-model of the entire test was used for the thermo-hydro-mechanical simulation of the entire CRT experiment. The modelling was done with the code Abaqus and is described in detail in Börgesson et al. (2015).

Model

Figure 7-8 shows the geometry and the element mesh of the 2D model. The model includes a total of five different bentonite materials (ring shaped blocks, solid blocks, bricks, pellets and the empty slot) and four other materials (canister, rock, concrete plug and steel lid).

The dimensions and material names of the different parts in the model are shown in Table 7-1.

Table 7-1. Dimensions and material name of the different parts of the model

Model part	Radial thickness (m)	Axial thickness (m)	Material name
Steel plug	r=0.875	0.2	Steel
Concrete plug	r=0.875	0.5	Concrete
Bentonite top blocks	r=0.82	1.5	Blocks
Bentonite bricks	r=0.535	0.25	Bricks
Canister	r=0.525	4.75	Canister
Bentonite bottom block	r=0.82	0.5	Blocks
Empty slot	r=0.01	4.75	Slot
Bentonite rings	r=0.285	5.0	Rings
Pellets filled slot	r=0.055	7.0	Pellets
Bottom rock	r=0.875	0.1	Rock
Radial rock	r=0.12	8.55	Rock

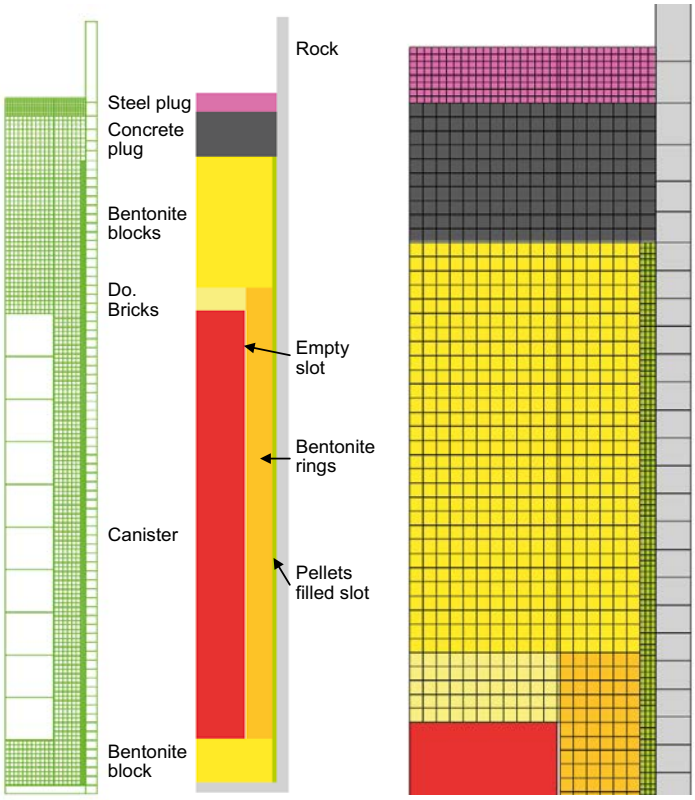

Figure 7-8. *Element mesh and property areas of the 2D model. The model is axial symmetric around the left boundary.*

The model is composed of eight different materials, of which four are different bentonite-based components. The bentonite material MX-80 is used for all bentonite components but with different densities and water contents, resulting in the same material model but different initial conditions, as shown in Table 7-2. In this table Pellets I refers to the pellets filled slot before water filling and Pellets II after water filling.

The three types of blocks were modelled as water unsaturated bentonite with the models developed for Abaqus. The pellet filling changes its density significantly during the wetting due to the swelling of the blocks. Since the model of unsaturated bentonite used is not well suited for large volume changes and since the degree of saturation after the water filling is very high the pellets filling was modelled as completely water saturated.

In addition there is a slot of 1 cm between the canister and the bentonite rings that has been assumed to be filled during the initial water filling of the outermost pellets fill. This slot was modelled as water filled space between two contact surfaces.

The material models are in detail described in Börgesson et al. (2015).

The canister and the rock were modelled as rigid impermeable bodies. The concrete plug and the steel lid were modelled as impermeable elastic materials. In order to simulate the elasticity in the anchor rods the steel plate was defined as having an E-modulus that gives the same deformation as the lengthening of the rods.

The contacts between the buffer and the rock and canister were mechanically modelled with contact surfaces.

Results

The 2D model of the entire test yielded good agreement between modelled and calculated results.

For ring 5 the results were equal to the 1D calculation with exception of the density distribution that differed slightly due to the vertical displacements that could not take place in the 1D model and also due to the difference in element mesh. The element mesh was much finer in the 1D calculation which yielded a better density distribution that captured the influence of the inner gap and the outer pellets filled slot better.

The modelled moisture history just above the canister in section R5 and further up in section C3 agreed well with measurements but the degree of saturation at the end of the test was a little higher than measured in both sections.

Figure 7-9 shows the modelled and measured evolution of Relative Humidity in ring 10 and block C3, both located just above the top of the canister. Figure 7-10 shows the modelled and measured degree of saturation at the end of the test in block C3.

Table 7-2. Basic properties of four of the five bentonite parts.

Section	Density (kg/m^3)	Water ratio	Dry density (kg/m^3)	Void ratio	Degr. of saturation
Solid block	1,991	0,172	1,699	0,636	0,751
Ring shaped block	2,087	0,171	1,782	0,560	0,849
Bricks	1,883	0,165	1,616	0,720	0,637
Pellets I (dry)	1,101	0,100	1,001	1,778	0,156
Pellets II (water filled)	1,574	0,572	1,001	1,778	0,895

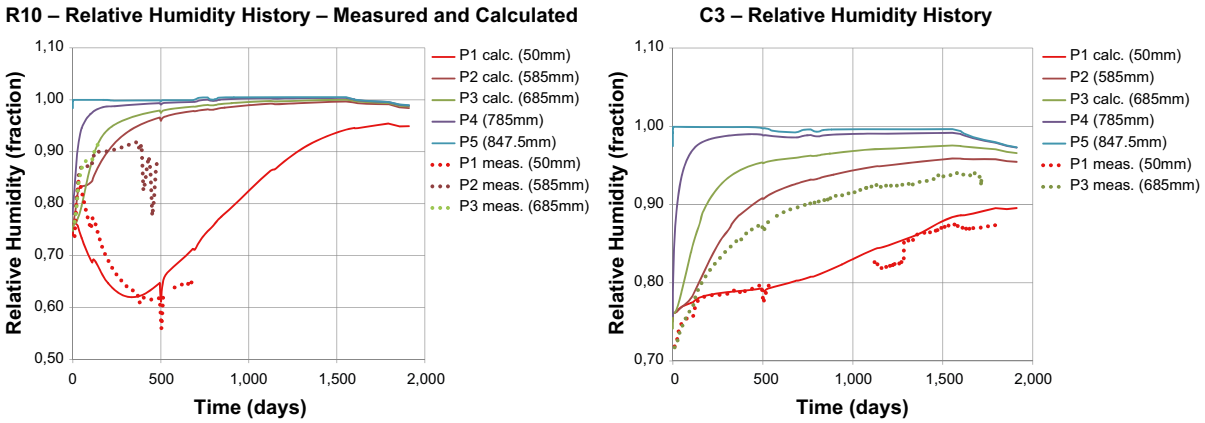

Figure 7-9. *Modelled and measured evolution of RH above the canister.*

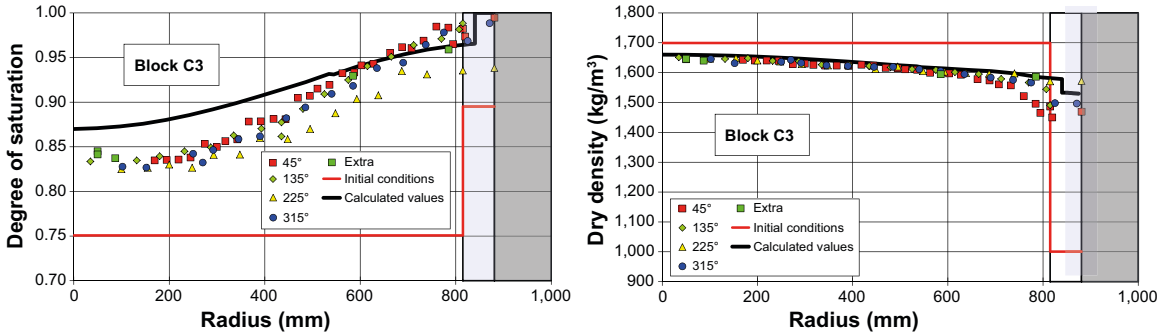

Figure 7-10. *Modelled and measured distribution of degree of saturation and dry density in block C3 at the end of the test.*

The modelled density distribution in sections R10 and C3 agreed well with measured as shown for block C3 in Figure 7-10.The small discrepancy at the brick filled part of section R10 above the canister was concluded to depend on that the sampling was done in the bricks while the average initial density used in the model was lower and also included a layer filled with bentonite powder. The modelled total axial stress was higher than measured, which can be explained by the transducer design and is especially critical when the bentonite is not water saturated as analysed in earlier.

The modelled history of the force on the plug agreed very well with measured, which additionally support that the modelled stresses are more correct than the measured ones. The disagreement between the measured and modelled displacement of the plug could be explained by early effects before start of the actual test as analysed earlier.

The overall conclusion is that the test was well modelled and that the material models and calculation technique have been validated.

7.2 Modelling outside of EBS-TF

Buffer homogenization taking place in the CRT has also been studied and reported outside of EBS-TF using the second EBS-TF sub-task as a base for the studies.

Modelling of the buffer homogenization in CRT was presented at the 4th international meeting on clay confinement properties, held in Nantes, France (April 2010) and was subsequently published (Kristensson and Åkesson 2011).

When buffer homogenization was studied for SR-Site (Åkesson et al. 2010, Chapter 5) the modelling of CRT as described above defined a base case from which alterations were made. Changes from the base case were made with respect to material parameters, material models, geometry, character of saturation, and simulated time (the model of the entire experiment was continued until full saturation of the buffer was obtained).

7.2.1 Pellet slot width variation

One case within SR-Site (Åkesson et al. 2010, Section 5.7) studied how variation of the pellet slot width affected the numerical solution obtained. The basis for this investigation was the Code_Bright model used in the EBS-TF sub-task 2, but now with a pellet slot width of 3, 5, or 9 cm. One conclusion which could be drawn immediately when designing the models was the necessity of using individualized parameter settings regarding the mechanical material model (a modified version of Barcelona Basic Model) in order to achieve representative void ratio profiles.

As clearly seen in Figure 7-11, when properly calibrated, the models produced void ratio profiles which agreed well with what was expected; both when compared with each other and the CRT-data. Thus, the wider the pellet slot the higher the void ratio profile and the 5 cm width model agrees well with the CRT-data (the average pellet slot width was about 6 cm in CRT).

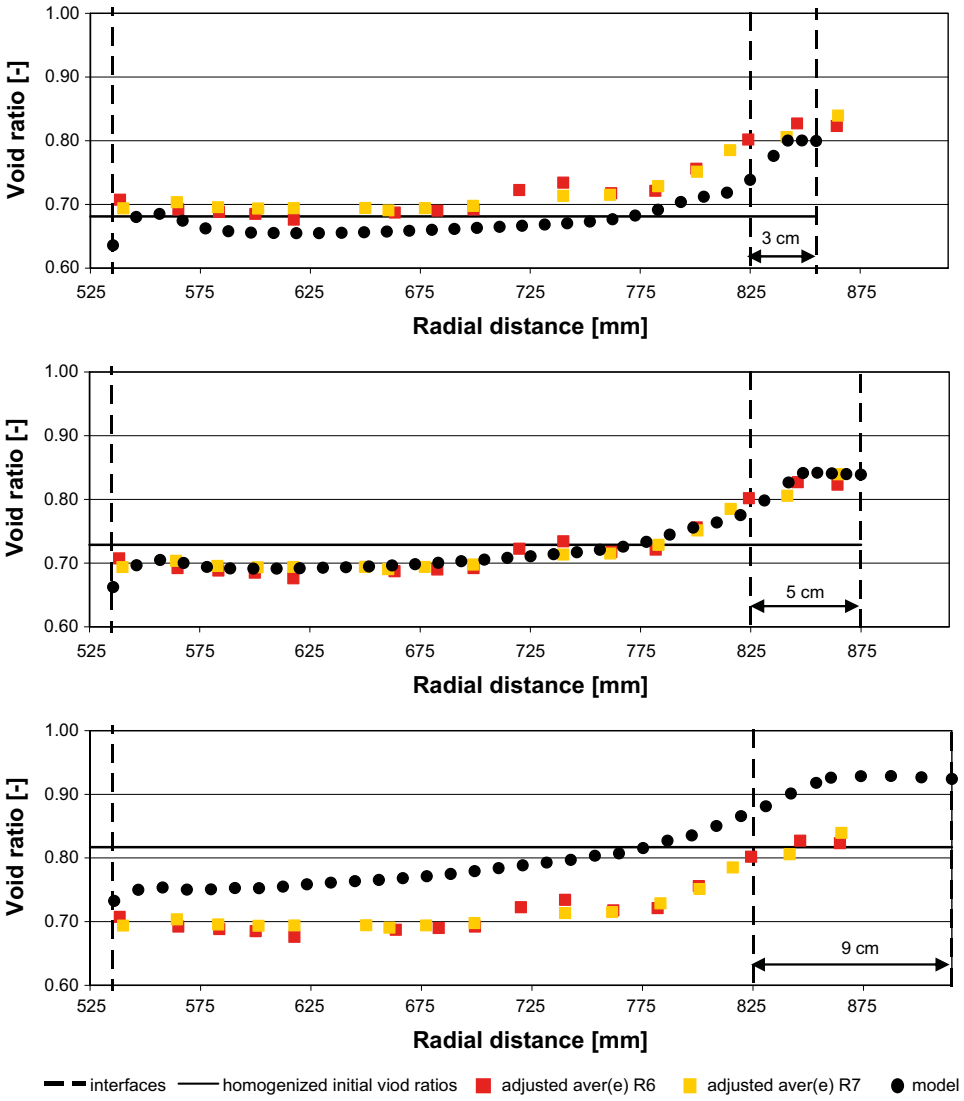

Figure 7-11. *Calculated void ratio profiles obtained for 3, 5 and 9 cm pellet slot together with CRT-data.*

Since some safety function criteria are expressed in terms of total pressure, a study of this variable was also of interest for the three cases. To evaluate the pressures at the end of the simulation, volume averages of the total pressures in the pellet slot, block and the total model were calculated. The obtained values, shown in Figure 7-12, depend on void ratios and volume relations between pellet slot and block for the different models. The lower the void ratio the higher the pressure and the wider the slot the lower the total average pressure as compared to the block average pressure (a wider slot increases the relative volume of pellets).

7.2.2 Investigation of remaining heterogeneity

Yet another investigation in connection with SR-Site (Åkesson et al. 2010, Sections 5.3 and 5.8) dealt with the heterogeneity (in terms of density/void ratio) which remains after full saturation has taken place. From basic thermodynamical considerations a simple analytical model was developed; block and pellet slot were treated as two homogeneous materials in mechanical balance. This gave a possibility to study the influence of wetting sequence and total pressure difference (total pressure will be denoted by pressure only in the forthcoming) in the two materials on remaining heterogeneity. The wetting sequence had, since it "acted through" the path dependence of the retention curve (a.k.a. hysteresis), a significant effect as well as prescribing different pressure ratios, $\alpha = p^p/p^b$.

Both influences can be studied in Figure 7-13 where two extreme wetting sequences, serial (pellet slot first and block second) and parallel (simultaneous wetting of pellet slot and block), are paired with pressure ratios 1, 0.9, 0.8, and 0.7. The red circle indicates the state of CRT and the black line indicates extrapolations from CRT to states where constant volume is assumed. The four graphs to the right in Figure 7-13 show the obtained void ratio profiles corresponding to points A, B, C, and D respectively.

It should be noted that the correspondence with CRT and the line "serial wetting and α=1.0" do not indicate that this process is describing what actually happened in CRT. This is merely one possible combination that gives the correct final state. A more likely combination should have a pressure ratio about 0.85 (based on the FE solution presented above) and thereby the wetting process could be described as "closer to serial than parallel" when studying Figure 7-13. This actually mimics what took place in CRT where the pellet slot was filled with water at the very start of the experiment.

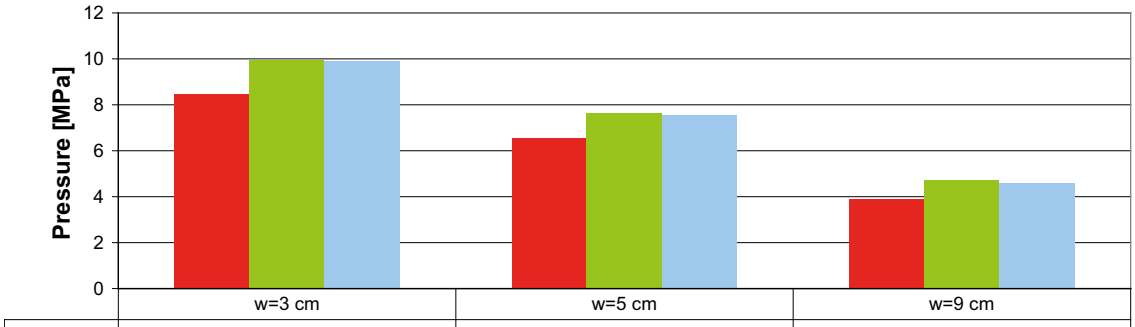

	w=3 cm	w=5 cm	w=9 cm
pellet slot	8.48	6.54	3.89
block	9.97	7.65	4.72
tot	9.91	7.55	4.57

Figure 7-12. *Averages of pressure for 3, 5 and 9 cm pellet slot.*

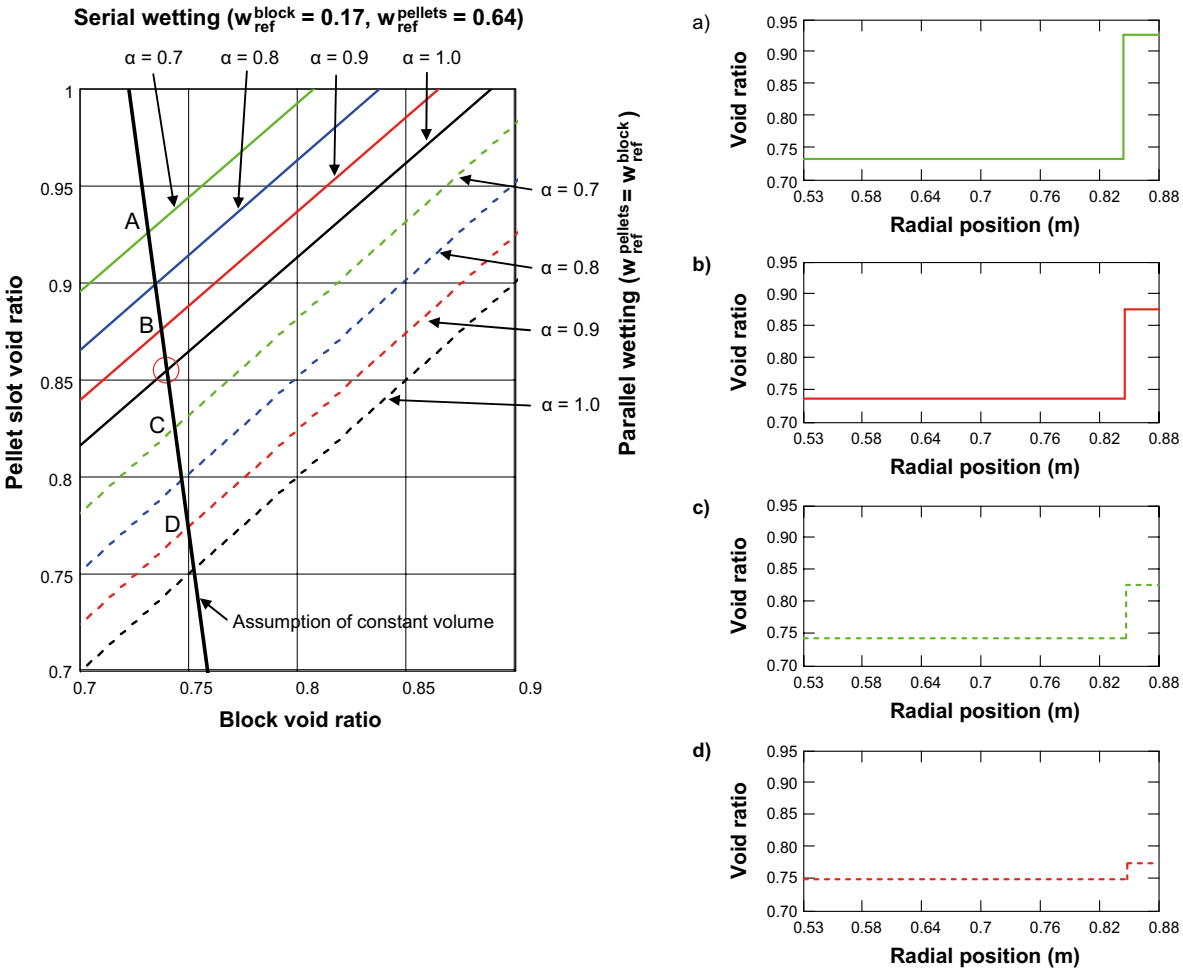

Figure 7-13. *Compilation of the analytical model results for serial (solid lines) and parallel wetting (hatched lines) assuming different pressure ratios. The obtained average void ratio profiles are shown for four different choices in wetting process and pressure ratio along the constant volume assumption with the CRT state as a reference.*

8 Conclusions and remarks

8.1 Freeing and retrieving the canister

The hydrodynamic/chemical freeing technique worked very well for dissolution and removal of bentonite. A prerequisite for its efficiency, however, is that it is used in an environment free of disruptive materials such as bits of tubing, rags, strings etc. The retrieval of the canister was unproblematic using the same machinery as used at installation.

8.2 Buffer sample analyses

At time of excavation the buffer was unsaturated above the canister and saturated elsewhere. A density homogenization process had been taking place during the water uptake but heterogeneity still prevailed at fully saturated conditions.

Autotropic acetogens and sulphate-reducing bacteria were found in the CRT buffer despite the harsh conditions during the five year experiment. The number of them was however low, as compared to the surrounding groundwater. Viable bacteria were mostly found at locations where the maximum temperature had not been too high.

Chemical-mineralogical analyses showed that: calcium sulfate had accumulated near the canister; the proportion of exchangeable Mg had a small decrease in the outer parts of the analysed blocks; a non-exchangeable insoluble form of Cu was incorporated in the bentonite at the canister/block interface; and no evidence of structural changes could be found by crystal chemistry, the X-ray diffraction characteristics, and cation exchange properties.

When compared to reference material properties the hydro-mechanical analyses of the buffer samples showed: no significant change in swelling pressure, somewhat lower hydraulic conductivity (especially so at higher density), a reduction in strain at failure for samples in the proximity of the canister, and no significant change in deviator stress at failure.

The final conclusion from chemical-mineralogical and hydro-mechanical analyses was that the conditions of the CRT experiment did not result in significant changes of the buffer properties.

8.3 Modelling

Modelling of CRT has been performed within the framework of the task force on engineered barrier systems, where it was given as one of the full scale experiment assignments. In addition, a model and experimental data concerning CRT was used in SR-Site (the safety assessment) when homogenization process and remaining heterogeneity after the water uptake process were investigated.

The capability for modelling the thermal problem seems to be rather good. It was found that when performing detailed studies of temperatures at the canister surface and within the buffer the saturation dependence of the thermal conductivity and the effect of the initially empty inner gap, between the canister and blocks, are influential.

If studying the agreement between the simulations and the experimental sensor data, concerning suction and RH, the overall trends of the wetting process seem to be well captured. It should however be remembered that the presently used models were not formulated with unsaturated bentonite clay in mind in the first place and they were also developed under certain assumptions such as confined conditions and unchanged groundwater chemistry.

When studying total vertical stress as recorded by the sensors and comparing them with what the models simulate and the buffer sample analysis gave, the sensor data is showing lower magnitudes of stress than what is expected. This probably comes from an installation effect due to low density volumes around the sensors. The simulated overall trends and relation of stresses agree well with what is measured.

In the Code_Bright simulation a fictional “open slot material” was used, and its presence gave rise to some disturbances in the numerical solutions in the close vicinity of the slot. Abaqus used contact surfaces to represent the gap and the solution did not seem to suffer from any of the disturbances observed for the Code_Bright model. The parameter setup of the fictional material in Code_Bright could however probably be calibrated as to significantly decrease the observed disturbances.

The calculated dry density profile at the end of the test was in good agreement with experimental data for both Abaqus and Code_Bright. The homogenization process had been mimicked well; the high density buffer block had swollen and compressed the low density pellet slot to a reasonable degree. There were some anomalies in the profiles, however. The Abaqus solution showed a distinct discontinuity at the buffer/pellet slot interface and for Code_Bright the fictional “open slot material” gave a disturbance at the canister side. It should be noted that the pellet slot material in the Code_Bright model was calibrated to give a continuous profile at the interface whereas the Abaqus model was closer to being a true blind prediction.

The pellet slot material model used in Abaqus did not account for unsaturated states, full water saturation was assumed from the start. This was due to limited capability of the unsaturated model to cope with the large density variations that were present in the pellet slot material.

Regarding the Code_Bright simulations, the mechanical material model used for representing the buffer (a modified version of Barcelona Basic Model) showed what may be called “process dependency”. It was experienced that the user had to have knowledge about the process which was going to take place and calibrate the model with respect to this in order to obtain representative responses. A probable reason for the difficulties regarding the mechanical material model is that it was developed with clays possessing low expansive potential in mind, which bentonite is not.

One example of such a difficulty occurred when it was found necessary to calibrate the pellet slot mechanical model by trial and error in order to obtain a dry density profile which was representative. Another related example occurred when investigating the influence of different initial pellet slot widths. The material parameters were recalibrated for each of the adopted widths in order to obtain representative void ratio profiles.

The simulations of CRT cannot with the above in mind therefore be considered an unbiased indication of the predictive capacities of the model formulated using Code_Bright.

It should finally be mentioned that a mechanical material model which is intended for highly expansive clays is now available in Code_Bright (it was not at the time when the simulations were performed) and this might resolve much of the experienced difficulties described above.

8.4 Remarks

Some remarks/issues with respect to the CRT experiment are here given.

There are matters regarding freeing and retrieval which have not been considered and tested in CRT:

- Excavation of tunnel backfill prior to buffer removal.
- Handling of radiation shielding during retrieval.
- Techniques for handling potentially radiologically-polluted buffer and washing water.

The CRT experiment differed from the KBS-3V design:

- There was no tunnel backfill.
- A ramped slot from the tunnel floor to the deposition hole wall, intended to facilitate the canister installation, was lacking (the status of this feature is however uncertain at the moment).
- There was initial artificial water filling of the pellet filled slot at installation.
- An artificial wetting system was present (filter strips, tubing, and cement between strips).
- Sensors with connections/cables were present.
- Heater power cables were present.
- There was an extra lid on top of the heater (to protect the power cables).

8.4.1 Heater malfunction

The heater power cable used was not reliable. The cable shield could not withstand the conditions within the buffer and then moisture caused short circuits which led to ongoing heater failures, see Section 4.

8.4.2 Issues monitoring the experiment

The reported total volume of water added to the experiment, at installation and through filters, is not considered to be reliable; it does not match the final state given by sample analyses (see Section 4.1).

The plug heave measurements are not consistent between the monitoring points and the readings obtained appeared to be inconsistent for each sensor individually (see Section 4.1); manual measurements would have been valuable as a reference.

The total pressure sensor data suffered from an installation effect; probably due to volumes of lower density around the sensors. This gave lower stress levels than what is considered representative within the block material (see Section 4.1).

Buffer displacement could have been estimated directly by measuring the position of the block surfaces at installation and dismantling; the block interfaces were clearly visible at dismantling.

References

SKB's (Svensk Kärnbränslehantering AB) publications can be found at www.skb.se/publications.

Ageskog L, Blix P, 2000. Äspö Hard Rock Laboratory. Canister retrieval test. Temperature on the canister surface. SKB IPR-00-18, Svensk Kärnbränslehantering AB.

Börgesson L, Åkesson M, Kristensson O, Dueck A, Hernelind J, 2015. EBS TF – THM modelling. BM 2 – Large scale field tests. SKB TR-13-07, Svensk Kärnbränslehantering AB.

Dueck A, Johannesson L-E, Kristensson O, Olsson S, 2011a. Report on hydro-mechanical and chemical-mineralogical analyses of the bentonite buffer in Canister Retrieval Test. SKB TR-11-07, Svensk Kärnbränslehantering AB.

Dueck A, Johannesson L-E, Kristensson O, Olsson S, Sjöland A, 2011b. Hydro-mechanical and chemical-mineralogical analyses of the bentonite buffer from a full-scale field experiment simulating a high-level waste repository. Clays and Clay Minerals 59, 595–607.

Eng A, 2008. Äspö Hard Rock Laboratory. Canister Retrieval Test. Retrieval phase. Project report. SKB IPR-08-13, Svensk Kärnbränslehantering AB.

Gentzschein B, 1999. Äspö Hard Rock Laboratory. Canister retrieval test. Flow and pressure measurements in the pilot holes. SKB IPR-00-10, Svensk Kärnbränslehantering AB.

Goudarzi R, Börgesson L, Röshoff K, Edelmann M, 2006. Äspö Hard Rock Laboratory. Canister Retrieval Test. Sensors data report (Period 001026–060501). Report No:12. SKB IPR-06-35, Svensk Kärnbränslehantering AB.

Hardenby C, 2002. Äspö Hard Rock Laboratory. Tunnel for the canister retrieval test. Geological mapping of tunnel and deposition holes. SKB IPR-02-49, Svensk Kärnbränslehantering AB.

Johannesson L-E, 1999. Compaction of full size blocks of bentonite for the KBS-3 concept. Initial tests for evaluating the technique. SKB R-99-66, Svensk Kärnbränslehantering AB.

Johannesson L-E, 2007. Äspö Hard Rock Laboratory. Canister Retrieval Test. Dismantling and sampling of the buffer and determination of density and water ratio. SKB IPR-07-16, Svensk Kärnbränslehantering AB.

Kalbantner P, Sjöblom R 2000. Techniques for freeing deposited canisters. SKB TR-00-15, Svensk Kärnbränslehantering AB.

Karnland O, Olsson S, Nilsson U, 2006. Mineralogy and sealing properties of various bentonites and smectite-rich clay materials. SKB TR-06-30, Svensk Kärnbränslehantering AB.

Kristensson O, Åkesson M, 2011. Homogenization of engineered barriers, simulations verified against Canister Retrieval Test data. Physics and Chemistry of the Earth, Parts A/B/C 36, 1848–1856.

Luo S, 2006. Äspö Hard Rock Laboratory. Canister Retrieval Test. Investigation of possible therminal induced stress damage by UCS testing and simulations. SKB IPR-06-37, Svensk Kärnbränslehantering AB.

Lydmark S, Pedersen K, 2011. Äspö Hard Rock Laboratory. Canister Retrieval Test. Microorganisms in buffer from the Canister Retrieval Test – numbers and metabolic diversity. SKB P-11-06, Svensk Kärnbränslehantering AB.

Nirvin B, 2007. Äspö Hard Rock Laboratory. Retrieval of deposited canister for spent nuclear fuel. Freeing – slurrying of saturated bentonite buffer around a canister at Äspö HRL, Technology, equipment and results in connection with freeing for the Canister Retrieval Test. SKB IPR-08-04, Svensk Kärnbränslehantering AB.

Nowak T, Kunz H, 2010. Äspö Hard Rock Laboratory. Äspö Task Force on Engineered Barrier System. Modelling of THM-coupled processes for benchmark 2.2 with the code GeoSys/RockFlow. SKB IPR-10-07, Svensk Kärnbränslehantering AB.

Pedersen K, 1993. Bacterial processes in nuclear waste disposal. Microbiology Europe 1, 18–23.

Pettitt W, Baker C, Young R P, 1999. Äspö Hard Rock Laboratory. Acoustic emission and ultrasonic monitoring during the excavation of deposition holes in the Canister Retrieval Test. SKB IPR-01-02, Svensk Kärnbränslehantering AB.

Sandén T, Börgesson L, 2000. Äspö Hard Rock Laboratory. Canister Retrieval Test. Report on instrument positions and preparation of bentonite blocks for instruments and cables. SKB IPR-00-14, Svensk Kärnbränslehantering AB.

Svemar C, 1999. Äspö Hard Rock laboratory. Canister Retrieval Test. Test plan. Part 1 – Geotechnical characterisation, test installation and monitoring during saturation. SKB IPR-99-26, Svensk Kärnbränslehantering AB.

Thorsager P, Börgesson L, Johannesson L-E, Sandén T, 2002. Äspö Hard Rock Laboratory. Canister Retrieval Test. Report on installation. SKB IPR-02-30, Svensk Kärnbränslehantering AB.

Åkesson M, Kristensson O, Börgesson L, Dueck A, Hernelind J, 2010. THM modelling of buffer, backfill and other system components. Critical processes and scenarios. SKB TR-10-11, Svensk Kärnbränslehantering AB.

Appendix A

Volume and swelling estimations

A.1 Volume estimations

From the data in Table A-1 and Table A-2 together with the specified geometry, see Box A-1, an estimate of the available pore volume at installation can be calculated as shown in Box A-3. The calculated total available pore volume, also accounting for the empty slot of 1 cm between canister and rings and a heave of the plug of 34 mm, motivated from measurements, becomes 2,264 litres.

Figure A-1 shows the accumulative measured volume of artificially supplied water to the CRT-experiment. During operation, the accumulated measured filter inflow was as given by Figure A-1 when reading the left of the scales. Thus, according to measurements, a total of 670 litres was added through the filters. At installation, water was being fed into the outer pellet filled slot through tubes, which were withdrawn after usage. According to Thorsager et al. (2002) the water volume added through the tubes at installation was about 950 litres. The right of the scales in Figure A-1 gives the accumulated volume of total added water, i.e. the water volume of 950 litres, added at installation, is included, which ends up about 1,620 litres at the end of the test. Thus, 72% of the available pore volume was filled according to the measured and reported water volumes.

If using density and water content data at installation, given in Table A-1 and Table A-2, and excavation, reported in Johannesson (2007), together with the specified geometry, an estimation of the added water volume may be calculated according to

$$V_w = \frac{m_w}{\rho_w}$$

$$m_w = \int dm_w = \int \frac{\rho}{1+\frac{1}{w}} dV \approx \sum \frac{\rho}{1+\frac{1}{w}} \Delta V$$

, see chapter A.3 for some details. An estimate of 2,113 litres was obtained using the assumptions:

- 36 mm total swelling occurred,
- the lower ring-shaped buffer blocks, R1–R5, contain the same water volume as R6, and
- the bottom buffer block, C1, contain the same water volume as C2.

The difference between the estimate and measured value is significant, 2,104–1,620 = 484 litres. According to the estimate 93% of the available pore volume was filled.

Table A-1. Average data for buffer blocks at installation, dimensions from Thorsager et al. (2002) and other from Johannesson (2007).

Type	Dimensions [mm]	Density [kg/m^3]	Water content	Dry density [kg/m^3]	Void ratio
Cylinders	H=504[1]	1,991	0.172	1,699	0.636
Rings	H=510[1]	2,087	0.171	1,782	0.560
Bricks[2]	H=125[3]	1,883	0.165	1,616	0.720

[1]The average value and an additional 3 mm representing interface volumes between blocks.
[2]The total volume including bentonite bricks, pellets, and powder.
[3]This value is obtained from subtracting the canister height from the height of 10 rings as described in the table.

Table A-2. Data for pellet filled gap at installation, from Johannesson (2007).

Type	Width [mm]	Density [kg/m^3]	Water content	Dry density [kg/m^3]	Void ratio
Pellet slot (dry)	61	1,101	0.1	1,001	1.778
Pellet slot (wet[1])	61	1,574	0.572	1,001	1.778

[1]The state when the pore volume between the pellets has been water filled.

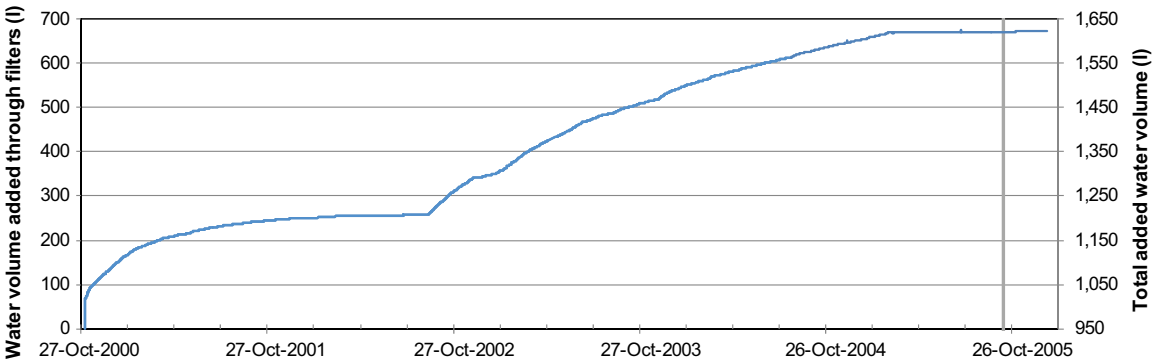

Figure A-1. *Accumulative volume of water added through filters (left scale) and reported accumulative volume of total added water (right scale).*

One potentially uncertain component in the total added water volume is the water volume of about 950 litres that was reported to be added when installing the pellet filled slot (Thorsager et al. 2002). If using the data in Table A-2 together with the specified geometry, a value of 1,096 litres is obtained for the available volume between the pellets, see Box A-4 for details. Also, sensor responses indicate that the open volume of 166 litres between the canister and buffer rings was water filled at installation as well. If so, this gives a total volume of 1,096+166 = 1,261 litres as compared to the reported 950 litres. If calculating a new total added water volume based on the measured inflow from the filters and the estimated volume that was water filled (volume between pellets and the inner slot volume) we obtain 670+1,261 = 1,931 litres which is more in line with that obtained from evaluating excavation data. According to this estimate 85% of the available pore volume was filled. The volumes discussed above are listed in Table A-3 and graphically represented in Figure A-2.

Table A-3. Compilation of the volumes discussed in the text.

Description	Volume [litres]	Ratio [%]
Estimation of available pore volume at installation	2,269	100
Added water volume 1: Reported at pellet filling + Measured filter inflow	1,620	71
Added water volume 2: Calculated from excavation data	2,104	93
Added water volume 3: Calculated available ”macro pore volume” in pellet filling and volume of inner slot + Measured filter inflow	1,931	85

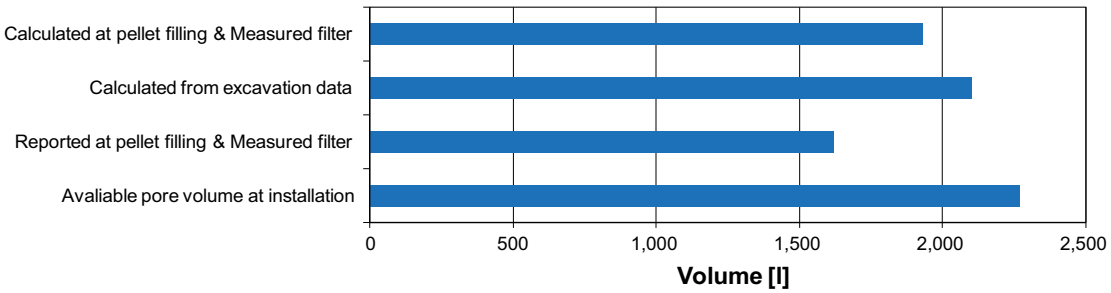

Figure A-2. *Graphical view of the volumes discussed in the text above.*

A.2 Swelling estimation

The axial swelling of buffer sections was estimated by using a relation between initial and final dry density. When performing the estimation three assumptions were made; the solid mass is constant within a considered control volume (buffer section), this volume has a homogeneous thickness also at the final state, and excavation samples taken at a given radius are representative for that radius throughout the block.

$$\rho_d = \frac{dm_s}{dV} = \frac{\rho}{1+w}$$

$$m_s = \int \rho_d dV = \bar{\rho}_d V$$

$$\bar{\rho}_d V = h \int \frac{\rho}{1+w} dA \approx h \sum \frac{\rho}{1+w} \Delta A$$

$$m_s{}^{final} = m_s{}^{init} \Rightarrow h^{final} = \frac{\bar{\rho}_d{}^{init}}{\bar{\rho}_d{}^{final}} h^{init}$$

A.3 Details of the analysis

Below, details of the calculations involved when estimating the volumes and swelling discussed above are given. In Table A-4 the calculation files and their location are compiled. Box A-1 to Box A-4 show how calculations were performed, and Figure A-3 and Figure A-4 show how the data were treated.

Location: ”Administrativa dokument on”: Projekt\CRT\rapporter\Final report\data\Final state*

Table A-4. Compilation of the files used in the analysis.

MathCad-document	
‘Estimate of water in CRT 3B.xmcd’	
‘Estimate dry density and swelling in CRT 3B.xmcd’	
Excel-documents	*** in Location given above**
‘Sammanst C2.xls’	\Block C2
‘Sammanst C3.xls’	\Block C3
‘Sammanst C4.xls’	\Block C4
‘Sammanst R6.xls’	\Block C6
‘Sammanst C7.xls’	\Block C7
‘Sammanst C8.xls’	\Block C8
‘Sammanst C9.xls’	\Block C9
‘Sammanst C10.xls’	\Block C10

Calculate initial water volume

$\rho_w := 1{,}000$ $\quad r_o := \frac{1.64}{2}$ $\quad r_i := \frac{1.07}{2}$ $\quad \Delta r := 0.061$

Cylinders	$H_C := 0.504$	$\rho_C := 1991$	$w_C := 0.172$
Rings	$H_R := 0.510$	$\rho_R := 2087$	$w_R := 0.171$
Bricks	$H_B := 0.123$	$\rho_B := 1883$	$w_B := 0.165$
Pellet slot	$H_P := 4 \cdot H_C + 10 \cdot H_R$	$\rho_P := 1101$	$w_P := 0.1$

$$V_{w\_init\_cylinders} := H_C \cdot r_o^{\,2} \cdot \pi \cdot \frac{1}{1 + \frac{1}{w_C}} \cdot \frac{\rho_C}{\rho_w}$$

$$V_{w\_init\_rings} := H_R \cdot \left(r_o^{\,2} - r_i^{\,2}\right) \cdot \pi \cdot \frac{1}{1 + \frac{1}{w_R}} \cdot \frac{\rho_R}{\rho_w}$$

$$V_{w\_init\_bricks} := H_B \cdot r_i^{\,2} \cdot \pi \cdot \frac{1}{1 + \frac{1}{w_B}} \cdot \frac{\rho_B}{\rho_w}$$

$$V_{w\_init\_pellet} := H_P \cdot \left[\left(r_o + \Delta r\right)^2 - r_o^{\,2}\right] \cdot \pi \cdot \frac{1}{1 + \frac{1}{w_P}} \cdot \frac{\rho_P}{\rho_w}$$

$$V_{w\_init} := 4 \cdot V_{w\_init\_cylinders} + 10 \cdot V_{w\_init\_rings} + V_{w\_init\_bricks} + V_{w\_init\_pellet}$$

$V_{w\_init} = 3.392$

Box A-1. *Calculation of initial water volume. Densities in [kg/m³], dimensions in [m].*

Calculate final water volume

$C4\_sol := vol(FC4, 55, H_C, 0)$ $C4\_sol_0 = 0.501$ $V_{w\_final} := C4\_sol_0$

$C3\_sol := vol(FC3, 55, H_C, 0)$ $C3\_sol_0 = 0.491$ $V_{w\_final} := V_{w\_final} + C3\_sol_0$

$C2\_sol := vol(FC2, 60, H_C, 0)$ $C2\_sol_0 = 0.511$ $V_{w\_final} := V_{w\_final} + 2 \cdot C2\_sol_0$

$C10\_sol := vol(FR10, 55, H_B, 0)$ $C10\_sol_0 = 0.121$ $V_{w\_final} := V_{w\_final} + C10\_sol_0$

$R10\_sol := vol(FR10, 55, H_R - H_B, 1)$ $R10\_sol_0 = 0.257$ $V_{w\_final} := V_{w\_final} + R10\_sol_0$

$R9\_sol := vol(FR9, 55, H_R, 1)$ $R9\_sol_0 = 0.338$ $V_{w\_final} := V_{w\_final} + R9\_sol_0$

$R8\_sol := vol(FR8, 55, H_R, 1)$ $R8\_sol_0 = 0.333$ $V_{w\_final} := V_{w\_final} + R8\_sol_0$

$R7\_sol := vol(FR7, 55, H_R, 1)$ $R7\_sol_0 = 0.335$ $V_{w\_final} := V_{w\_final} + R7\_sol_0$

$R6\_sol := vol(FR6, 55, H_R, 1)$ $R6\_sol_0 = 0.335$ $V_{w\_final} := V_{w\_final} + 6 \cdot R6\_sol_0$

$V_{w\_final} = 5.408$

Calculate added water volume and compare with measurement

$\Delta V_{w\_calc} := (V_{w\_final} - V_{w\_init})$

$\Delta V_{w\_calc} = 2.016$

$\Delta V_{w\_calc} := \Delta V_{w\_calc} + V_{av\_init\_swell}$

$\Delta V_{w\_measured} := 1.620$

$\Delta V_{w\_calc} = 2.104$

$\Delta V_{w\_calc} - \Delta V_{w\_measured} = 0.484$

$$\frac{\Delta V_{w\_calc}}{V_{av\_init}} = 0.927$$

Box A-2. *Calculation of the final water volume and added water volume. Dimensions in [m].*

Calculate initial avaliable pore volume

Cylinders $e_C := 0.636$ $H_{swell} := 0.036$

Rings $e_R := 0.56$ $\Delta r_{slot} := 0.01$

Bricks $e_B := 0.72$

Pellet slot $e_P := 1.778$

$$V_{av\_init\_cylinders} := H_C \cdot r_o^{\,2} \cdot \pi \cdot \frac{e_C}{1 + e_C} \cdot \left(1 - \frac{\rho_s}{\rho_w} \cdot \frac{w_C}{e_C}\right) \qquad 4 \cdot V_{av\_init\_cylinders} = 0.411$$

$$V_{av\_init\_rings} := H_R \cdot \left(r_o^{\,2} - r_i^{\,2}\right) \cdot \pi \cdot \frac{e_R}{1 + e_R} \cdot \left(1 - \frac{\rho_s}{\rho_w} \cdot \frac{w_R}{e_R}\right) \qquad 10 \cdot V_{av\_init\_rings} = 0.336$$

$$V_{av\_init\_bricks} := H_B \cdot r_i^{\,2} \cdot \pi \cdot \frac{e_B}{1 + e_B} \cdot \left(1 - \frac{\rho_s}{\rho_w} \cdot \frac{w_B}{e_B}\right) \qquad V_{av\_init\_bricks} = 0.017$$

$$V_{av\_init\_pellet} := H_P \cdot \left[\left(r_o + \Delta r_{pellets}\right)^2 - r_o^{\,2}\right] \cdot \pi \cdot \frac{e_P}{1 + e_P} \cdot \left(1 - \frac{\rho_s}{\rho_w} \cdot \frac{w_P}{e_P}\right) \qquad V_{av\_init\_pellet} = 1.253$$

$$V_{av\_init\_slot} := \left(10 \cdot H_R - H_B\right) \cdot \left[r_i^{\,2} - \left(r_i - \Delta r_{slot}\right)^2\right] \cdot \pi \qquad V_{av\_init\_slot} = 0.166$$

$$V_{av\_init\_swell} := H_{swell} \cdot \left(r_o + \Delta r_{pellets}\right)^2 \cdot \pi \qquad V_{av\_init\_swell} = 0.088$$

$$V_{av\_init} := 4 \cdot V_{av\_init\_cylinders} + 10 \cdot V_{av\_init\_rings} + V_{av\_init\_bricks} + V_{av\_init\_pellet}$$

$$V_{av\_init} := V_{av\_init} + V_{av\_init\_slot} + V_{av\_init\_swell}$$

$$V_{av\_init} = 2.269$$

Box A-3. *Calculation of the initially available pore volume. Densities in [kg/m³], dimensions in [m].*

Calculate estimate of water volume added at installation

$w_{P\_wet} := 0.572$

$$\Delta V_{init\_pellet\_wet} := H_P \cdot \left[\left(r_o + \Delta r_{pellets} \right)^2 - r_o^{\,2} \right] \cdot \pi \cdot \frac{e_P}{1 + e_P} \cdot \left(\frac{\rho_s}{\rho_w} \cdot \frac{w_{P\_wet}}{e_P} - \frac{\rho_s}{\rho_w} \cdot \frac{w_P}{e_P} \right)$$

$\Delta V_{init\_pellet\_wet} = 1.096$

$V_{av\_init\_slot} = 0.166$

$\Delta V_{init\_pellet\_wet} + V_{av\_init\_slot} = 1.261$

Box A-4. *Calculation of estimate of the water volume added at installation. Densities in [kg/m³], dimensions in [m].*

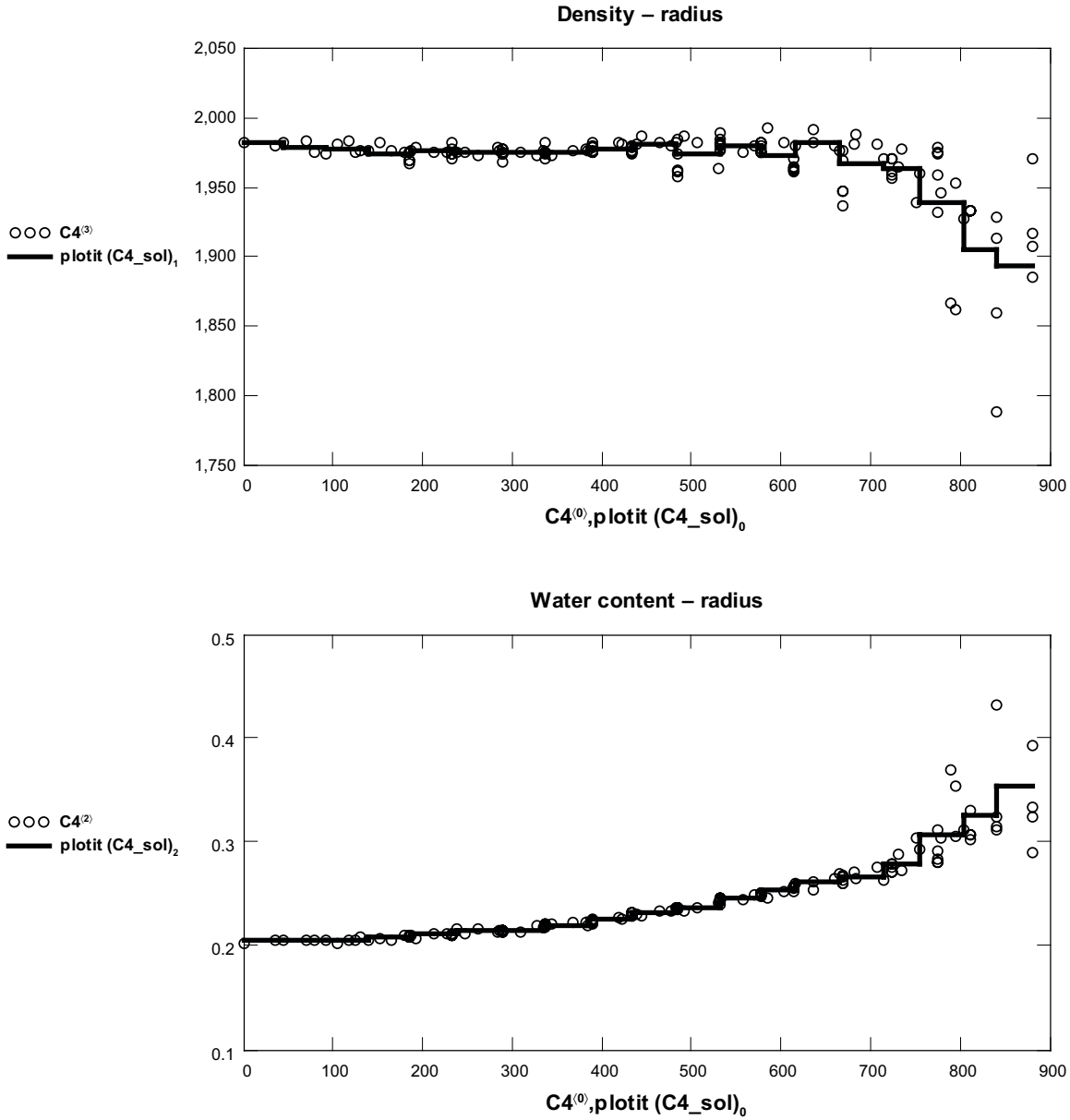

Figure A-3. *Example showing the analysis of block C4. Density in [kg/m³], radius in [mm].*

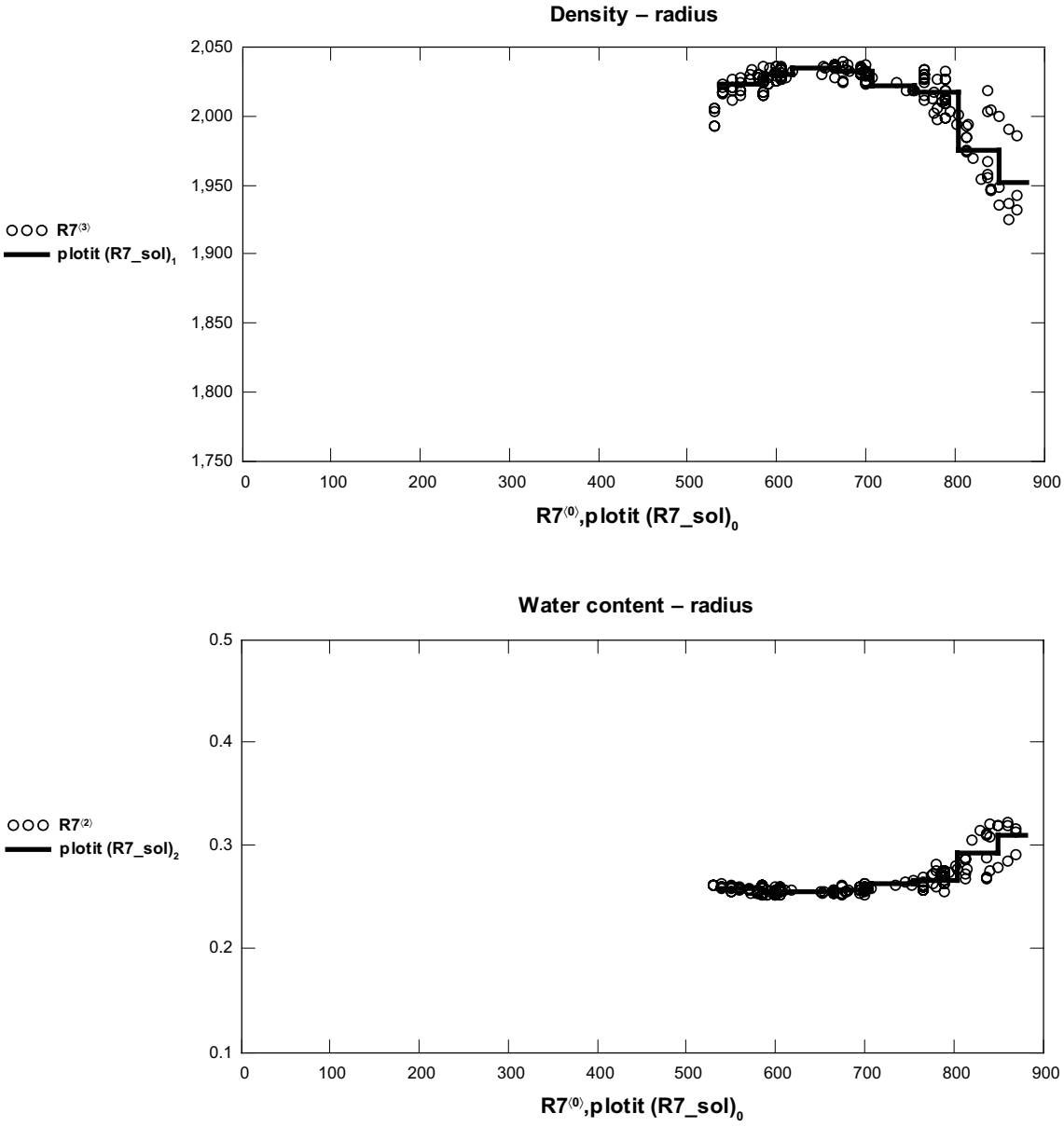

Figure A-4. *Example showing the analysis of block R7. Density in [kg/m^3], radius in [mm].*

Appendix B

RH and suction of Äspö-water

Prepared from work done in June 2008 by A. Dueck, Clay Technology AB.

B.1 Water sample

Water from borehole HD0025A was taken 2007-10-09 for the purpose of saturating laboratory samples from the CRT project.

B.2 RH measurement

The relative humidity was measured above a surface of Äspö-solution as shown in Figure B-1. Psychrometers (Wescor) were installed in calibrators and measurements were made above Äspö solution and controlled above a saturated solution of K_2SO_4 (RH = 97.6% at 20°C). The suction was measured both by the psychrometer method (PS) and by the dew point method (DP). Two sensors were used represented by red and blue lines.

After approximately 150h RH = 99.5% and RH = 99.6% were measured in this limited investigation. The average of the measurements was RH = 99.55%.

B.3 Calculations of activity from measured salt content

Data from the database SICADA gave the contents (mg/l) of Na, Ca, Cl, K, Mg, HCO_3 and SO_4 (2003-04-02) as shown in Table B-1. The contents of SO_4_S, BR, F, Si, Fe, Fe_{tot}, FeII, Mn, Li and Sr were not considered since the total weight was small.

From the concentrations (mmolar) of the elements the water activity was calculated with the program PHREEQC by M. Birgersson. The given data represents large contents of the elements. Data representing lower contents of the elements was also analysed and the resulting activity for this data is shown in brackets. The salt content as weight-%, calculated from the data in Table B-1, was 0.9% (0.5%).

The relative humidity measured above a surface of the solution should be the same as the activity in the solution, i.e. $RH = 100 \cdot p/p_s$ = 99.5% (99.7%).

B.4 Conclusion

The relative humidity above Äspö water is between 99.5% and 99.7%. The corresponding suction calculated from Kelvins equation, given below, is ψ = 404–678 kPa at 20°C. Kelvins equation reads,

$$\psi = -\frac{R \cdot T}{\nu_{w0} \cdot \omega_v} \ln\left(\frac{p}{p_s}\right),$$

where

ψ = suction (kPa)

T = absolute temperature (K)

R = universal gas constant (8.31432 J/(mol K))

v_{w0} = specific volume of water ($1/\rho_w$ m^3/kg)

ρ_w = density of water (kg/m^3)

ω_v = molecular mass of water vapour (18 kg/kmol)

p = partial pressure of pore-water vapour (kPa)

p_s = saturation pressure of water vapour over a flat surface of pure water of the same temperature (kPa)

Table B-1. Chemical data of Äspö water (SICADA) and calculated water activity.

Ion/element	mg/l[1]	Molecular weight[1]	mmolar	Calculated activity[2]
Na	1,810	23	78.7	
Ca	1,310	40.1	32.7	
Cl	5,560.8	35.5	156.6	
K	15.90	39,10	0.4	99.50%
Mg	71.5	24.3	2.9	(99.7%)
HCO_3	101.00	61.00	1.7	
SO_4	365.00	96.10	3.8	
Total	9,234.20			

[1] Assumed to be mg per litre of the solution.
[2] Calculated with PHREEQC.

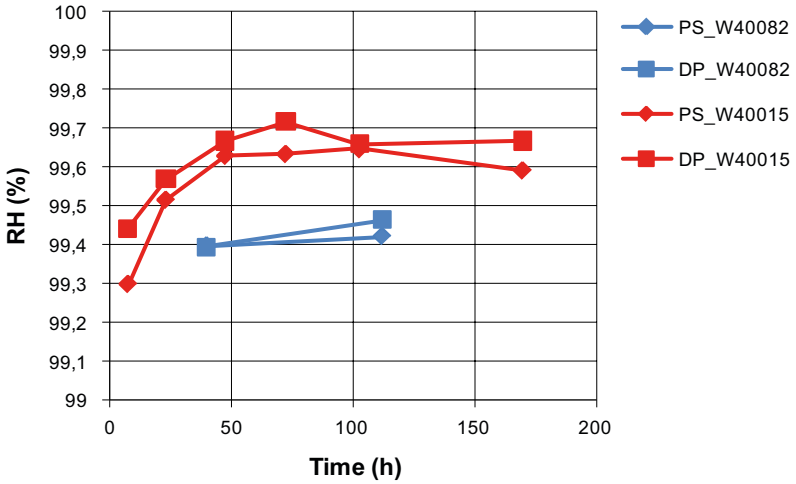

Figure B-1. *Measurement of RH by two psychrometers.*

Appendix C

Test of the sensor installation effect

Based on work performed November 2007 by U. Nilsson, Clay Technology AB

C.1 Introduction

A test of the Geokon total pressure transducers used in CRT has been performed by Ulf Nilsson at Clay Technology. This test was designed to investigate the cause of the unexpectedly low total pressures (or rather stress in the direction of the sensor) measured in CRT.

C.2 Experimental setup

The test setup, shown in Figure C-1, measured the axial total stress at full water saturation under confined conditions, by using one of the Geokon transducers that was used in the CRT experiment, and the radial stress at two different heights, by using two load cells.

The installation of the pressure sensor was done using the same technique as in CRT, where a hole was drilled in the block, bentonite powder was compacted in the bottom of the hole, the sensor was inserted into the hole, and finally the hole was backfilled with more bentonite powder. The bentonite powder initially compacted at the bottom of the drilled hole was used to fill the cone-shaped excavation, caused by the shape of the drill bit, so that a good contact between the block material and the sensor tip was obtained.

The sample used in the sensor test setup was taken from an uninstalled ring-shaped block that was manufactured for the Prototype Repository experiment. The ring-shaped blocks used in the Prototype Repository had an initial density of 2,075 kg/m^3 and an initial water content of 17.3%. The sample was cut so that it fitted tightly into the steel cylinder, obtaining at most a 1mm gap between the cylinder wall and the sample surface.

The sample had free access of water at atmospheric pressure through an upper and a lower cylindrical filter section installed at the cylinder wall. The time duration of the water saturation at atmospheric water pressure was about 3 months; the increase of the monitored pressures had then been insignificant during two months which indicated that full swelling pressure had been obtained.

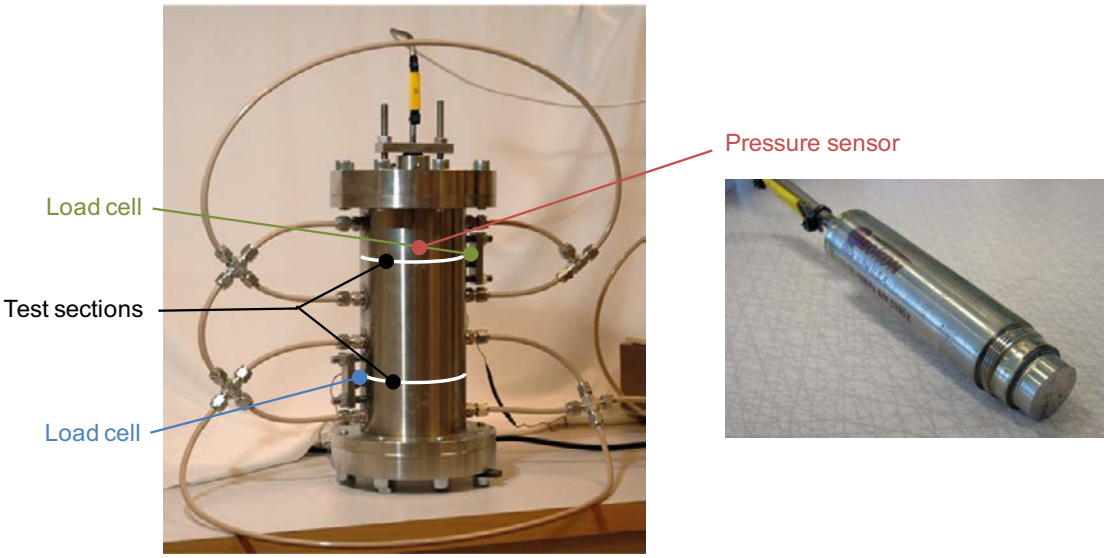

Figure C-1. *The experimental setup and Geokon pressure sensor.*

C.3 Results and discussion

The measured stress responses are shown in Figure C-2 where the blue curve corresponds to the lower load cell, the green curve corresponds to the upper load cell and the red curve corresponds to the Geokon pressure sensor. The curves level out at approximately 15 MPa, 13 MPa and 9 MPa, for the blue, green and red curve respectively. The step in the curves at 2007-10-10 comes from that a 1 MPa water pressure was imposed on the system at this time. The different pressures indicate that the installed Geokon sensor have an effect on the stress response and that it does not measure the stress representative for "undisturbed conditions", here considered to be best captured by the lower load cell.

Thus, the stress measurement obtained at the lower test cell (15 MPa) is considered most representative for undisturbed conditions in the buffer material and the pressure sensor measurement (9 MPa) represents the sensor data of the CRT experiment. If the "installation effect" is to be compensated for in models where the local conditions around the sensors are not included, the present study motivates that the calculated stress might be multiplied with the ratio 9/15 = 0.6 (or the sensor data could be divided by 0.6).

After dismantling the experiment, the water content w and the density ρ was evaluated for samples of 1 cm length in the two test sections indicated in Figure C-1. From these properties the dry density can be calculated according to,

$$\rho_d = \frac{\rho}{w+1}.$$

The obtained profiles of dry density are shown in Figure C-3. It can be seen that the profile corresponding to the upper test section is lower and has more heterogeneous appearance as compared to the lower test section profile. This indicates that the presence of an installed sensor affects the state of the buffer after being saturated.

The obtained dry density profiles averaged over the two test sections (excluding the outermost samples) give ρ_d = 1,630 and 1,648 kg/m^3, for the upper and lower test section respectively. These dry densities are considered suitable to associate with the radial stresses measured at the two different heights, i.e. 13 MPa for ρ_d = 1,630 kg/m^3 and 15 MPa for ρ_d = 1,648 kg/m^3.

It is more difficult, with the data given, to estimate a dry density suitable to associate with the vertical stress measured by the Geokon sensor. A typical dry density will instead be estimated by comparing the obtained axial stress with data from other swelling pressure experiments where a characteristic trend in pressure-dry density can be used.

With the data plotted in a graph, where also data from other swelling pressure experiments are shown, see Figure C-4, it is possible to:

- evaluate if the obtained test section dry densities and measured radial stresses are representative for the material,
- estimate a dry density typical for the obtained sensor pressure.

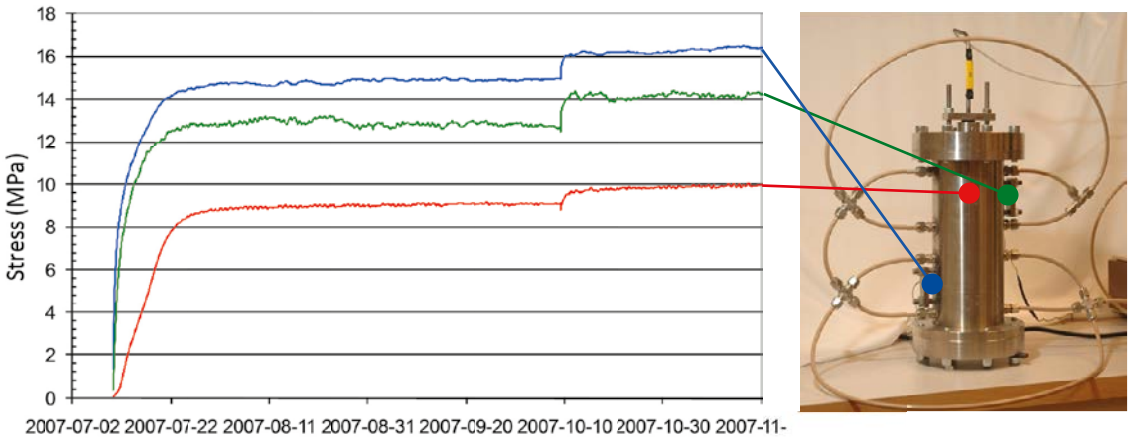

Figure C-2. *Measured stress component evolutions in MPa.*

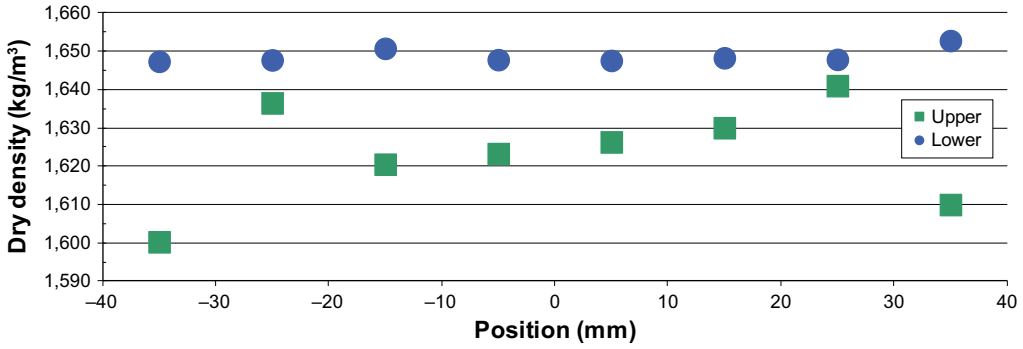

Figure C-3. *Dry density profiles in the upper and lower test section.*

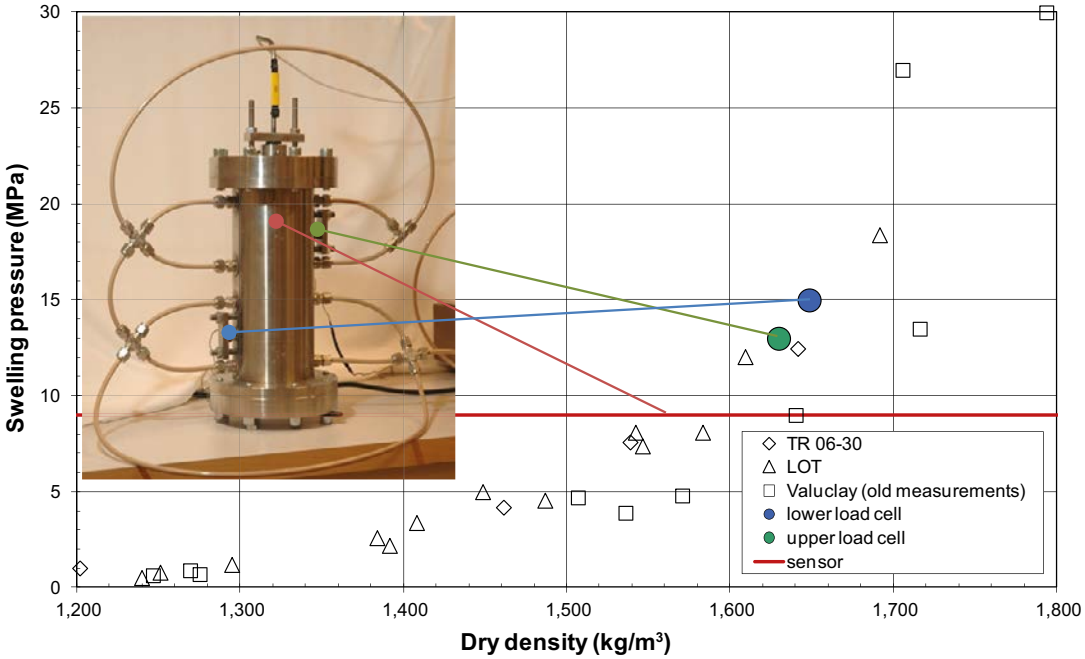

Figure C-4. *Swelling pressure given as a function of dry density. The measurements from this experiment (coloured symbols/lines) and other experiments (unfilled symbols).*

It should be noted that the data denoted Valuclay is quite old and the accuracy of these measurements should probably be regarded somewhat lower as compared to the other data.

It can be seen that the datasets consisting of the two load cell pressures and the corresponding dry densities agree well with the trend of the other measurements. The pressure sensor measurement can be seen to correspond to a dry density somewhere about 1,560 kg/m^3, which is 0.95 of the undisturbed dry density (1,648 kg/m^3).

Some of the discrepancy is believed to stem from locally lower average density around the pressure sensor, which arises as a result from using the technique with bentonite powder backfill at the hole bottom when installing the pressure sensor.

Another possible reason for low total pressures in the CRT experiment, which is not investigated using the present test setup, is that the sensor is not installed "firmly" in the buffer block. With the present test setup, the sensor is fixated with respect to the block by a beam, see Figure C-1, whereas in CRT, the entire sensor was embedded in backfilled bentonite powder which allowed for displacement with respect to the block.

It can be noted that the swelling pressure is very sensitive to changes in dry density at the high dry densities that are considered here. Thus, small deviations in the determination of water content and density make a significant impact on the result.

Appendix D

Testing of CRT sensors

Based on work performed June 2006 by U. Nilsson, Clay Technology AB.

D.1 Introduction

This appendix describes the testing of sensors previously mounted in the Canister Retrieval Test (CRT). The tested sensors were used in measuring pressure, humidity and displacements.

At the time of ending the CRT, the majority of the pressure sensors were functioning and showing small deviations. The humidity sensors were mostly either non-functional or had unreliable readings. One linear displacement sensor was showing correct values, one was damaged by corrosion and the last was bent, probably during dismantling.

When the sensors arrived at the laboratory they were examined for obvious damage and checked for serial number/channel number. Sensors with obvious damages were not further tested. If possible, tests of cable integrity were made.

D.2 Total Pressure sensors

14 Geokon total pressure sensors were examined. The sensors were emplaced in a pressure vessel and the pressure source was then connected. A Single channel logger 8001 (S/N 2623) was used for reading and a GDS controller (S/N 2352) acted as pressure source. The sensors were tested by applying determined pressures, reading the obtained frequency, and translating this to pressure using the Linear Gage Factor from factory calibration and the Regression zero from this measurement. The Regression zero from this measurement was used since the zero reading can be affected by the installation. The deviation from zero in the table is the difference between this measurement and the factory zero. Some sensors had longitudinal scratches interfering with the sealing which limited the max pressure. With the exception of P210 the sensors output were about 2–4% lower than their initial as-installed value. P210 had also an offset error of 0.97 MPa higher than the applied pressure. For all results, see Table D-1.

Table D-1. Total pressure sensors.

		Calibration 0–3 MPa				
			Linear regression			
Mark	S/N	Dev at 0	A*x	+B	R^2	Comment
P201	52951	–0.062	0.9751	–0.0030	1	
P202	52955	–0.059	0.9737	–0.0036	1	
P203	52959	0.014	0.9844	0.0013	1	Longitudinal scratches, 2MPa
P204	52961	–0.086	0.9680	–0.0172	0.9999	
P207	52960	–0.041	0.9608	0.0009	1	
P209	52958	0.007	0.9656	–0.0010	1	Scratches
P210	52965	–0.971	0.9350	0.0029	1	Tested twice
P211	52976	–0.038	0.9703	–0.0026	1	
P212	52957	–0.051	0.9733	–0.0025	1	
P214	52952	0.014	0.9859	0.0440	0.9995	
P218	52939	–0.011	0.9690	–0.0088	1	
P219	52963	–0.023	0.9743	0.0016	1	
P220	52940	0.056	0.9785	–0.0010	1	
P225	52945	–0.004	0.9765	–0.0046	1	
P226	52949	–0.136	0.9678	0.0037	1	

D.3 Pore pressure sensors

9 Geokon pore pressure sensors were examined with the same methodology as used for the total pressure sensors. With two exceptions the readings for these sensors were about 2–3% lower than their initial calibration values. For all results see Table D-2. U204 had an offset error of 0.55 MPa lower than applied. U212 had a proportional error of 11%.

Table D-2. Pore pressure sensors.

		Calibration 0–3 MPa				
			Linear regression			
Mark	S/N	Dev at 0	A*x	+B	R^2	Comment
U201	52944	0.052	0.9813	0.0019	1	
U202	52972	–0.019	0.9756	–0.0017	1	
U203	52954	–0.007	0.9691	–0.0018	1	
U204	52973	0.554	0.9746	–0.0021	1	
U205	52969	–0.052	0.9697	–0.0055	1	
U206	52967	–0.039	0.9729	–0.0037	1	Without filter
U209	52975	0.048	0.9723	0.0011	1	
U212	52950	–0.092	0.8901	5.00E–05	1	Without filter
U213	52937	–0.015	0.9759	–0.0017	1	

D.4 Humidity sensors

The humidity sensors were of two makers with different sensing technique, one a capacitive sensor (Vaisala) and one with dew point measurement (Wescor). The Vasiala sensor requires that the cable is intact since it affects the measurement. Wescor sensors do not require this but have a smaller range. Since a number of sensors were found to be damaged on receipt from the CRT decommissioning only a few were actually tested. All results from the humidity sensors recovered and installed are gathered in Table D-3.

Vaisala

Since the sensor cable was cut from the electronics box when dismantled, the first test concerned the integrity of the cable and the Pt100 element in the sensor. Of the 23 sensors only 12 had realistic values. A standard Pt 100 at room temperature is expected to have a resistivity of ca 108 Ω, other values indicating either cable damage or deposits on the sensor. The electronics boxes were also inspected. Out of 13 boxes 9 were intact with no visible corrosion on the circuit board. Among the nine intact boxes, 3 were missing sensors and only 2 had sensors with realistic temperature values. These were reconnected with the electronic box by soldering. Once attached, the box indicated errors in the humidity sensor's operation. One was dismantled and had unknown substance on the sensor membrane. An attempt to clean it with deionised water failed. See Figure D-1 below.

No Vaisala sensor could be tested.

Wescor

23 Wescor humidity sensors were retrieved. Initial tests, reading of room temperature and cooling of the element, showed that 6 sensors could not be tested either due to missing parts (2 sensors) or probable cable errors (elements were moulded in epoxy and could not be further investigated). When a filter was removed some brown residue was found on the inside of the filter, see Figure D-2. The other 17 sensors responded with correct values and were tested in a closed environment against free water (100% RH).

Six sensors were tested against 0.5 Molal and 1.0 Molal NaCl solution. Results are given in Table D-4. As can be seen, none of the sensors gave a correct reading.

Table D-3. Humidity sensors.

								From protocol			
Sensor	**Date**	**Make**	**Test temp**	**Test Rh**	**Inside box**	**Outside box**	**Comment**	**Serial no.**		**Temp corr**	**Factor µV/bar**
W201	2006-07-27	Vaisala	OK		Corroded	Corroded					
W202	2006-07-27	Vaisala	Missing		OK	OK					
W203	2006-07-27	Vaisala	OK		Corroded	Corroded					
W204	2006-07-27	Vaisala	OK		OK	OK					
W205	2006-07-27	Vaisala	OK		OK	Corroded					
W206	2006-07-27	Vaisala	Missing		OK	OK					
W207	2006-07-26	Wescor	OK	OK				40171	9.2	9.46	0.377
W208	2006-07-25	Wescor	OK	OK				40176	9.8	10.07	0.401
W209	2006-07-26	Wescor	OK	OK				40178	9.2	9.46	0.377
W210	2006-07-27	Vaisala	dubious		OK	OK	95.158 Ohm				
W211	2006-07-27	Vaisala	Faulty		Seriously Corroded	Seriously Corroded	Cable cut, 1.2kohm, Cable ok				
W213	2006-07-26	Wescor	OK	Faulty			Zeroing not possible				
W214	2006-07-26	Wescor	OK	Faulty			Zeroing not possible				
W216	2006-07-26	Wescor	OK	OK				40182	10.2	10.48	0.418
W217	2006-07-26	Wescor	OK	OK				40172	9.4	9.66	0.385
W218	2006-07-27	Vaisala	Faulty		OK		Yellow/black ok blue/green OC				
W219	2006-07-27	Vaisala	Faulty				4.1kOhm, Yellowl/black OK, Angle grinder damage				
W220	2006-07-27	Vaisala	Faulty				Cable cut, 130kOhm, Cable ok				
W221	2006-07-27	Vaisala	Faulty		OK	Corroded	5.8 kohm				
W222	2006-07-26	Wescor	OK	Faulty			Zeroing not possible				
W224	2006-07-26	Wescor	OK	Faulty			Zeroing not possible				
W225	2006-07-27	Vaisala	Missing		Corroded	Corroded					
W226	2006-07-27	Vaisala	Missing		OK	Corroded					
W227	2006-07-27	Vaisala	Faulty		OK	OK	3kOhm, Yellow/black OK				
W228	2006-07-26	Wescor	OK	Faulty			No sensor				
W230	2006-07-26	Wescor	OK	Faulty			Can zero but no cooling, damage to the pipe				
W231	2006-07-26	Wescor	OK	Faulty			No sensor				
W232	2006-07-26	Wescor	OK	OK				40161	9.8	10.07	0.401
W233	2006-07-26	Wescor	OK	OK				40167	9.6	9.87	0.393
W234	2006-07-27	Vaisala	OK		Missing						
W235	2006-07-27	Vaisala	OK		Missing						
W236	2006-07-27	Vaisala	OK		Missing						
W237	2006-07-27	Vaisala	Faulty		Missing		Cable missing				
W238	2006-07-27	Vaisala	OK		Missing						
W239	2006-07-26	Wescor	OK	OK				40165	8.6	8.84	0.352
W240	2006-07-26	Wescor	OK	OK				40184	10.2	10.48	0.418
W241	2006-07-26	Wescor	OK	OK				40162	10	10.28	0.409
W242	2006-07-27	Vaisala	Faulty		Missing		753 ohm?				
W243	2006-07-27	Vaisala	dubious		Missing		111.447 ohm				
W244	2006-07-27	Vaisala	Faulty		Missing		3 Mohm, cable OK				
W245	2006-07-26	Wescor	OK	OK				40180	10.4	10.69	0.426
W246	2006-07-26	Wescor	OK	OK				40157	10.8	11.10	0.442
W247	2006-07-26	Wescor	OK	OK				40183	10.8	11.10	0.442
W248	2006-07-26	Wescor	OK	OK				40166	9	9.25	0.369
W249	2006-07-26	Wescor	OK	OK				40163	10	10.28	0.409
W250	2006-07-27	Vaisala	OK		Missing						
W251	2006-07-27	Vaisala	OK		Missing						
W252	2006-07-27	Vaisala	Faulty		Missing		Cable missing				
W253	2006-07-27	Vaisala	OK		Missing						
W254	2006-07-27	Wescor	OK	OK				40177	10.4	10.69	0.426
W255	2006-07-27	Vaisala	OK		Missing		Damaged cable				

Figure D-1. *Vaisala Sensor membrane, exposed W204 and new.*

Figure D-2. *Wescor filter (W214), the damage on the rim occurred when the filter was removed from the holder.*

Table D-4. Readings from Wescor sensors, correct values in curly brackets.

Sensor	233	239	240	241	245	246
Bar {22.6}	–	2.84	16.7	17.1	9.4	24.9
Bar {46}	3.8	7.1	16.7	19.6	164	33.9

D.5 Displacement sensors

The displacement sensors were tested with micrometer and gauge block of 25 and 50 mm. The feed was +15, 0 and –15 V. Output was measured with a Fluke 8840A multimeter. The sensor tips were heavily corroded and in some case completely worn away, see Figure D-3.

Sensor one had a faulty circuit board due to corrosion products and did not function, see Figure D-4.

Sensor two was working properly and the obtained linear coefficient was:

Output/Deformation = 0.2005 V/mm, with R^2=1.0000.

Sensor three was bent out of shape and could not be tested, see Figure D-5. This probably happened during dismantling of the sensor. The electronics were intact on this sensor so it would probably work.

Figure D-3. *Top row, tip of sensor 1 and 2, Bottom row tip of sensor 3 and a new tip.*

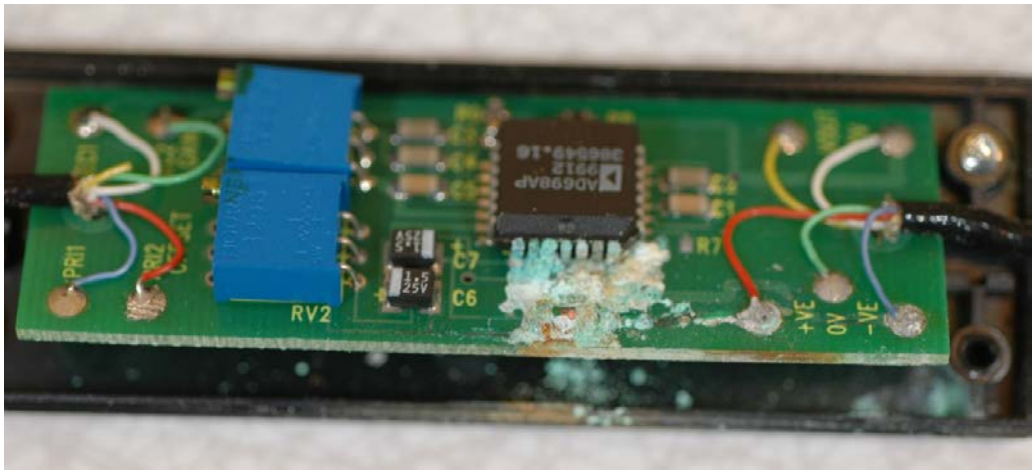

Figure D-4. *Electronics of displacement sensor 1.*

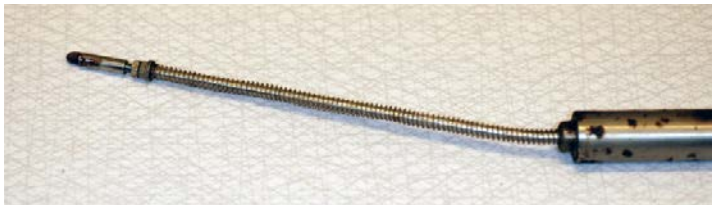

Figure D-5. *Bent displacement sensor 3.*